UNIVERSITÉ LAVAL

Optimization of design and operation of synergetic heating and cooling networks based on the energy hub concept

Thèse

Hossein Ahmadisedigh

Doctorat en génie mécanique
Philosophiæ doctor (Ph. D.)

Québec, Canada

UNIVERSITÉ LAVAL

Optimization of design and operation of synergetic heating and cooling networks based on the energy hub concept

Thèse du Doctorat en Génie Mécanique

Hossein Ahmadisedigh

Sous la direction de :

Louis Gosselin

2022

Résumé

Dans le présent travail, un modèle de « hub énergétique » a été utilisé pour concevoir des réseaux combinés de chauffage et de refroidissement afin de bénéficier des synergies potentielles. Les réseaux de chauffage et de refroidissement font partie intégrante de divers bâtiments, campus ou villes. Le concept de réseau thermique intelligent et de « hub énergétique » plaide en faveur de l'intégration thermique pour bénéficier des synergies potentielles et faciliter l'utilisation des sources d'énergie renouvelables. Dans ce système intégré, les pompes à chaleur peuvent être utilisées pour récupérer la chaleur de la boucle de refroidissement et la fournir à la boucle de chauffage. La récupération de la chaleur résiduelle peut aider à réduire les coûts d'exploitation et les émissions de gaz à effet de serre. Les charges de chauffage et de refroidissement du réseau peuvent être satisfaites par des chaudières au gaz naturel, des radiateurs électriques, des refroidisseurs et des pompes à chaleur. La conception du système et son fonctionnement ont été optimisés en termes de coût et d'émissions de gaz à effet de serre sous différentes combinaisons de charges de chauffage et de refroidissement. Les configurations de hub optimisées pour les scénarios avec et sans récupération de chaleur perdue ont été comparées, montrant que les pompes à chaleur étaient bénéfiques dans tous les scénarios. La capacité optimale des pompes à chaleur pour minimiser le coût total s'est avérée être d'environ 80% de la valeur maximale possible à partir d'une analyse thermodynamique des charges. La minimisation simultanée des coûts et des émissions a révélé une transition relativement nette du chauffage au gaz au chauffage électrique, car l'accent est davantage mis sur les émissions que sur les coûts, mais dans tous les cas, la récupération de la chaleur perdue avec des pompes à chaleur a été largement utilisée pour satisfaire les charges de chauffage et de refroidissement.

Ensuite, en gardant le même cadre conçu ci-dessus, une méthode a été développée pour indiquer comment les unités de stockage d'énergie thermique (SET) peuvent contribuer à réduire le coût total d'un réseau thermique. Nous avons développé une méthode montrant comment les unités SET, couplées à des pompes à chaleur, peuvent contribuer à réduire le coût total d'un réseau thermique. Un modèle d'optimisation est introduit, basé sur un modèle de hub énergétique comprenant des chaudières au gaz naturel, des radiateurs électriques et des refroidisseurs. Pour différents profils de charge, les réseaux thermiques intégrant des pompes à chaleur seules, SET seules ou une combinaison des deux sont comparés à un hub de référence sans intégration thermique. Il a été constaté que l'inclusion à la fois du SET et des pompes à chaleur génère plus de bénéfices que lorsqu'elles sont utilisées séparément, étendant l'utilisation synergique des pompes à chaleur pour satisfaire à la fois les charges de chauffage et de refroidissement. De plus, l'intérêt du SET lorsque les composants du système (refroidisseur ou chaudière) sont sous-dimensionnés est évalué. Il a été observé que dans ces cas, le SET

contribue à satisfaire les demandes thermiques. Cependant, en raison de la configuration du système, il existe une limite de sous-dimensionnement du refroidisseur que les unités SET peuvent compenser.

Ensuite, l'influence du fonctionnement à charge partielle des dispositifs du hub énergétique a été étudiée pour le même hub énergétique. Dans la pratique, l'efficacité à charge partielle des équipements tels que les refroidisseurs, les chaudières et les pompes à chaleur doit être prise en compte dans la conception et le contrôle des réseaux de chauffage et de refroidissement car elle peut fortement affecter leurs performances globales. Cependant, les modèles d'optimisation tels que les hubs énergétiques considèrent généralement des efficacités constantes en raison du défi de mettre en œuvre l'efficacité à charge partielle dans de tels modèles. Par conséquent, l'impact des courbes d'efficacité à charge partielle sur les résultats d'optimisation des hubs énergétiques n'est souvent pas clair, en particulier lorsque plusieurs appareils sont inclus. Dans ce travail, le coût total sur la vie d'un système de réseaux combinés de chauffage et de refroidissement a été optimisé sur la base d'un hub énergétique dans lequel des dispositifs d'efficacité à charge partielle (chaudières à gaz naturel, radiateurs électriques, refroidisseurs électriques et pompes à chaleur) ont été modélisés. Le modèle a été linéarisé et étudié sous différentes combinaisons de charges thermiques. Une méthode itérative a été développée pour optimiser la conception et l'exploitation du pôle énergétique dans ce contexte. Pour déterminer l'impact des efficacités à charge partielle, chaque appareil a été examiné individuellement tandis que l'efficacité des autres appareils est restée constante. L'erreur résultant de l'hypothèse d'un rendement constant a ensuite été calculée sur la base d'un hub de référence avec des rendements constants. Les résultats ont indiqué une erreur maximale sur le coût total de 1,85 %, 0,6 % et 0,16 % en supposant un rendement constant pour les chaudières, les refroidisseurs et les pompes à chaleur respectivement. Les charges pour lesquelles ces erreurs maximales se produisent ont ensuite été choisies pour optimiser le hub avec tous les appareils modélisés avec une courbe d'efficacité à charge partielle. Les erreurs ont augmenté à 1,9 %, 0,71 % et 1.49 %, respectivement.

Enfin, le potentiel de récupération de chaleur perdue (WHR) d'un atelier de fabrication a été évalué. Dans un premier temps, les sources de chaleur résiduelle ont été identifiées et évaluées, ce qui a conduit à la préparation d'une carte de chaleur résiduelle pour l'entreprise. Par la suite, trois principales méthodes de récupération de la chaleur ont été choisies et analysées pour l'usine. Pour les étés, la possibilité de remplacer les refroidisseurs actuels de bureaux par un refroidisseur à absorption simple effet de 52 kW a été étudiée, ce qui coûterait 8,000 CAD de plus que les refroidisseurs actuels sur 20 ans. Pour les hivers, le flux de chaleur résiduelle conditionné peut être utilisé à des fins de chauffage local au lieu d'utiliser les systèmes de chauffage électrique actuellement utilisés, ce qui permettrait d'économiser environ 110,000 CAD sur 20 ans. Pour le reste de l'année, la consommation interne d'eau chaude de l'entreprise peut être fournie en utilisant un chauffe-eau hybride (WHR + électricité), ce qui permettrait d'économiser environ 2,000 CAD sur la même période.

Abstract

In the present work, an “energy hub” template was employed to design combined heating and cooling networks to benefit from potential synergies. Heating and cooling networks are integral components of various buildings, campuses, or cities. The concept of smart thermal grid and “energy hub” argue in favor of thermal integration to benefit from potential synergies and facilitate the use of renewable energy sources. In this integrated system, heat pumps can be used to recover heat from the cooling loop and supply it to the heating loop. Waste heat recovery can help reducing operation costs and greenhouse gas emissions. Heating and cooling loads of the network can be satisfied by natural gas boilers, electric heaters, chillers, and heat pumps. The design of the system and its operation were optimized with respect to cost and greenhouse gas emissions under different combinations of heating and cooling loads. The optimized hub configurations for scenarios with and without waste heat recovery were compared, showing that heat pumps were beneficial in all scenarios. The optimal capacity of heat pumps to minimize total cost was found to be ~80% of the maximal possible value from a thermodynamic analysis of the loads. The simultaneous minimization of cost and emissions revealed a relatively sharp transition from gas to electric heating as more emphasis is put on emissions than cost, but in all cases, waste heat recovery with heat pumps was heavily used to satisfy the heating and cooling loads.

Next, keeping the same framework designed above, a method was developed to indicate how thermal energy storage (TES) units can contribute to reduce the total cost of a thermal grid. We developed a method showing how TES units, coupled with heat pumps, can contribute to reducing the total cost of a thermal grid. An optimization model is introduced, based on an energy hub model including natural gas boilers, electric heaters, and chillers. For different load profiles, thermal grids integrating heat pumps alone, TES alone, or a combination of both are compared to a reference hub with no thermal integration. It was found that the inclusion of both TES and heat pumps together results in more profits than when they are used separately, extending the synergic use of the heat pumps to satisfy both heating and cooling loads. Furthermore, the benefit of TES when components of the system (chiller or boiler) are under-sized is assessed. It was observed that in these cases, TES contributes to satisfying the thermal demands. However, due to the configuration of the system, there is a limit of chiller under-sizing that TES units can compensate.

Then, the influence of part-load operation of energy hub devices was studied for the same energy hub. In practice, part-load efficiency of equipment such as chillers, boilers, and heat pumps need to be taken into account in the design and control of heating and cooling networks as it can strongly affect their overall performance. However, optimization models such as energy hubs usually consider constant efficiencies due to the challenge of implementing part-load efficiency in such models. Therefore, the impact of part-load efficiency

curves on energy hub optimization results is often unclear, in particular when multiple devices are included. In this work, the lifetime cost of a combined heating and cooling networks system was optimized based on an energy hub in which part-load efficiency devices (natural gas boilers, electric heaters, electric chillers, and heat pumps) were modeled. The model was linearized and studied under different combinations of thermal loads. An iterative method was developed to optimize the design and operation of the energy hub in this context. To determine the impact of part-load efficiencies, each device was individually examined while the efficiency of other devices remained constant. The error resulting from assuming a constant efficiency was then calculated based on a reference hub with constant efficiencies. The results indicated a maximum error on the total cost of 1.85%, 0.6%, and 0.16% by assuming constant-efficiency for the boilers, chillers, and heat pumps respectively. The loads for which these maximum errors occur were then chosen to optimize the hub with all devices modeled with a part-load efficiency curve. The errors increased to 1.9%, 0.71%, and 1.49%, respectively.

Finally, the waste heat recovery (WHR) potential of a manufacturing workshop was assessed. First, the sources of waste heat were identified and evaluated, leading to preparation of a waste heat map for the company. Subsequently, three main WHR methods were chosen and analyzed for the plant. In the summer, the possibility of replacing the current office chillers with a 52 kW single-effect absorption chiller was investigated, which would cost 8,000 CAD more than the present chillers over 20 years. For winters, t waste heat can be used for local heating purposes instead of using the electric heating systems currently used, which would save approximately 110,000 CAD over 20 years. For the rest of the year, the internal hot water consumption for the company can be supplied by using a hybrid (WHR + electricity) water heater, which would save around 2,000 CAD over the same period.

Table des matières

Liste des figures

Liste des tableaux

I am dedicating this work to my beloved wife, ***Elnaz****, who has patiently helped me in the most difficult moments of my life, and to my precious parents, Laleh and Parviz who encouraged and supported me to pursue my dreams.*

Remerciements

First, I appreciate my supervisor, Louis Gosselin, who has accepted me as his Ph.D. student, and who has not only supervised my research through these five years but also raised me as a researcher. From when I decided to speak French, he was the first person who encouraged me to do so. I am now proudly capable of speaking French, what I had even never dreamed of. Next, I would like to thank all my lab mates, particularly former students who have always been helping me in learning everything required for studying, living and for being integrated into my new country. Also, I would like to offer my warmest gratitude to my dearest friends who facilitated living abroad for me: Moslem, Alireza, Takuya.

Avant-propos

This thesis is the result of the research accomplished during doctoral studies from Sep. 2016 to August 2021, mainly in the Laboratoire de Transfert Thermique et d'Énergétique (LaTTÉ) de l'Université Laval, and partly in APN company in Parc Technologique de Québec. The covered topics and the procedures are presented in the Introduction section. Next, chapters 1-4 are constituted of the four articles that were prepared during this research, including three journal papers, and one conference paper. The conclusions are drawn subsequently. The articles are as follows:

Chapter 1:

H. Ahmadisedigh and L. Gosselin, "COMBINED HEATING AND COOLING NETWORKS WITH WASTE HEAT RECOVERY BASED ON ENERGY HUB CONCEPT", Applied Energy, vol. 253, p. 113495, Nov. 2019, doi: https://doi.org/10.1016/j.apenergy.2019.113495.

Hossein Ahmadisedigh: Conceptualization, Methodology, Software, Validation, Formal analysis, Investigation, Data Curation, Writing – Original Draft, Visualization.
Louis Gosselin: Conceptualization, Methodology, Resources, Writing – Review & Editing, Supervision, Project administration, Funding acquisition.

Chapter 2:

H. Ahmadisedigh and L. Gosselin, "OPTIMAL IMPLEMENTATION OF THERMAL ENERGY STORAGE WITHIN COMBINED HEATING AND COOLING NETWORKS BASED ON ENERGY HUB CONCEPT", Energy, vol. 243, p. 123112, March 2022, doi: https://doi.org/10.1016/j.energy.2022.123112.

Hossein Ahmadisedigh: Conceptualization, Methodology, Software, Validation, Formal analysis, Investigation, Data Curation, Writing – Original Draft, Visualization.
Louis Gosselin: Conceptualization, Methodology, Resources, Writing – Review & Editing, Supervision, Project administration, Funding acquisition.

Chapter 3:

H. Ahmadisedigh and L. Gosselin, "OPTIMIZATION OF COMBINED HEATING AND COOLING NETWORKS CONSIDERING VARIABLE-EFFICIENCY DEVICES BASED ON ENERGY HUB CONCEPT", Applied Energy, vol. 307, p. 118245, Feb. 2022, doi: https://doi.org/10.1016/j.apenergy.2021.118245.

Hossein Ahmadisedigh: Conceptualization, Methodology, Software, Validation, Formal analysis, Investigation, Data Curation, Writing – Original Draft, Visualization.
Louis Gosselin: Conceptualization, Methodology, Resources, Writing – Review & Editing, Supervision, Project administration, Funding acquisition.

Appendix 1:

H. Ahmadisedigh, L. Gosselin, and S. Lemelin, “WASTE HEAT ASSESSMENT OF THE WORKSHOP OF A MANUFACTURING PLANT: EVALUATION OF THE WASTE HEAT AMOUNT, AND WASTE HEAT RECOVERY SOLUTIONS”, 2020, Young Energy Researchers Conference, 2-6 March 2020, 1-13 p. "https://www.rls-sciences.org/uploads/5/5/4/4/55448469/ahmadisedigh_poster.pdf ".

Hossein Ahmadisedigh: Conceptualization, Methodology, Software, Validation, Formal analysis, Investigation, Data Curation, Writing – Original Draft, Visualization.
Louis Gosselin: Conceptualization, Methodology, Resources, Writing – Review & Editing, Supervision, Project administration, Funding acquisition.
Simon Lemelin: Conceptualization, Methodology, Resources, administration, Data Curation, Funding acquisition.

Introduction

Heating and cooling demands can be supplied using different energy resources, depending on where the energy system is situated. It also depends on the sector for which this system supplies energy, i.e., residential, commercial, and industrial sectors. In Canada, for instance, the majority of the energy consumption in the residential and commercial/institutional sectors are devoted to thermal satisfaction, as demonstrated in Figure 1. This figure indicates that more than 60% of the final energy use in Canada is allocated to fulfillment of heating and cooling demands.

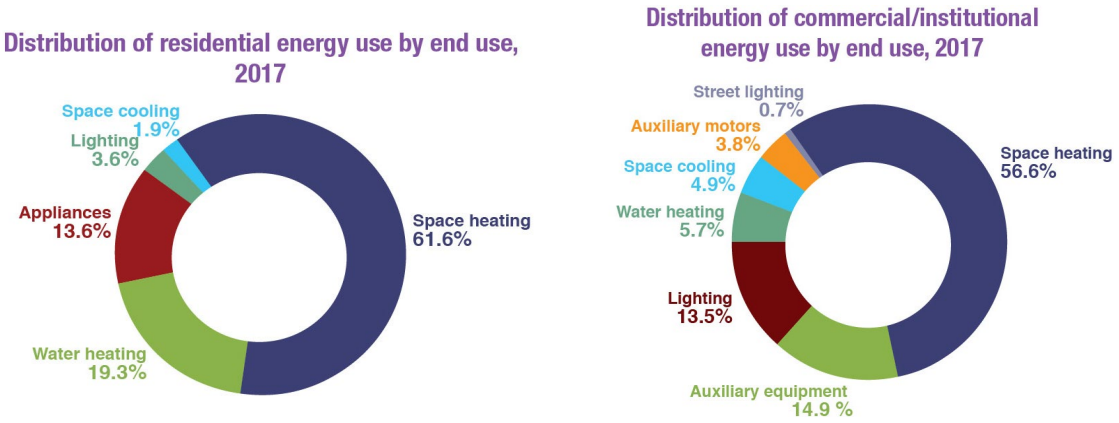

(a) (b)

Figure 1. Distribution of (a) Residential, and (b) Commercial energy use in Canada in 2017 [1], [2].

Integrated heating and cooling networks can be seen as smart thermal grids satisfying the heating and cooling needs of buildings, campuses, districts or cities. They are found abundantly, at different scales, and throughout the world. According to the International Energy Agency (IEA), district heating systems are a proven solution to facilitate the energy transition and the decarbonization of the heating sector (one of the major energy end-uses in many countries) [3]. The recourse to such system is on the rise, with an average increase of 2.4% per year over the two last decades. IEA indicates the necessity to develop innovative concepts to fully exploit waste heat, relying on a deep integration of heating and cooling networks. Providing optimization and decision-making tools, design guidelines and operational best practices for a wide range of possible load configurations thus helps the deployment of synergetic heating and cooling systems, and in the end, allows reducing significantly energy consumption and costs for many end-users.

Recently, the “energy hub” concept was found to be quite useful for optimizing the design and operation of integrated heating and cooling networks [4], an important category of applications which is the topic of interest in the present work. Using this approach, a complex energy system can be treated as a set of equipment coupling the available energy sources to the demand of end-users. This concept defines a framework in which the energy

resources available in an area can be linked to the end-users' thermal and electrical demands. Because of their flexibility, energy hub models are capable of handling various types of energy sources and carriers. Hence, depending on the energy sources that are available at the hub inlet, adapted equipment and technologies can be used to convert, transform or store energy. Therefore, it is important to determine which sources are more appropriate to satisfy the loads of interest and which converters may offer the best performance.

The main components of the energy hub thus include: (i) available sources of energy (e.g., fossil fuels, renewable energy, electricity from the grid or generated on-site, waste heat sources available nearby, etc.), (ii) technology for energy conversion, transfer, or storage, and (iii) loads (energy required by end-users for heating, cooling, etc.). An example of a typical energy hub is shown in Fig. 2, where Res., Conv., TR, and ESS indicate energy resources, conversion units, transformers, and energy storage systems, respectively. As is observable in this figure, converted energy can either be directly sent to the hub outlet for the consumers' requirements or stored in ESS to be used when needed.

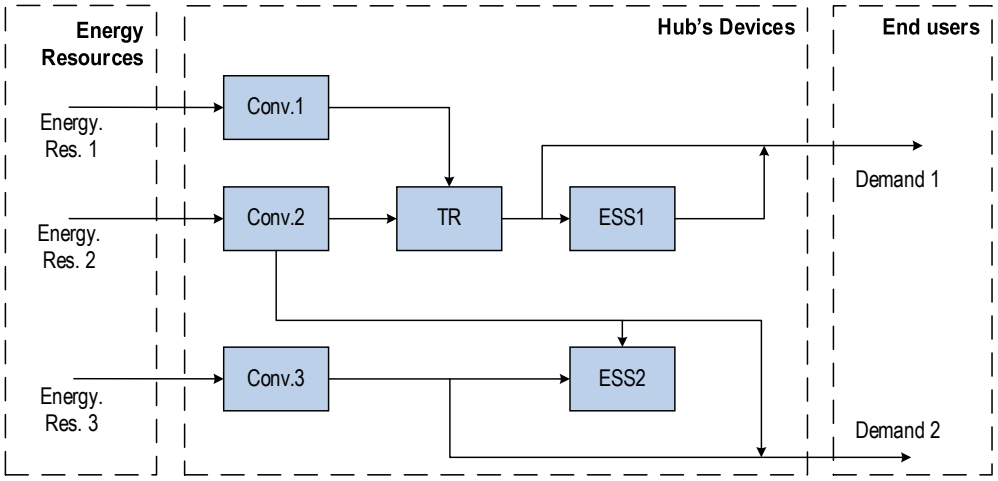

Figure 2. Example of an energy hub that contains energy convertors, transformers, and storage facilities.

The basic question in hub optimization is to determine at which rate each energy resource should be consumed by the system and at which rate each converter should contribute in supplying the loads (i.e., operational optimization). Furthermore, one may be interested in optimizing the hub configuration itself and the choice of technologies on which it relies (i.e., design optimization). The possible combinations of the available technologies and energy sources should not only meet the imposed heating, cooling and electricity demands on the end-user side of the energy hub, but also satisfy other considerations that might apply. Providing optimization and decision-making tools, design guidelines and operational best practices for a wide range of possible load

configurations thus offers an opportunity for reducing significantly energy consumption, costs, and CO2 emission for many end-users.

Various available energy sources can cooperate in a synergetic way with other energy flows. For instance, in Fig. 2, the block Conv,2 is a multi-generation unit from which two energy flows are extracted. Multi-generation devices such as heat pumps are characterized by the fact that they can supply two different forms of useful energy at the same time. Heat pumps can provide simultaneous heating and cooling, and intrinsically provide a way to recover the waste heat from electricity or cold production. Thermal networks thus can be combined using heat pump units in order to form an integrated network. A schematic view of such integration is given in Fig. 3. Due to their complexity, though, a proper framework is required to model and optimize such combined energy systems, in particular for a dynamic system in which the loads constantly change over time.

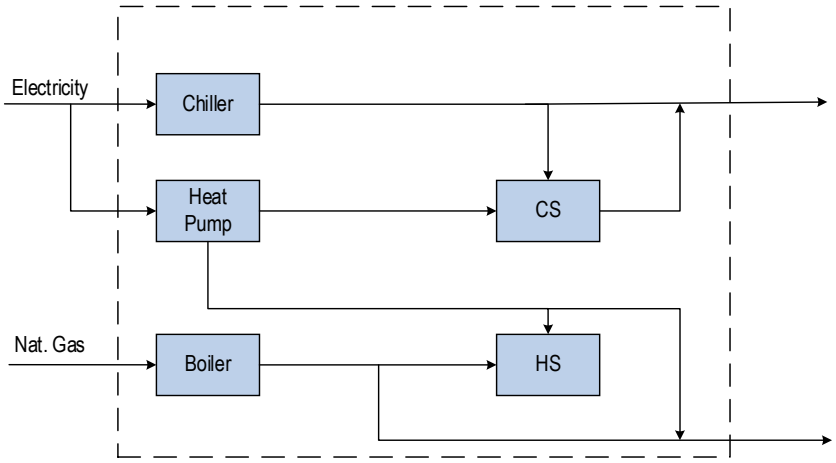

Figure 3. A schematic view of the integrated thermal networks using heat pumps.

In this figure, CS, and HS represent cold and hot storage units, respectively. As can be seen, the chiller and heat pump feed the cooling demand, while the boiler and heat pump satisfy the heating load. This combined thermal network is the result of heat pump use in this energy hub in order to recover the waste heat from the cooling loop that would otherwise be released into the environment if not recovered by the heat pump. Nevertheless, it should be noted that such integration depends strongly on the simultaneous existence of both thermal loads on the consumer's side, because heat pumps requires both a heat source (cooling load) and a heat sink in order (heating load) to function.

Objectives

The main objective of this research is to develop a method in order to optimize design and operation of synergetic heating and cooling networks using the energy hub concept. Such energy hub could look like the one portrayed in Fig. 3. Toward this target, we have split the main objective into a three subobjectives, for which three scientific articles have been prepared (one per subobjective):

- Elaborate a method for optimizing combined heating and cooling networks through the hub concept.
- Determine the benefits and optimal design and operation of thermal storage within a combined heating and cooling network for a wide range of scenarios.
- Model and optimize combined heating and cooling networks with part-load efficiency (PLE) energy conversion equipment.

The fourth article was not originally planned but was made possible thanks to a research internship opportunity in a machining plant to work on waste heat recovery. Since the idea behind the present thesis originated from research on waste heat recovery, it seemed interesting to consider that paper to finish the thesis. In the future, that industry can actually serve as a good candidate for developing smart thermal grids. The objective of the internship and of the related paper was to develop a mapping of the waste heat and potential recovery applications in that industry.

Contribution of the articles

As a result of this study, an energy hub template was designed to optimize integrated thermal networks in which heat pumps can be employed to recover the heat absorbed by cooling loops. The heating and cooling loads of the network can be satisfied by natural gas boilers, electric heaters, chillers, heat pumps, and thermal storage facilities. This system forms the main framework for the three journal articles that were prepared throughout this research project. These articles are provided in a chronological order so that new features are considered in each step using the same method. A conference paper is another outcome of this research wherein different WHR devices that can be implemented in an industrial plant are compared, but that paper does not present thermal network integration and heat pumps as a WHR technology.

In the first paper, the design of the system and its operation over one year is optimized with respect to cost and greenhouse gas emissions under different thermal load combinations. The contribution of each possible energy source and technology as well as the sizing of the heat pump system are optimized. The optimized hub configurations for scenarios with and without WHR (heat pump) were compared in order to demonstrate the extent of the profits that may be achieved by WHR use. The optimizations are accomplished for two cases focusing on two different objectives. In the first case, only cost minimization matters, and in the second, dual-objective optimization reduces both cost and GHG emissions. In this paper, however, only the purchase cost of heat pumps is considered, and the remaining devices are assumed to be already available in the plant. The efficiency of the energy hub facilities remained constant in these analyses. The challenges that were addressed in the first paper include:

- Development a better understanding of how and when waste heat recovery can be integrated in heating and cooling networks.

- Assessment the impact of the heating, cooling and electric loads on the features of the optimal hub design and operation.

- Identification of the configuration and operation of energy system in cases where cost, GHG emission or a dual objective of both is to be minimized.

The second article considers the same energy hub as developed in the first paper, except that it includes hot and cold thermal energy storage (TES) facilities. A method is adopted in this paper to illustrate how heat pumps and TES units can contribute to reducing the total cost of a combined thermal grid. In particular, the focus is on the added value provided by TES addition into the system in different scenarios. Next, the energy hub is examined in order to analyze the effect of various parameters on its design and operation. These parameters involve variations in boiler and chiller size, thermal loads, and unit TES purchase cost. The purchase costs of the heat pumps, TES units, and electric heaters are assumed to be variable here, while the boilers and chillers are already in the system. The efficiencies of the energy hub devices are held constant in these analyses. The gaps that were filled by this research include:

- Quantification of the effects of TES inclusion in energy hubs, mainly when undersized devices are part of the hub.

- Assessment of the influence of TES unit purchase cost on design and operation of energy hubs.

- Development of design charts for various load combinations from which one could obtain information on the potential financial benefits resulting from the installation of TES within a given energy hub, in particular in the predesign stage.

Articles 1 and 2 developed the idea of WHR implementation in combined thermal networks; however, they neither account for variable-efficiency equipment nor the purchase costs of the relevant technology. Those considerations are addressed in the third article, where an iterative method is developed in order to optimize the design and operation of energy hubs equipped with the devices with part-load ratio (PLR) efficiency. The model here addresses non-linearities arising from PLR-based facility operations for which efficiency and power are correlated. Each device is individually examined, while the efficiency of other pieces of equipment remains constant in the first section. Therefore, the extent of the error resulting from the assumption of a constant efficiency is revealed. Then, the energy hub is optimized, while all devices operate on a part-load efficiency basis in order to determine the errors. The novelties introduced in this paper is as follows:

- A linear formulation capable of minimizing lifetime cost, i.e. capable of sizing equipment with PLE curves and of simulating more than one day.

- Guidelines regarding the best design and operational practices for different load scenarios to help practice engineers design and manage energy systems with PLE devices.

- Flexible and generalized way to account for efficiency curves in order to facilitate the resolution of the problem.

Lastly, a conference paper which resulted from an internship in an industrial workshop in Québec revealed the least-expensive WHR technology for that workshop on a lifetime-basis calculation. The waste heat from this company originates from cutting and machining processes, and also from three compressors that supply high-pressure air for the cutting machines. In the first phase of the associated studies, the magnitude of the waste heat generated by each piece of equipment is determined, and a waste heat map is prepared for the workshop. Next, by conducting experiments, how the waste heat can be captured and which WHR technologies are appropriate for particular conditions is studied. Based on the amount and temperatures of the waste heat flows in summer and winter, different WHR methods are proposed and then compared in order to introduce feasible solutions.

Chapitre 1 COMBINED HEATING AND COOLING NETWORKS WITH WASTE HEAT RECOVERY BASED ON ENERGY HUB CONCEPT

1.1 Résumé

La récupération de la chaleur résiduelle peut contribuer à réduire les coûts d'exploitation et les émissions de gaz à effet de serre. Dans la présente étude, un modèle de « hub énergétique » a été utilisé pour concevoir des réseaux combinés de chauffage et de refroidissement dans lesquels des pompes à chaleur peuvent être utilisées pour récupérer la chaleur de la boucle de refroidissement et la fournir à la boucle de chauffage. Les charges de chauffage et de refroidissement du réseau peuvent être satisfaites par des chaudières à gaz naturel, des chaudières électriques, des refroidisseurs et des pompes à chaleur. La conception du système et son fonctionnement au cours de l'année ont été optimisés en termes de coût et d'émissions de gaz à effet de serre sous différentes combinaisons de charges de chauffage et de refroidissement. L'introduction de charges synthétiques de 8760 heures a permis de couvrir plusieurs profils de charges possibles entraînant le hub énergétique. L'apport de chaque source d'énergie et technologie possibles et le dimensionnement du système de pompe à chaleur sont optimisés, tout en garantissant la satisfaction des demandes de chauffage et de refroidissement. Les configurations de hub optimisées pour les scénarios avec et sans récupération de chaleur perdue ont été comparées, montrant que les pompes à chaleur étaient bénéfiques dans tous les scénarios. La capacité optimale des pompes à chaleur pour minimiser le coût total s'est avérée être d'environ 80% de la valeur maximale possible résultant d'une analyse thermodynamique des charges. La minimisation simultanée des coûts et des émissions a révélé une transition relativement nette du chauffage au gaz au chauffage électrique, car l'accent est mis davantage sur les émissions que sur le coût, mais dans tous les cas, la récupération de la chaleur perdue avec des pompes à chaleur a été largement utilisée pour satisfaire les charges de chauffage et de refroidissement.

1.2 Abstract

Waste heat recovery can help reducing operation costs and greenhouse gas emissions. In the present work, an “energy hub” template was employed to design combined heating and cooling networks in which heat pumps

can be used to recover heat from the cooling loop and supply it to the heating loop. Heating and cooling loads of the network can be satisfied by natural gas boilers, electric heaters, chillers, and heat pumps. The design of the system and its operation over the year were optimized with respect to cost and greenhouse gas emissions under different combinations of heating and cooling loads. The introduction of 8760-hour synthetic loads allowed covering several possible load profiles driving the energy hub. The contribution of each possible energy source and technology and the sizing of the heat pump system are optimized, while ensuring satisfaction of the heating and cooling demands. The optimized hub configurations for scenarios with and without waste heat recovery were compared, showing that heat pumps were beneficial in all scenarios. The optimal capacity of heat pumps to minimize total cost was found to be ~80% of the maximal possible value from a thermodynamic analysis of the loads. The simultaneous minimization of cost and emissions revealed a relatively sharp transition from gas to electric heating as more emphasis is put on emissions than cost, but in all cases, waste heat recovery with heat pumps was heavily used to satisfy the heating and cooling loads.

1.3 Introduction

Over the last years, the concept of “energy hub” has emerged as an appealing way to model complex energy conversion systems. The energy hub concept was introduced in Ref. [5], and the details of the corresponding project and its outcomes were discussed in [6], [7]. The energy hub concept models energy flows from various energy sources to different loads in an organized framework [8]. An energy hub contains three main components: (i) energy resources, (ii) energy convertors & storages, and (iii) energy demand (loads), and can be applied to a wide variety of systems.

Because of their flexibility, energy hub models are capable of handling various types of energy sources and carriers. Hence, depending on the energy sources that are available at the hub inlet, adapted equipment and technologies can be used to convert, transform or store energy. The energy sources can be fossil fuels, biomass, electricity from the grid or produced on-site, waste heat of a nearby plant, etc.

Since for a given set of electricity, heating, and cooling needs, there might be different combinations of energy sources to be used, it is important to determine which sources are more appropriate to satisfy the designated loads and which converters may offer the best performance. These various available energy sources can also cooperate in a synergetic way with other energy flows. For example, multi-generation facilities such as heat pumps or combined heat and power (CHP) systems are characterized by the fact that they can supply two different forms of useful energy at the same time. Heat pumps can provide simultaneous heating and cooling,

whereas in CHP, both electricity and heat can be produced. These systems intrinsically provide a way to recover the waste heat from electricity or cold production. However, due to their complexity, a proper framework is required to model and optimize such energy systems, for example as that developed in the work of Geidl and Andersson [9]–[12].

The basic question in hub optimization is to determine at which rate each energy resource should be consumed by the system and at which rate each converter should contribute in supplying the loads (i.e., operational optimization). Furthermore, one may be interested in optimizing the hub configuration itself and the choice of technologies on which it relies (i.e., design optimization). These optimization problems can be formulated and analyzed using various criteria such as cost, GHG emissions, etc.

In operational optimization of energy hubs, studies focus on finding the optimal contributions of each energy carrier in order to satisfy the end-user demands. In this line, Schulze, Friedrich and Gautschi [13] presented an application of energy hub as a modeling framework for optimal power flow problems with integrated energy systems and multiple energy carriers. They modeled an energy hub within a single time step with constant efficiencies and illustrated the application of the model with a realistic hub comprising five different energy sources.

A dual-objective optimization aiming to minimize both cost and GHG emissions with the weighted-average sum method is presented by Maroufmashat, Elkamel, Fowler et al. [14]. They used the optimization tool General Algebraic Modeling System (GAMS) to solve a Mixed-Integer Linear Problem (MILP) with the CPLEX solver. Each part of the objective function (i.e., cost and GHG emissions) is normalized by its minimum value when it is regarded as the only objective function. A comprehensive study of normalization methods for the weighted average sum approach is discussed in [15].

The optimization problem proposed by Moghaddam, Saniei and Mashhour [16] includes a detailed model of a residential energy hub designed to meet the heating, cooling, and electrical needs of a building. The possibility to sell electricity to the grid is also considered. The analysis of the daily scheduling of the energy hub is performed in GAMS as a Mixed-Integer Non-Linear Program (MINLP). On the contrary, a MILP formulation is employed in [17], in which the possibility of using different combinations of energy converter and storage devices is assessed. The approach taken in the latter involves a comprehensive model for planning the energy hub configuration.

To adapt energy hubs to interconnected regions with different energy resources and policies, the concept of Regional Energy Hub is developed by Guler, Çelebi and Nathwani [18]. In this approach, each participating region can get benefits from the mutual advantages of a shared hub. Reducing carbon emissions and costs are the major targets. From the recent work presenting more complex and comprehensive methods to model energy

hubs, the research by Ayele, Haurant, Laumert and Lacarrière [19] can be mentioned here. Their model analyzes complex couplings of local heating and electricity networks. The couplings are modeled within an energy hub framework using Matlab.

A network of four interconnected energy hubs is optimized from the cost standpoint by Maroufmashat, Fowler, Sattari Khavas et al. [20]. The capital cost of hydrogen refueling stations and operation cost of energy hubs were taken into account. The associated MILP is solved with the CPLEX solver for 8,760 hours (i.e., 1 year). The study calculates the optimal operation of various pieces of equipment for energy conversion and storage in order to satisfy the demand for a single objective (i.e., cost) problem.

In some studies, authors begin with a set of predefined possible scenarios for the system configuration and compare these configurations. In [21], the authors used Mixed Complimentary Problem (MCP) in GAMS to deal with an economic model. They developed different scenarios that combine different energy generation technologies and evaluate generated energy, cost, and emissions. A similar approach was adopted in [22]. They regarded emissions as an element in the cost function of their MCP to find the best operational and design criteria among the available scenarios. In both aforementioned papers, all efficiencies are held constant over the year, and a time step of 1 h is used which requires 8,760 time steps to simulate 1 year. Togawa, Fujita, Dong, Fujii and Ooba [23] studied the replacement of a boiler with different scenarios to meet the heating demand of a greenhouse.

Reliability and uncertainty of energy hubs are assessed in [24] and [25], respectively. In [24], reliability is imposed as a constraint during the modeling phase, compared to [25], in which cost and emissions are minimized as objective functions. The optimization operates under uncertainty of electricity price, electricity demand, and wind power in different scenarios. Both above-mentioned articles have optimized their models with a CPLEX solver. All capital costs entered as presumed constant values in the cost analysis and optimization procedures.

In the work done by Brahman, Honarmand and Jadid [26], Demand Response (DR) and energy storage are highlighted, and single and multi-objective optimization are performed for a 24-hour time period with mixed-integer linear programming (MILP) via the CPLEX solver. A similar research by Batić, Tomašević, Beccuti, Demiray, and Vraneš [27] also focuses on Demand Side Management (DSM) with a time step of 15 minutes during a special day of the year. Heating loads are estimated using Matlab and the single objective optimization is performed by CPLEX. Energy Management System using Dynamic Pricing (DP) and Time-of-Use methods is investigated in Ref. [28] thorough an energy hub concept. A 24-hour time step is used for time series input and output. Operational cost of fuel, water, and electricity, as well as discomfort costs (due to load shifting) is the objective function. Efficiencies are constant and the model is linear.

So far, only 8% of the articles related to energy hubs have employed heat pump technology in their hub modeling and/or optimization [29]. In Refs. [12] and [13], the possibility of using an electric heat pump, a CHP, and an absorption chiller (all three can work as waste heat recovery (WHR) modules) within an energy hub is analyzed. In the former, the implementation of the WHR component is discussed at a residential scale, whereas in the latter, it models an overall energy hub is assumed without any predetermined configuration for the hub. The hub comprising energy converters and storages is optimized from operational and structural points of view with respect to the total cost.

In Refs. [30]–[32], the inclusion of Combined Heating and Power (CHP) and Combined Cooling, Heating and Power (CCHP) in the energy hub are assessed. Optimal operational and configuration characteristics of a hub including CHP units are addressed in a MILP by Moradi, Ghaffarpour, Ranjbar and Mozaffari [30], with respect to supply reliability. In [31], [32], the optimization of an energy hub, with a focus on Combined Cooling, Heating and Power (CCHP) systems, is studied. A single objective optimization is used based on cost to find the optimum size of hub elements such as gas turbine, heat exchanger, absorption chiller, boiler, storage system and electricity transformer. GHG emissions are accounted for as an imposed cost on the system. GAMS and COMFAR are used to solve the associated non-linear problem. All efficiencies are assumed constant in their modeling.

Through the above literature review, several limitations and gaps were identified and will be addressed in the present work. Thermal integration of heating and cooling networks through the hub concept has not received a lot of attention, even though these energy systems are among the most common, ranging from small systems in individual buildings to more elaborate ones in districts and plants. Developing a better understanding of how and when waste heat recovery can be integrated in heating and cooling networks is thus required and could be quite impactful in terms of energy conservation. Furthermore, the impact of the heating, cooling and electric loads on the features of the optimal hub design and operation is typically not investigated, as only one or a few load profiles are used in a given study. It would thus be useful to evaluate this impact of the load on the optimal design and provide designers with general charts of the best designs as a function of the load context.

In this paper, we introduce a hub model to optimize the operation and design of a combined cooling and heating network. In particular, waste heat recovery opportunities with the use of heat pumps through the integration of these networks are studied. In Section 1.4, the energy hub model is introduced, along with the formulation of the optimization problem. The solver is presented in Section 1.5. Section 1.6 presents the resulting design and operation of the combined heating and cooling network when minimizing total cost, and Section 1.7 introduces correlations to easily size the system based on the parameters of the problems. Finally, a dual-objective problem (minimizing simultaneously cost and GHG emissions) is introduced and solved in Section 1.8. The paper aims

at facilitating the design and implementation of waste heat recovery strategies such as the integration of heat pumps in a combined heating and cooling network. It provides a detailed design methodology, as well as new design charts and correlations for easily pre-sizing the system in practice.

1.4 Energy hub optimization model

1.4.1 Modeling of the system

The energy system that is studied in this paper is schematized in Figure 1.1 in the form of an energy hub. It consists in a heating and cooling system, which was initially inspired by the district heating and cooling network of the campus of Université Laval (Québec City, Canada). Chillers (labeled "CH" in Fig. 1.1) produce chilled water that circulates in a loop from which buildings are cooled. The heat extracted from the buildings is delivered to the cold loop, and is eventually rejected to the ambient in cooling towers that are connected to the chillers, and thus becomes waste heat. Heating is provided to the buildings by a vapor or a hot water network which constitutes a second loop. Two types of boilers are considered depending on the source of energy (i.e., electricity and natural gas, respectively "EH" and "FB" in Fig. 1.1). Once heat is taken from the vapor/hot water, the condensate/water is returned to the boilers. In general, these two loops (e.g., chilled water and vapor/hot water) are considered independent. In this paper, we assume that the system (without heat pumps) already exists and we investigate the potential to recover heat from the cold loop with new heat pumps in order to supply heat to the buildings and produce chilled water at the same time. Note that because of the temperatures involved in this type of system are close to the ambient, the actual exergy of the waste heat is quite low, even though the amount of energy available can be significant. This emphasizes the recourse to a direct use of the waste heat as proposed here, rather than using it to produce electricity.

Because there is no local electricity generator or power plant in the system considered, the electricity demand should be met directly by the grid. In the present model, the electricity demand was separated into four parts: the electricity required by the chiller, by the heat pumps, by the electric heater and the remaining electricity demand (which is labeled L_e in Fig. 1.1). In this way, it is possible to assess how changes to the design or operation of the hub affect the electricity cost, which is also a function of the monthly peak demands as will be shown below. As can be seen in Fig. 1.1, the cooling load L_c is satisfied by the chillers and heat pumps, and the heating load L_h, by the heat pumps and the two types of boilers. The different loads identified in Fig. 1.1 (i.e., L_e,

L_h and L_c) pull energy fluxes from the two available sources, i.e. from the electric grid (i.e., P_e) and from natural gas (i.e., P_f). Note that since L_e, L_h and L_c vary in time, so do P_e and P_f.

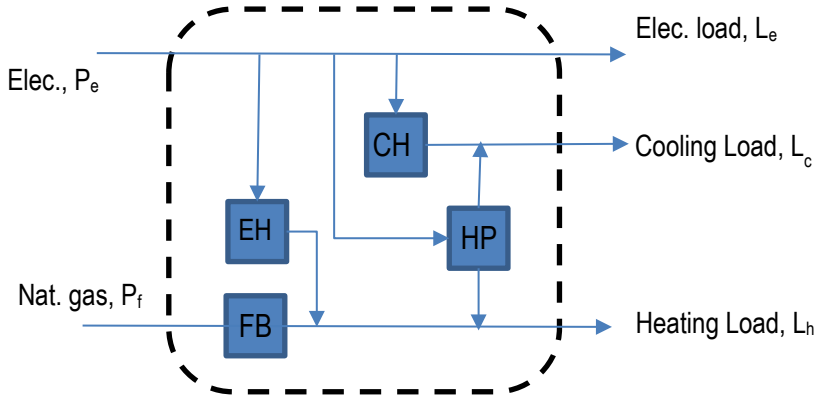

Figure 1.1. Hub representation of a heating and cooling network including electrical and natural gas boilers (EH and FB), chillers (CH) and heat pumps (HP).

The general equation of an energy hub relates the energy resource vector P and the load vector L, and can be expressed by

$$\underbrace{\begin{pmatrix} L_e \\ L_c \\ L_h \end{pmatrix}}_{\mathbf{L}(t)} = \underbrace{\begin{pmatrix} C_{ee} & C_{fe} \\ C_{ec} & C_{fc} \\ C_{eh} & C_{fh} \end{pmatrix}}_{\mathbf{C}} \underbrace{\begin{pmatrix} P_e \\ P_f \end{pmatrix}}_{\mathbf{P}(t)} \tag{1.1}$$

where $\boldsymbol{C}$ is the coupling matrix and includes all the conversion and transformation coefficients corresponding to the hub technologies. P denotes the power of each energy resource that has been shown by f, e representing fuel (natural gas), and electricity, respectively. The subscripts c, h also indicate cold and heat on the demand side. This way, the subscript fe, for instance, means the conversion factor for fuel (natural gas) to electricity.

In the present case, the coefficients C_{fe} and C_{fc} are equal to zero, since the fuel is not used to satisfy the electric load, nor the cooling load. The C-coefficients involve the share of the energy resources that are used by the different end-uses, and the efficiency of the different technologies. Again, it should be reminded that Eq. (1.1) must hold true at each time step.

In the present model, it was decided to rewrite the hub model by splitting the total electricity consumed from the grid, P_e, as the summation of the different contributions mentioned above, i.e. electric heaters ($P_{e,EH}$), heat pumps ($P_{e,HP}$), chillers ($P_{e,CH}$), and other end-uses (L_e):

$$P_e = P_{e,EH} + P_{e,HP} + P_{e,CH} + L_e \tag{1.2}$$

Note that the share of the electricity used for the other end-uses was written as L_e since this correspond to the electric load in the present problem (see Fig. 1.1). An equivalent form to Eq. (1.1) is obtained by expressing the heating and cooling loads as a function of these different electricity consumptions and of the fuel consumption:

$$L_h = \eta_{fh}^{FB} P_f + \eta_{eh}^{EH} P_{e,EH} + \eta_{eh}^{HP} P_{e,HP} \tag{1.3}$$

$$L_c = \eta_{ec}^{CH} P_{e,CH} + \left(\eta_{eh}^{HP} - 1\right) P_{e,HP} \tag{1.4}$$

Note that *HP*, *B*, *CH*, *EH*, *h*, *c*, *ec*, and *eh* denote heat pump, natural gas boiler, chiller, electric heater, heat, cold, electricity to cold and electricity to heat, respectively. The η-values are the efficiency of each energy convertor. In the present study, these efficiency values are kept constant (η_{fh}^{FB} = 0.85, $\eta_{eh}^{HP} = 6$, $\eta_{ec}^{CH} = 4$, $\eta_{eh}^{EH} = 0.95$), but future work could include a dependency on time, part-load ratios, temperature, etc. Note that η_{eh}^{HP} can be seen as the coefficient of performance of the heat pump based on heating mode, whereas ($\eta_{eh}^{HP} - 1$) is the coefficient of performance of the heat pump based on cooling mode (COP_c). Typical values of COP_c vary between 3 to 5 for water-to-water heat pumps [33]. It should be noted that advanced heat pumps are considered in the present study, with large *COP* values and with variable speed drive. This feature allows to modulate the load that is "taken in charge" by the heat pump as seen in Eqs. (1.3), (1.4). Having several different heat pumps would also be a way to help modulating their load. If one single speed heat pump would have been used (e.g., see Setlhaolo, Sichilalu and Zhang [34]), on/off decision variables for the heat pump could be introduced in the problem instead of optimizing the load to the heat pump system.

In a matrix form, the energy balance of Eqs. (1.3), (1.4) becomes:

$$\begin{pmatrix} L_c \\ L_h \end{pmatrix} = \begin{pmatrix} \eta_{ec}^{CH} & \left(\eta_{eh}^{HP} - 1\right) & 0 & 0 \\ 0 & \eta_{eh}^{HP} & \eta_{eh}^{EH} & \eta_{fh}^{B} \end{pmatrix} \begin{pmatrix} P_{e,CH} \\ P_{e,HP} \\ P_{e,EH} \\ P_f \end{pmatrix} \tag{1.5}$$

This model will be used to represent the behavior of the hub. The loads L_e, L_h and L_c are assumed to be known at all time steps, as well as the different efficiencies of the convertors. The problem consists in finding the optimal vector P at all time steps (i.e. to what extent each technology should be used to supply heat and cold). The hub model of Eq. (1.5) will serve as an equality constraint in the optimization process that will be described below.

In order for the hub model to be physically sound, it is necessary to invoke other constraints. First, all P-values must always be larger or equal to zero at each time step, i.e.:

$$\begin{pmatrix} L_c \\ L_h \end{pmatrix} = \begin{pmatrix} \eta_{ec}^{CH} & \left(\eta_{eh}^{HP} - 1\right) & 0 & 0 \\ 0 & \eta_{eh}^{HP} & \eta_{eh}^{EH} & \eta_{fh}^{B} \end{pmatrix} \begin{pmatrix} P_{e,CH} \\ P_{e,HP} \\ P_{e,EH} \\ P_f \end{pmatrix} \tag{1.6}$$

Furthermore, the different convertors have a limited capacity due to the sizing of each piece of equipment, which translates as:

$$\begin{aligned} \eta_{ec}^{CH} P_{e,CH} &\le Q_{CH,\max} \\ \left(\eta_{ec}^{HP} - 1\right) P_{e,HP} &\le Q_{HP,\max} \\ \eta_{eh}^{EH} P_{e,EH} &\le Q_{EH,\max} \\ \eta_{fh}^{B} P_f &\le Q_{B,\max} \end{aligned} \tag{1.7}$$

In this series of inequalities, $Q_{CH,max}$ is the maximal capacity of the chillers, $Q_{HP,max}$, the maximal cooling capacity of the heat pumps, $Q_{EH,max}$, the maximal capacity of the electric heaters, and $Q_{B,max}$, the maximal capacity of the natural gas boilers. In the present problem, we assumed that $Q_{CH,max}$ and $Q_{B,max}$ were known and fixed. They would correspond to the current system (i.e. they are already in place) and their value should be large enough to satisfy the different loads. For the sake of simplicity, it was assumed that $Q_{CH,max} \to \infty$ and $Q_{B,max} \to \infty$. Similarly, the size of the electric heater ($Q_{EH,max}$) was known and fixed, and in this study it assumed a value of 5,133 kW (i.e., 20,000 *lbm/h*).

Finally, the size of the heat pump system, $Q_{HP,max}$, was considered as a decision variable. In other words, one wants to find whether it is profitable to purchase heat pumps and determine what capacity is needed. In order to obtain only non-negative values, the following constraint needs to be invoked:

$$Q_{HP,\max} \ge 0 \tag{1.8}$$

1.4.2 Objective functions and optimization problem

The first objective function is the total cost, including annual operation cost C_{op} and the purchase cost C_{init}^{HP}:

$$C_{tot} = C_{init}^{HP} + \frac{(1+i)^n - 1}{i(1+i)^n} C_{op} \tag{1.9}$$

where i is the interest rate, and n the duration of the project. In the present work, we used i = 5% and n = 10 years. Since the present study is focused on the addition of heat pumps to an existing system, only the purchase cost of the heat pumps is considered in the initial costs. In other words, it is assumed that all other pieces of equipment are already in place and thus, do not need to be purchased. If a new system were to be designed from scratch, the cost of the other pieces of equipment (e.g., boilers, chiller, etc.) would need to be included. The unit price of heat pump is estimated based on the correlation introduced in [33], in such a way that:

$$C_{init}^{HP} = \phi_{HP} Q_{HP,\max} \tag{1.10}$$

with ϕ_{HP} = 230 CAD/kW.

The annual operation cost is related to the energy consumption of fuel and electricity,

$$C_{op} = C_{op,e} + C_{op,f} \tag{1.11}$$

where the cost associated to the fuel consumption is simply the amount of fuel consumed multiplied by the unit cost of fuel:

$$C_{op,f} = \frac{\lambda_f \nu_f}{LHV_f} \sum_{t=1}^{N} P_f(t) \Delta t \tag{1.12}$$

with λ_f as unit fuel cost, v_f as specific volume, and LHV_f as the lower heating value of the fuel. The unit cost of fuel is equal to 0.15 CAD/m^3 (0.016123 CAD/kWh) [35]. The cost of electricity includes two components, i.e. the cost for the amount of energy consumed and the cost for the monthly peak demand:

$$C_{op,e} = \lambda_{e,energy} \sum_{t=1}^{N} P_e(t) \Delta t + \lambda_{e,peak} \sum_{month=1}^{12} \max\left(P_e(t)\right) \tag{1.13}$$

where the unit costs $\lambda_{e,energy}$ and $\lambda_{e,peak}$ are respectively 0.0327 CAD/kWh and 12.87 CAD/kW, based on current price for large consumers in Quebec, Canada [36]. Note that the first summation is over all the time

steps, and the second summation is over the different months since peak demands are charged on a monthly basis.

A second objective function was also studied, namely the greenhouse gases emissions (GHG) in $CO_{2,eq}$ associated with a solution. The total annual energy-related emissions are:

$$CO_{2,tot} = CO_{2,e} + CO_{2,f} \tag{1.14}$$

where:

$$CO_{2,e} = \alpha_e \sum_{t=1}^{N} P_e(t)\Delta t \tag{1.15}$$

$$CO_{2,f} = \alpha_f \sum_{t=1}^{N} P_f(t)\Delta t \tag{1.16}$$

The emission intensities of electricity and fuel were respectively α_e = 0.02072 kg CO2,eq/kWh [37] and α_f = 0.17644 kg CO2,eq/kWh [38] for Quebec, Canada. Note that the GHG emissions related to electricity are very low because electricity in Quebec is almost entirely hydroelectricity.

1.5 Optimization solvers

The optimization problem introduced in Section 1.4 can be formulated as: minimize C_{tot} (Eq. (1.9)) and/or $CO_{2,tot}$ (Eq. (1.14)) with respect to the $4N$+1 decision variables (i.e., $Q_{HP,max}$, $P_{e,EH}$, $P_{e,HP}$, $P_{e,CH}$, P_f), while respecting $2N$ equality (Eq. (1.5)) and $8N$+1 inequality constraints (Eqs. (1.6)-(1.8)), where N is the number of time steps. With a one-hour time step, one has N = 8,760 in order to simulate one year of operation. In that case, the number of decision variables is 35,041 and the number of constraints is 87,601. Furthermore, the optimization problem introduced above is non-linear due to the peak of electricity demand, $max(P_e)$, which appears in the cost evaluation. Different solvers were considered to solve the problem. Although some non-linear solvers provided satisfying optimization results (e.g., SCIP, LINDO), the computational time was important. It was thus decided to linearize the problem.

The maximum function in Eq. (1.13) can be converted into a mixed-integer linear problem using a binary variable K(t) [39]. This variable will be zero in every time slot except that with the maximum electricity demand for which

K = 1. Therefore, max(P_e) in Eq. (1.13) is replaced by $P_{e,peak}$ (which becomes a new decision variables in the linearized problem), given that the following constraints are respected:

$$P_{e,peak} \geq P_e(t) \tag{1.17}$$

$$P_{e,peak} \leq P_e(t) + M\left(1 - K(t)\right) \tag{1.18}$$

$$\sum_t K(t) = 1 \tag{1.19}$$

where M is a large number that must be chosen so that it is larger than the difference between the maximum and minimum values of P_e(t). Eq. (1.17) ensures that $P_{e,peak}$ is large enough to be above or equal to P_e(t). In Eq. (1.18), when K=1 at a given time step (i.e. when the peak occurs at that time step), the inequality forces $P_{e,peak}$ to be limited by the actual value of P_e(t). In our case, since 12 peak months must be taken into account, there are 12 $P_{e,peak}$ variables (one per month), and Eqs. (1.17)-(1.19) are treated on a monthly basis. The linearization introduces N binary variables, 12 continuous variables, and $2N$ inequality constraints. Different MILP solvers were tested. In the end, the CPLEX solver was chosen. The computational time for one optimization run is approximately 40 *s*. It should be noted that this linearization method is only a reformulation of the *Max* function, and no estimation is used within this process. We can eliminate a non-linearization from the program accepting new constraints to be added to the optimization.

The model was carefully tested to ensure that it contained no errors. For example, a scenario with no cooling load was modeled. It was verified that chillers were not used and that heat pumps were not present in the design. Similarly, when no heating is present, it was verified that heat pumps, boilers and electric heater did not contribute in the network. In the limit where the purchase cost of heat pumps tends to infinity, heat pumps are not employed, and thus, chiller is generating the entire needed cold; also, the heating load is totally fed by electric and natural gas boilers. In the limit where the peak cost was increased to large values, the usage of electricity in all devices tend to fall by using as much fuel as possible in boilers, and the cooling load is met solely by the heat pump.

1.6 Analysis of cost-minimal systems under different load scenarios

In the optimization problem introduced above, loads need to be provided. For the sake of simplicity, the following synthetic load functions were used in the present work:

$$L_x = A_{x,a} + A_{x,y} \sin\left(2\pi \frac{t}{\tau_y} + \theta_{y,x} \right) \tag{1.20}$$

where "*x*" can be either "*h*" or "*c*", depending on whether heating or cooling loads is considered. τ_y is the duration of a year. In the end, each load is characterized by 3 parameters (i.e., $A_{x,a}$, $A_{x,y}$, and $\theta_{y,x}$). This synthetic load representation was chosen for its simplicity and its capacity to represent realistic loads.

Although the synthetic load of Eq. (1.20) is only a simulated profile of the heating and cooling demands, it provides the optimization model with a realistic approximation of typically encountered situations (e.g., maximum cooling load during summer and minimum cooling in the winter, and vice versa for the heating load). Even though differences between real-case profiles and the synthetic curves could lead to different optimal design and operational solutions for the system, the methodology proposed here to optimize the system can still be applied.

In the present work, we assumed that the cooling load Lc was zero in the beginning of the year, reaching its maximal value in the middle of the year (i.e. $\theta_{c,y} = -\pi/2$) with an amplitude $A_{c,y}$ varying from 0 to 50 MW. The heating load was defined similarly, except that the maximum occurred in the beginning/end of the year and that a zero load was found in the middle of the year (i.e., $\theta_{c,y} = \pi/2$) with an amplitude $A_{h,y}$ between 0 and 50 MW. An important feature of this problem is that the solution to the cost minimization problem is not influenced by L_e in this case. It should be remembered that the electricity load L_e is the total electricity load minus the electricity used for heating and cooling, and that the electricity share of the pieces of equipment that are used for heating and cooling (i.e., heat pump, chiller and electric heater) is calculated separately, as described above, Eqs. (1.5) and (1.13). Thus, optimal heat pump size and GHG emissions depend only on heating and cooling demands. The electric load Le itself represents a certain cost, calculated within Eq. (1.13). As the optimization takes place, some components consume more or less electricity (electric heater, chiller, heat pumps) which induces an additional cost for electricity. However, this additional cost is independent from the baseline cost for L_e. Therefore, performing the cost minimization for different combinations of heating and cooling loads (i.e., for several sets of $A_{h,y}$ and $A_{c,y}$) is sufficient to fully characterize the optimal system as a function of the load. The load profiles are summarized in Fig. 1.2.

The cooling and heating load amplitudes were varied independently between 0 and 50 MW, by 10 MW increments, and in each case, the system was optimized by the procedure described above. In the present section, only the total cost is considered as the objective function (one objective). It should be noted that cost-

minimal designs are of particular interest in practice. It is traditionally what practice engineers try to achieve. This justifies the relevance of the present section which presents resulting optimal design as a function of load scenarios. Simultaneous minimization of cost and GHG emissions will be treated subsequently. All possible combinations of $A_{h,y}$ and $A_{c,y}$ were simulated, for a total of 36 optimization runs. The resulting optimal systems (i.e., cost minimal system) were then compared to the reference systems, which correspond to the energy hub without heat pumps.

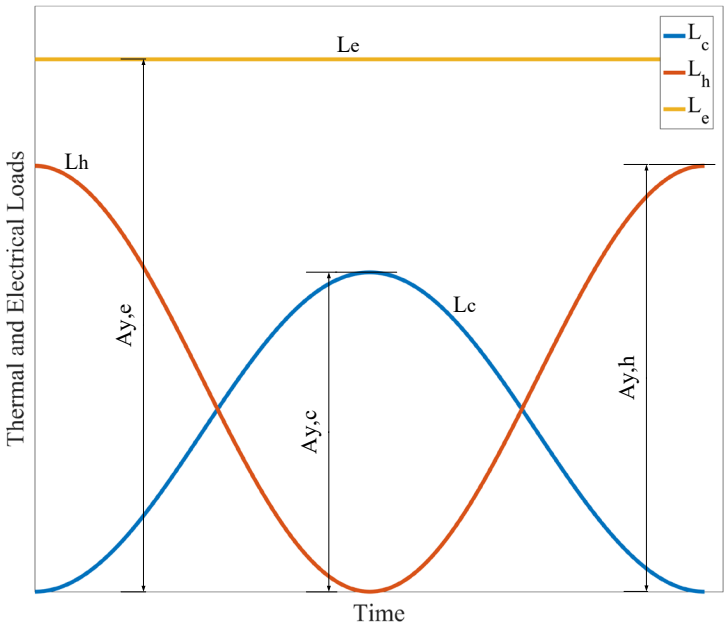

Figure 1.2. Schematic representation of the heating, cooling and electricity loads.

Figure 1.3 reports the energy savings ΔC achieved by introducing heat pumps into the hub compared to the reference case, i.e. the reference cost minus the minimized total cost of the hub with heat pumps. This figure is based on minimizing the total cost of the system. A positive value of ΔC means that savings are achieved with heat pumps, whereas zero or negative ΔC values would imply that the project is not profitable. It is visible in Fig. 1.3 that the integration of heat pumps becomes more and more beneficial as the thermal loads are increased, and in particular when they both increase simultaneously.

Figure 1.4 shows the optimized size of the heat pump as a function of the thermal loads. As expected, the higher the heating and cooling loads, the bigger the optimal capacity (size) of the heat pump. Note that the yellow points in Fig. 1.4 correspond to specific load scenarios that will be analyzed below. It should be remembered that Figs. 1.3, 1.4 were obtained by minimizing the total cost only. As mentioned above, cost is often the driving objective in this type of project. In that case, Figs. 1.3, 1.4 can be seen as practical design charts for sizing heat pumps in synergetic heating and cooling networks, and estimating the potential annual savings.

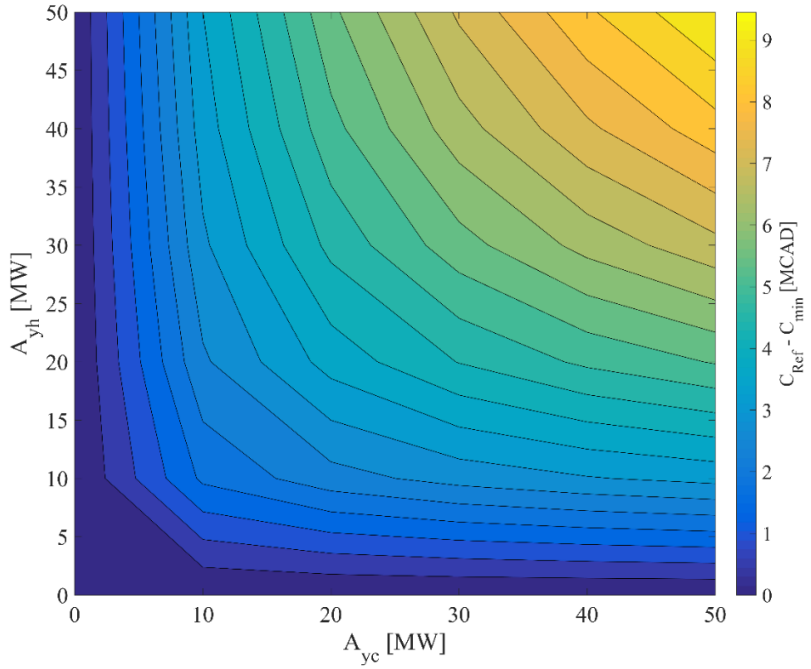

Figure 1.3. Savings caused by heat pumps (cost difference between the reference hub and that cost-minimized hub with the heat pumps) as a function of the heating and cooling.

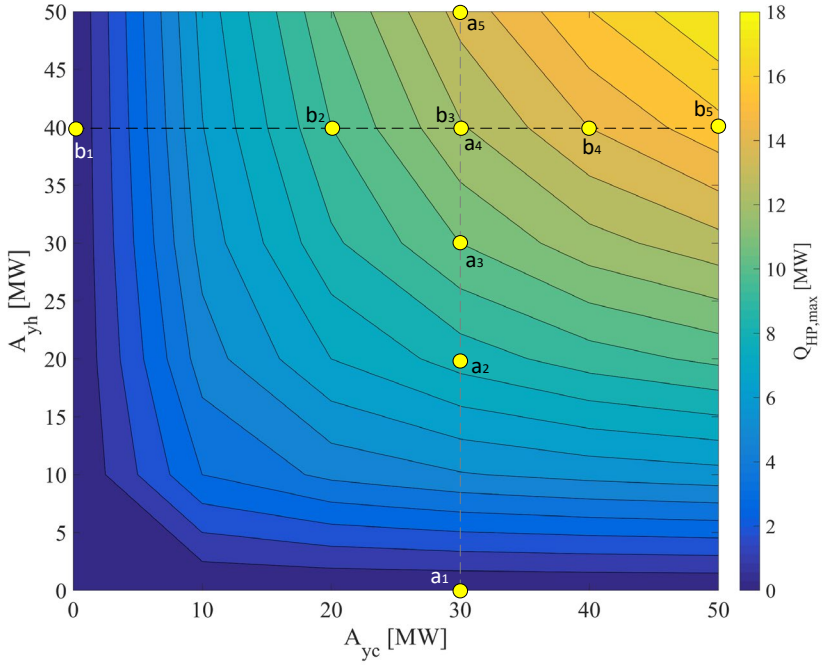

Figure 1.4. Optimal heat pump capacity as a function of the heating and cooling loads with constant electrical load.

1.7 Scale analysis to explain cost-minimal results

A scale analysis is developed in the present section. As will be shown below, this approach helps developing a better understanding of the features of cost-minimal systems both in terms of their design (i.e., size of the heat pump) and operation (i.e., how the heat pump is used). Furthermore, simple expressions will be obtained from this analysis to predict the optimal size of heat pumps integrated in an existing cooling and heating network. These expressions could be used in practice at the pre-design stage of a project.

The analysis starts by realizing that in the optimized hub, the consumption of electricity by the heat pump must always be smaller than the following limit:

$$P_{e,HP}(t) \leq \min\left\{\frac{L_c(t)}{\eta_{eh}^{HP}-1}, \frac{L_h(t)}{\eta_{eh}^{HP}}\right\} \tag{1.21}$$

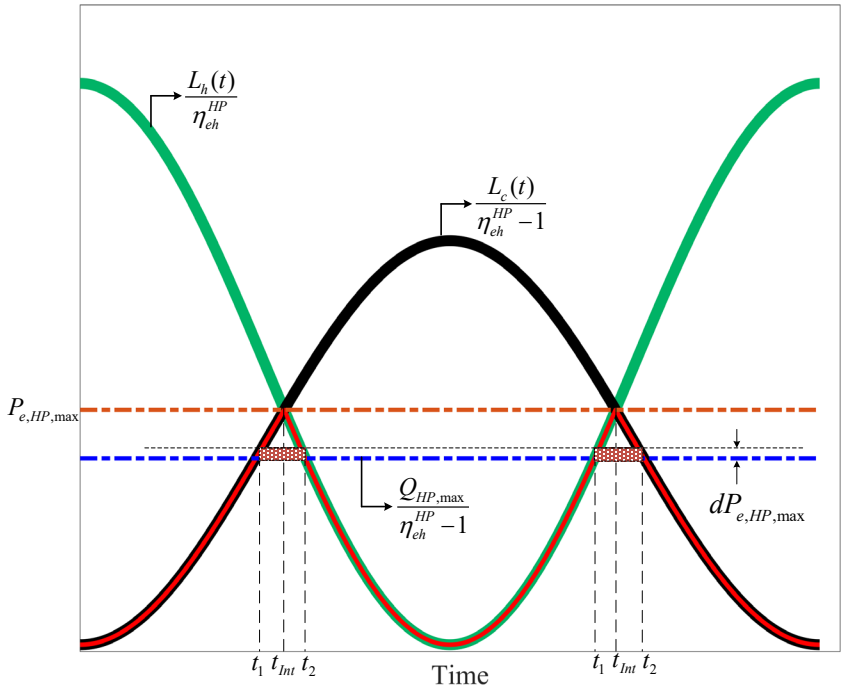

Figure 1.5. Schematic representation of the ceiling value of the heat pump electricity consumption.

The first term in the accolade is the heat pump electricity load that would be obtained if the entire thermal cooling load of the system served by the hub was to be satisfied by the heat pump. Equivalently, the second term is the electricity required at the heat pump in order to satisfy entirely the heating load. In the end, whichever of these two terms is smaller provides a maximal ceiling value of what the heat pump could provide at a given time step. In other words, during the optimization, it is not useful for the heat pump to provide more heating or cooling than that dictated by the smallest loads. For the sake of illustration, $L_c(t)/(\eta_{eh}^{HP}-1)$ and $L_h(t)/\eta_{eh}^{HP}$ are plotted in Fig.

1.5. The right-hand side of Eq. (1.21) is also shown by the red envelope in Fig. 1.5 and defines the maximal possible value of $P_{e,HP}(t)$ at each time.

Moreover, the peak of the red envelope in Fig. 1.5 provides a ceiling value for the heat pump sizing. In other words, it would make no sense for the optimized heat pump capacity to be such that it would require more electricity than that peak. It is possible to obtain an analytical expression for this peak, first by intersecting the "reduced" loads, i.e. by setting the expression $L_c(t)/(\eta_{eh}^{HP} - 1) = L_h(t)/\eta_{eh}^{HP}$, which yields the time at which the intersect occurs (see Fig. 1.5):

$$t_{Int} = \frac{\tau_y}{2\pi} \operatorname{Arc}\cos\left(\frac{A_c\,\eta_{eh}^{HP} - A_h(\eta_{eh}^{HP} - 1)}{A_c\,\eta_{eh}^{HP} + A_h(\eta_{eh}^{HP} - 1)} \right) \tag{1.22}$$

Then, the reduced load at this time is calculated, and one finds that the peak of the envelope in Fig. 1.5 is:

$$P_{e,HP,\max} = \frac{A_{h,y} A_{c,y}}{A_c\,\eta_{eh}^{HP} + A_h(\eta_{eh}^{HP} - 1)} \tag{1.23}$$

The optimized heat pump electricity consumption over time was then compared and normalized with respect to the envelope curve (in red) of Fig. 1.5 and to the peak of that envelope (Eq. (1.23)):

$$P_{e,HP,Norm}(t) = \frac{P_{e,HP}(t)}{P_{e,HP,\max}} \tag{1.24}$$

To have a better understanding of how heat pump contributes to the generation of heating and cooling in the system, heat pump normalized electricity usage $P_{HP,Norm}$ (see Eq. (1.24)) is shown in Fig. 1.6 as a function of time, as well as cooling and heating load amplitudes. Results from the optimization runs performed in the previous section were used. For the sake of visibility, from the 36 above-mentioned load combinations, only 9 cases with different cooling and heating amplitudes were chosen to illustrate the heat pump electricity consumption over time. On the left hand side of Fig. 1.6, the cooling load amplitude $A_{c,y}$ is 30 MW while the heating load amplitudes vary between 0 and 50 MW. These curves correspond to points a_1-a_5 in Fig. 1.4. Similarly, the right hand side of Fig. 1.6 represents the consumption of the heat pump with $A_{h,y}$ = 40 MW and $A_{c,y}$ between 0 and 50 MW, i.e. for points b1-b5 in Fig. 1.4. In this figure, we took advantage of the symmetry of each profile at mid-year to represent only half of each curve.

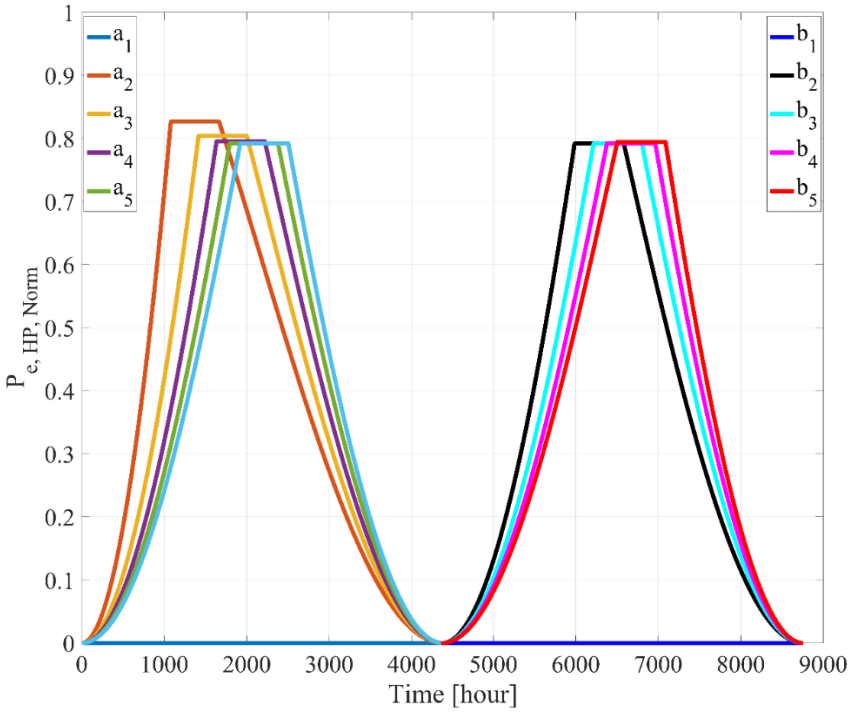

Figure 1.6. Normalized heat pump electricity consumption versus time for 9 load scenarios corresponding to the yellow points in Fig. 1.4.

As apparent in Fig. 1.6, the actual curves tend to follow the conceptual red envelope of Fig. 1.5, but also exhibit a flat portion during which heat pumps generate a constant amount of heat. On this plateau, the heat pump is used at full capacity and the extra heat required is supplied by boilers. The ratio of the maximum optimal heat pump electricity consumption to the maximum theoretical electricity usage of heat pump is defined as:

$$k = \frac{P_{e,HP,\max\,opt}}{P_{e,HP,\max}} = \frac{\left(A_c\,\eta_{eh}^{HP} + A_h(\eta_{eh}^{HP} - 1)\right)P_{e,HP,\max\,opt}}{A_{h,y}A_{c,y}} \tag{1.25}$$

In other words, the value of *k* corresponds to the value at which the plateau occurs in Fig. 1.6, i.e., the percentage of the maximal thermodynamic limit for the heat pump capacity based on the heating and cooling loads that should be installed. In Eq. (1.25), $P_{e,HP,max,opt}$ denotes the maximum electricity usage of the heat pump as a consequence of the optimization process. The value of *k* was found to be almost insensitive to the load scenario and varies only between 0.79 to 0.83 (see the plateaus in Fig. 1.6).

Based on the observation that there is an optimal value of *k* which is almost the same for all load cases, there is thus an opportunity to try predicting the heat pump optimal capacity (by multiplying $P_{e,HP,max,opt}\,(\eta_{eh}^{HP} - 1)$, even prior to optimization. In Fig. 1.7, the optimized heat pump capacity was plotted against the thermodynamic

ceiling value, Eq. (1.23), for all the load scenarios. Each point is the result of a full optimization as explained in the previous sections. A linear fitting was then applied and is also shown in Fig. 1.7. The slope of the linear fitting actually corresponds to the value of *k* that best-fits all the results (k = 0.7961). In other words, it is possible to predict the optimal capacity of the heat pump to be purchased with the following correlation:

$$Q_{HP,\max,\mathrm{Est}} \approx 0.7961 \underbrace{P_{e,HP,\max}}_{Eq.(23)} \left(\eta_{eh}^{HP} - 1\right) \tag{1.26}$$

where $Q_{HP,max,Est}$ represents the estimated optimal size of the heat pumps to be provided in the system.

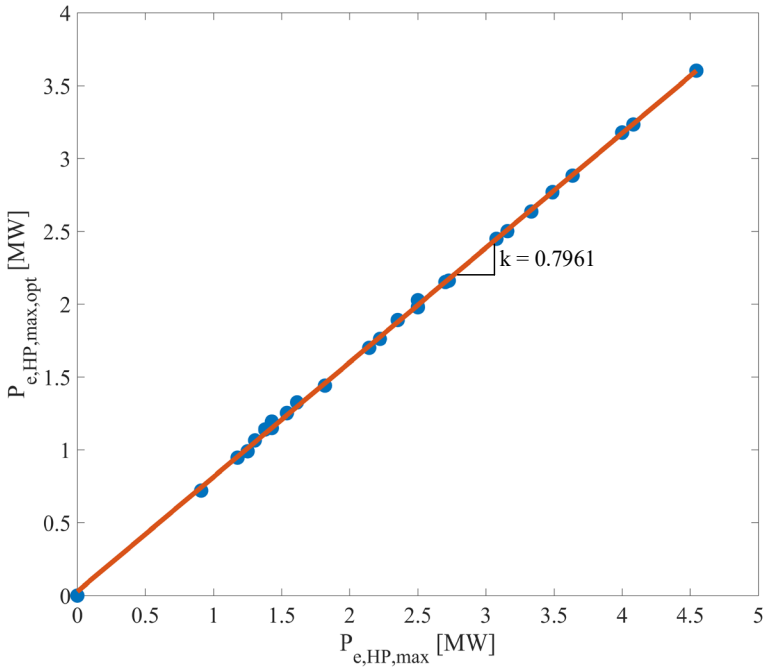

Figure 1.7. Optimized peak heat pump electricity consumption versus thermodynamic limit based on loads.

The value of *k* = 0.7961 means that the optimal heat pump capacity is about 80% of the theoretical maximum heat pump size based on the load analysis (i.e., when all possible portion of the heat and cold loads would be provided by the heat pumps). The fact that this *k* value is not 100% follows directly from cost minimization considerations. Sizing the heat pumps in such a way that it would be used at full capacity only one hour per year is not cost-effective and therefore, the optimal capacity is found to be smaller than the theoretical limit, resulting in heat pump electricity consumption profiles with a plateau as in Fig. 1.6.

Considering Fig. 1.5, it is possible to derive a direct mathematical relation for the optimal heat pump capacity, i.e. for the optimal *k* value. If the size of the heat pump is increased by a small increment *dQ*, the total cost will be changed by *dC* as

$$dC \approx \phi_{HP}\, dQ + \frac{(1+i)^n - 1}{i(1+i)^n}\begin{pmatrix} \phi_{e,tot}\int dP_{e,HP}dt - \phi_{e,tot}\int dP_{e,\mathrm{CH}}dt - \\ \phi_{e,tot}\int dP_{e,\mathrm{EH}}dt - \phi_f \int dP_{f,\mathrm{B}}dt \end{pmatrix} \tag{1.27}$$

where the right-hand side terms denote respectively cost variations for the heat pump purchase, heat pump consumption, chiller consumption, electric heater consumption cost, and fuel consumption due to the change of the heat pump capacity. As introduced before, the present value of the operation costs is used with the proper interest rate and number of years. The coefficient $\lambda_{e,tot}$ represent the total electricity cost coefficients. The value of these coefficients have been previously given (ϕ_{HP} = 230 CAD/kW, $\lambda_{e,tot}$ = 0.05057 CAD/kWh, and λ_f = 0.15 CAD/m^3). Note that $\lambda_{e,tot}$ is the total electricity cost coefficients resulted by the summation of the rates of electricity consumption (energy) and electricity peak (maximum power). Introducing the efficiencies, it can be shown that Eq. (1.27) can be expressed as:

$$dC \approx \phi_{HP}\, dQ + \left(\int dP_{e,HP}dt\right)\underbrace{\left(\frac{(1+i)^n - 1}{i(1+i)^n}\right)\begin{bmatrix} \phi_{e,tot} - \phi_{e,tot}\dfrac{\eta_{eh}^{HP} - 1}{\eta_{ec}^{CH}} - \\ \phi_{e,tot}\dfrac{\eta_{eh}^{HP}}{\eta_{eh}^{EH}} - \phi_f \dfrac{\eta_{eh}^{HP}}{\eta_{fh}^{B}} \end{bmatrix}}_{c_4} \tag{1.28}$$

and the minimal cost is achieved when dC = 0. The order of magnitude of the term $\left(\int dP_{e,HP}dt\right)$ can be estimated by evaluating the area of the two shaded areas Fig. 1.5, i.e. $2dQ(t_2 - t_1)/\left(\eta_{eh}^{HP} - 1\right)$. The time t_1 is found by intersecting $Q_{HP,max}/\left(\eta_{eh}^{HP} - 1\right)$ and the cooling load curve $L_c(t)/\left(\eta_{eh}^{HP} - 1\right)$. Similarly, the time t_2 is obtained by intersecting $Q_{HP,max}/\left(\eta_{eh}^{HP} - 1\right)$ by $L_h(t)/\eta_{eh}^{HP}$. One obtains:

$$\left(\int P_{e,HP}dt\right) \approx 4\frac{dQ}{(\eta_{eh}^{HP} - 1)}\frac{\tau_y}{2\pi}\begin{Bmatrix} \mathrm{Arc\,cos}\left(\dfrac{2\eta_{eh}^{HP} Q_{HP,\max}}{A_h(\eta_{eh}^{HP} - 1)} - 1\right) - \\ \mathrm{Arc\,cos}\left(1 - \dfrac{2Q_{HP,\max}}{A_c}\right) \end{Bmatrix} \tag{1.29}$$

In order to simplify the expression, the *Arccos* functions can be approximated by

$$Arc\cos(x) \approx -1.178\,x + 157 \tag{1.30}$$

as long as x is between -1 and 1, which is the case here. Introducing Eqs. (1.29) and (1.30) in Eq. (1.28) and isolating $Q_{HP,max}$, one finds

$$Q_{HP,\max,\mathrm{math}} \approx \frac{1+\dfrac{\pi c_1}{4(1.178)\,c_4\,\tau_y}}{\dfrac{\eta_{eh}^{HP}}{A_h(\eta_{eh}^{HP}-1)}+\dfrac{1}{A_c}} = \frac{1+\dfrac{\pi c_1(\eta_{eh}^{HP}-1)}{4(1.178)\,c_4\,\tau_y}}{\dfrac{\eta_{eh}^{HP}}{A_h(\eta_{eh}^{HP}-1)}+\dfrac{1}{A_c}} \tag{1.31}$$

The optimal heat pump capacity that we obtained in the previous section for different load scenarios versus Eq. (1.31) is plotted in Fig. 1.8. It is found that the heat pump capacity predicted by Eq. (1.31) is close to the one obtained from the full optimization. It is evident from Fig. 1.8 that the optimal heat pump sizing is almost 80% of thermodynamics limit, no matter how much the heating and cooling load amplitudes are.

The present scale analysis helps to understand how a cost-minimal heat pump system works in practice in a combined heating and cooling network. Correlations such as Eq. (1.31) can be used conveniently to estimate the cost-minimal sizing of the heat pumps, without having to perform the full optimization. The correlation also reveals explicitly how each parameter of the problem can influence the best solution. As a result, even if a different context was to be considered (e.g., different cost of energy, loads, cost of pump, etc.), the relations of the present section could still be used to estimate the cost minimal sizing of the heat pump without having to perform the full optimization presented before.

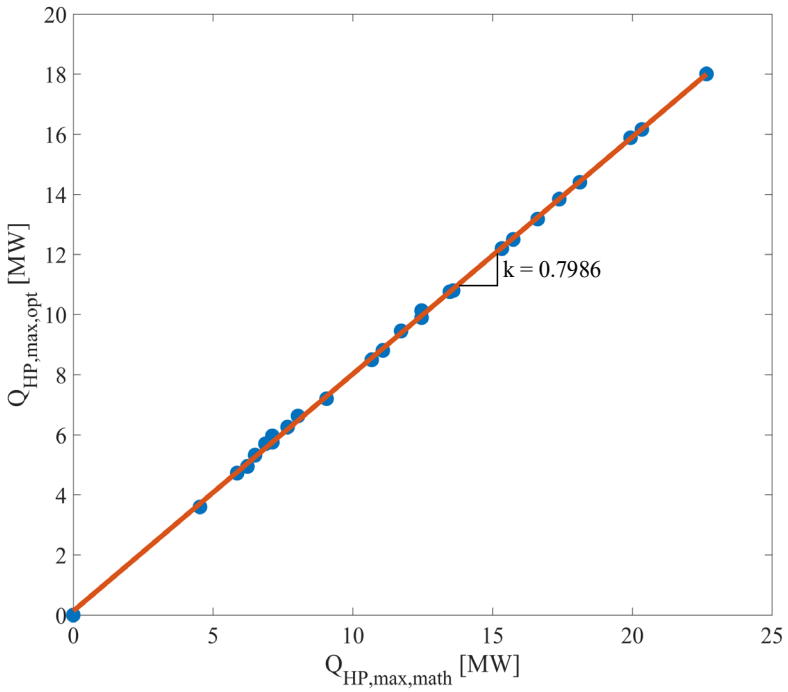

Figure 1.8. Optimized heat pump capacity from optimization versus thermodynamic limit based on loads.

1.8 Dual-objective optimization

As mentioned in Section 1.4, in addition to minimizing the total cost of the waste heat recovery strategy, it is also often desirable to minimize the GHG emissions of the project. So far, the results presented above only considered the minimization of total cost, not CO_2 emissions. A special attention was devoted to cost minimal solutions since this is often the most widely used criterion for sizing and operating heating and cooling systems. However, since more and more emphasis is put on reducing our environmental footprint, it becomes more and more relevant to include a second objective in the problem, namely the reduction of GHG emissions. Therefore, the present section introduces a dual-objective minimization of both cost and GHG emissions, based on the weighted average sum method. Although this method does not necessarily lead exactly to the Pareto front, it is still employed often in literature. In principle, every Pareto optimal solution can be found with this method, if convexity holds [15] (which is the case here since the problem has been linearized).

The weighted average sum method minimizes a combination of the different normalized objective functions. A normalization of the objectives introduced in Section 1.4 is recommended in order to obtain values of the two objectives having the same order of magnitude, as this will facilitate the creation of the Pareto front. In the present case, the dual-objective optimization problem can thus be formulated as:

$$\min\left(w\widetilde{C}_{tot} + (1-w)\widetilde{CO}_{2,tot} \right) \tag{1.32}$$

where w is the weight given to the first objective function and the symbol ~ is to remind us that these functions have been normalized. The same set of constraints as before apply. To normalize the cost and emission functions, so that they can be added together, the following method can be used [15]

$$\widetilde{C}_{tot} = \frac{C_{tot} - C_{\min}}{C_{\max} - C_{\min}} \tag{1.33}$$

$$\widetilde{CO}_{2,tot} = \frac{CO_{2,tot} - CO_{2,\min}}{CO_{2,\max} - CO_{2,\min}} \tag{1.34}$$

The parameters C_{min}, C_{max} represent respectively, the minimum and the maximum costs of the plant when the cost is considered as the only objective function of the optimization, with minimization and maximization objectives. Similarly, $CO_{2,min}$, and $CO_{2,max}$ stand for the minimum and the maximum GHG emission while the optimization takes emission into account as the sole objective function. These values are thus unique for a pair

of load amplitudes. The value of *w* must be between 0 and 1. By performing the optimization for different values of *w*, it is thus possible to build the equivalent of a Pareto front of non-dominated solutions.

The result of the dual-objective optimization is shown in Fig. 1.9. The minimized cost $\tilde{C}_{tot,min}$ and minimized emissions $\widetilde{CO}_{2,tot,min}$ are shown for 9 different combinations of the heating and cooling loads. Each point is the result of optimization for a given value of *w*. For each load combination, 50 values of *w* were considered in order to plot Fig. 1.9. As could be expected, in order to reduce GHG emissions, it is required to increase the total cost and vice versa, to reduce the cost involves increasing GHG emissions. In the context that is simulated, natural gas is cheaper than electricity, but its usage generates more GHG emissions. Therefore, when the emphasis is put on cost, gas is preferred over electricity to satisfy the heating load. On the other hand, when the focus is on emissions, electricity emerges as the best heating source. It should also be noted that in all load scenarios and for all values of *w*, the heat pumps are beneficial which will be demonstrated below.

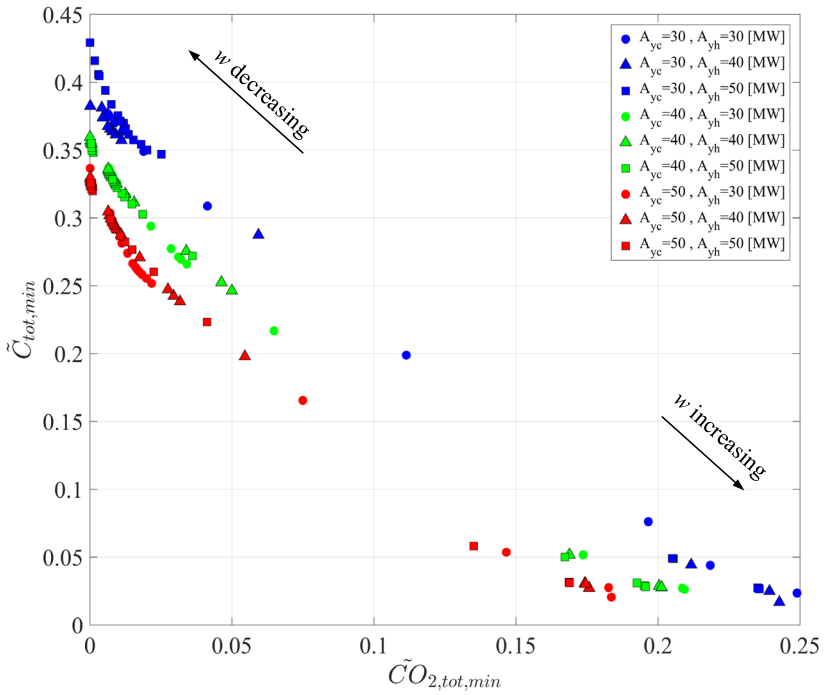

Figure 1.9. Pareto front associated with dual-objective optimization of cost and emission for 9 different sets of heating and cooling loads.

In order to better understand how the weight given to cost versus emissions affects the optimal solution, the features of the optimal solutions reported on the Pareto front of Fig. 1.9 have been analyzed. In Fig. 1.10, the optimized heat pump capacity is plotted for the nine load scenarios as a function of the weight value *w*. The case with *w* = 1 corresponds to the minimization of cost only, and the case with *w* = 0, the minimization of CO_2 emissions only. As explained in the previous sections, the heat pump optimal sizing involves a heavy utilization

of the heat pumps and is strongly affected by the load values. However, the heat pump sizing is essentially unaffected by *w*, as observable in Fig. 1.10.

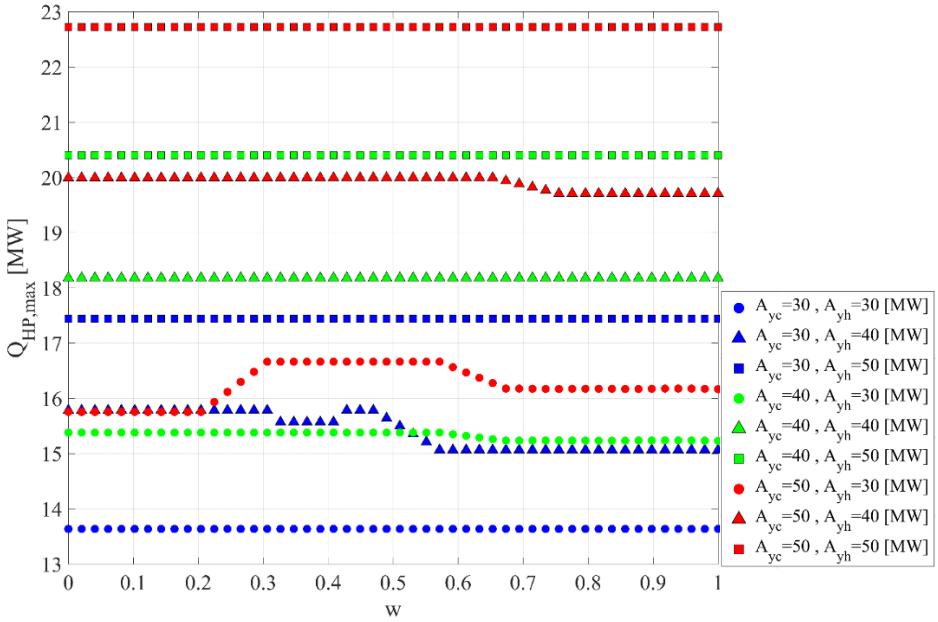

Figure 1.10. Optimized heat pump capacity as a function of the weight value w for nine load scenarios.

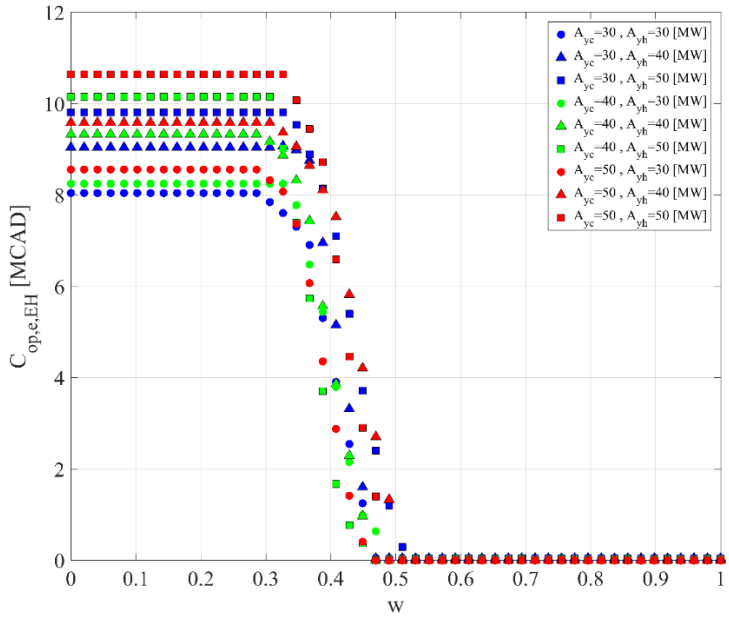

Figure 1.11. Electricity cost for electric heating as a function of the weight value w for nine load scenarios.

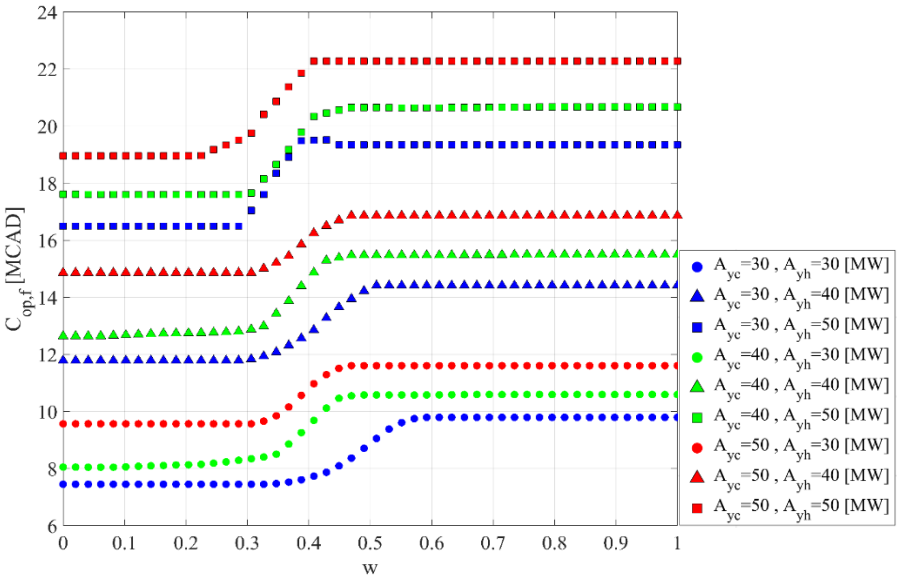

Figure 1.12. Cost for natural gas consumption as a function of the weight w for nine load scenarios.

Figure 1.11 presents the consumption of electricity of the electric heating system as a function of *w* and of the load scenario. It can be observed that for large *w*-values (i.e., more importance given to the cost), the electric heater is not used. This results from the fact that natural gas is cheaper, and would be preferred in that case. In Fig. 1.12, the consumption of natural gas is plotted and demonstrates that statement. The sharp transition around $w \sim 0.4$ corresponds to the point when electricity becomes a bon compared to gas in the overall objective function. The optimal operation strategy completely changes around that w-value, which explains why there is an empty space in the middle of the Pareto fronts of Fig. 1.9. For large *w*-values (i.e. $w > 0.4$), natural gas is used for heating providing a low cost with large emissions, whereas for small *w*-values (i.e. $w < 0.4$), electricity is preferred for heating to reduce the emissions, but at a higher cost. In other words, as *w* increases, there is at a specific *w* value a change in the optimal heating system which results in a "quantum" leap in terms of the objective function values (i.e. although the sum in Eq. (1.32) might not change at that *w* value, the repartition between cost and emissions does) and thus, creates a zone that is "unachievable" on the Pareto front. Note that due to the limited capacity of the electrical boiler, natural gas is still needed even when the emphasis is put on reducing GHG emissions (i.e. at low *w*-values).

The optimal use of equipment is illustrated via the Sankey diagrams of Fig. 1.13 for the case with $A_{h,y} = A_{c,y} = 50$ MW. In this figure, the yearly energy consumption (in MWh) of each hub technology is shown for three different values of *w* (i.e., $w = 0$, 0.37, and 1). As apparent, the yearly energy consumption of chiller and heat pump does not change significantly with *w*, and it is in accordance with what is expected according to Fig. 1.10. The main changes is how the electric heater and the natural gas boiler are used. The conclusion was found to be similar for the other load scenarios.

It is worth to mention that the benefits of heat pumps and their sizing for simultaneous heating and cooling described above is coherent with previous studies [40]. For example, based on simulations and interviews, Kontu, Rinne and Junnila [41] showed recently that the share of heat pumps in heating networks could be increased to reduce fossil fuel consumption. The viable amount of heat pump based on heat production was estimated between 10 and 25% in the Finland context. Simultaneous cooling and heating was not considered, but they mention that heat pumps would be even more beneficial in this case. Byrne, Miriel and Lénat [42] sized a heat pump system for simultaneous heating and cooling of a large building to 80% of the heating load, but this number was not optimized. Based on Fig. 1.9, the optimal ratio between the heat pump capacity and the maximal heating load ranges between 35 and 50% in the present case. Averfalk, Ingvarsson, Persson, Gong and Werner [43] indicated that recently "the installations of large heat pumps [in Sweden] created an important synergy for the introduction of district cooling" but these cases were not reviewed in their study. Four district heating systems relying 100% on the district cooling network as a source of heat were reported [44]. In a case study in Sweden, Brange, Euglund and Lauenburg [45] found that exploiting the excess heat with heat pumps could cover between 50 and 120% of the annual heat demand. As can be seen, the results depicted in Figs. 1.9-1.12 and in previous sections are thus consistent with test cases from literature and help to develop a better understanding of the potential synergy between heating and cooling networks. The approach proposed in this work is capable of estimating the benefits of a waste heat recovery strategy, size its components and operate it optimally.

1.9 Conclusions

Cooling and heating networks are among the most widely used energy systems. Thermally integrating them with heat pump is a practical way to improve their energy efficiency. The challenge to properly design such a system for it to be economically viable and yield as much GHG emission reduction as possible is quite complex and there is a lack of tools to do so in practice. In this work, we introduced an energy hub model to optimize the design and operation of a synergetic cooling and heating network. The system includes a chiller, an electric heater, a natural gas boiler and heat pumps. Specifically, we focused on the waste heat recovery provided by the heat pumps. Every hour of the year is considered in order to optimize how much each piece of equipment is used and to size the heat pumps for different load scenarios. The objective functions that are considered are the total cost and the CO_2 emissions.

The contributions of this investigation can be briefly summarized as follows:

- The energy hub concept was successfully adapted for the optimization of waste heat recovery in cooling and heating networks with heat pumps. We were able to achieve a linear model that solved relatively fast and that could provide a significant insight on the optimal features of the system;

- In the different scenarios investigated, the use of heat pumps to recover heat from the cooling loop always proved to be beneficial in terms of both cost and emissions. The heat pump optimal capacity is around 80% of the thermodynamic maximal value based on the load analysis.

- A theoretical analysis of the system was performed and was able to provide the correct order of magnitude for the optimal sizing of the heat pump. By comparing the analysis to the formal optimization results, we obtained correlations that can be used to easily size the heat pump system.

- The weighted sum average method allowed generating a Pareto front when minimizing simultaneously cost and GHG emissions. A relatively sharp transition between two families of solutions was noted at the point when electricity becomes more viable an option than gas for heating in the combined objective function as more emphasis is put on CO_2 than on cost.

The results were shown to be in line with current literature and help to fill the lack of knowledge on optimized synergetic heating and cooling networks. The figures and correlations that have been developed in this work can serve as straightforward design tools for practice engineers to properly size and operate such systems.

Future work could include a better representation of system. For example, the efficiencies could vary with part-load factors and outside temperature. The integration of other potential technologies such as energy storage and renewables (PV, geothermal, etc.) could be optimized. Finally, it would be interesting to perform a sensitivity analysis of uncertain parameters or parameters that could change over time (e.g., costs, loads, etc.).

Acknowledgments

This work was supported by the Natural Sciences and Engineering Research Council of Canada (NSERC).

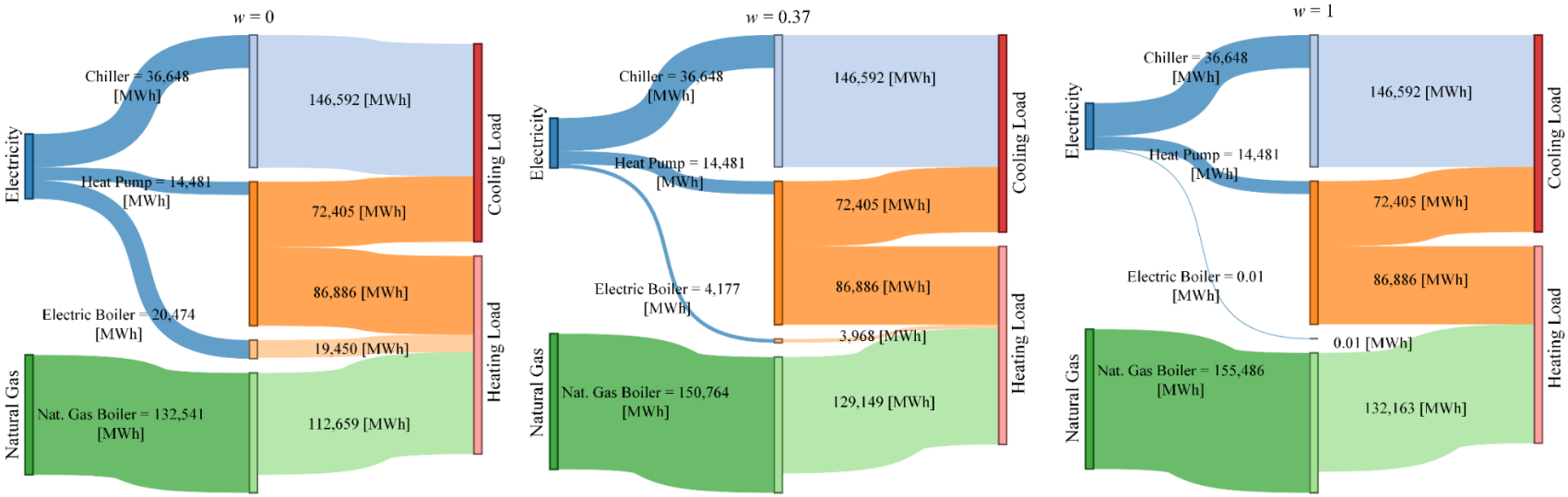

Figure 1.13. Sankey diagram of energy use for $A_{h,y} = A_{c,y} = 50$ MW and for three weights ($w = 0$, 0.37 and 1).

Chapitre 2 HOW CAN COMBINED HEATING AND COOLING NETWORKS BENEFIT FROM THERMAL ENERGY STORAGE? MINIMIZING LIFETIME COST FOR DIFFERENT SCENARIOS

2.1 Résumé

Les réseaux de chauffage et de refroidissement font partie intégrante de divers bâtiments, campus ou villes. Le concept de réseau thermique intelligent plaide en faveur de l'intégration thermique pour bénéficier des synergies potentielles et faciliter l'utilisation des sources d'énergie renouvelables. Ici, nous développons une méthode montrant comment des unités de stockage d'énergie thermique (SET), couplées à des pompes à chaleur, peuvent contribuer à réduire le coût total d'un réseau thermique. Un modèle d'optimisation est introduit, basé sur un modèle de hub énergétique comprenant des chaudières au gaz naturel, des radiateurs électriques et des refroidisseurs. Pour différents profils de charge, les réseaux thermiques intégrant des pompes à chaleur seules, SET seules ou une combinaison des deux sont comparés à un hub de référence sans intégration thermique. Il a été constaté que l'inclusion à la fois du SET et des pompes à chaleur génère plus de bénéfices que lorsqu'elles sont utilisées séparément, étendant l'utilisation synergique des pompes à chaleur pour satisfaire à la fois les charges de chauffage et de refroidissement. Avec la demande de charge maximale, le coût total a été réduit respectivement de 0,48 %, 6,37 % et 7,25 % avec l'ajout de SET uniquement, de pompes à chaleur uniquement et des deux à la fois. De plus, l'intérêt du SET lorsque les composants du système (refroidisseur ou chaudière) sont sous-dimensionnés est évalué. Il a été observé que dans ces cas, le SET contribue à satisfaire les demandes thermiques. Cependant, en raison de la configuration du système, il existe une limite de sous-dimensionnement du refroidisseur que les unités SET peuvent compenser.

2.2 Abstract

Heating and cooling networks are integral components of various buildings, campuses or cities. The concept of smart thermal grid argues in favor of thermal integration to benefit from potential synergies and facilitate the use of renewable energy sources. Here, we develop a method showing how thermal energy storage (TES) units, coupled with heat pumps, can contribute to reduce the total cost of a thermal grid. An optimization model is

introduced, based on an energy hub model including natural gas boilers, electric heaters and chillers. For different load profiles, thermal grids integrating heat pumps alone, TES alone or a combination of both are compared to a reference hub with no thermal integration. It was found that the inclusion of both TES and heat pumps at the same time results in more profits than when they are used separately, extending the synergic use of the heat pumps to satisfy both heating and cooling loads. With the maximal load demand, the total cost was reduced respectively by 0.48%, 6.37%, and 7.25% with addition of only TES, only heat pumps, and both. Furthermore, the benefit of TES when components of the system (chiller or boiler) are under-sized is assessed. It was observed that in these cases, TES contributes to satisfy the thermal demands. However, due to the configuration of the system, there is a limit of chiller under-sizing that TES units can compensate.

2.3 Introduction

The “energy hub” concept has been used more and more for the modeling of energy systems over the last decade. Using this approach, a complex energy system can be treated as a set of equipment coupling the available energy sources to the demand of end-users. The main components of the energy hub thus include: (i) available sources of energy (e.g., fossil fuels, renewable energy, electricity from the grid or generated on-site, waste heat sources available nearby, etc.), (ii) technology for energy conversion, transfer, or storage, and (iii) loads (energy required by end-users for heating, cooling, etc.).

The possible combinations of the available technologies and energy sources should not only meet the imposed heating, cooling and electricity demands on the end-user side of the energy hub, but also satisfy other considerations that might apply. In particular, cost is an important aspect to account for in the design and operation of energy systems. One of the strategies to minimize the cost of an energy hub is the recourse to energy storage. In synergetic systems, energy storage can help to handle the temporal mismatch between the different types of loads and energy sources. According to literature, energy storage can have several benefits, such as: (a) increase the energy efficiency of the system [46], [47], (b) improve the operation of cogeneration plants [48]–[51], (c) shift energy consumption to low-cost periods [52]–[55], (d) enhance system reliability [56], [57], (e) improve the HVAC system’s operation, and (f) facilitate renewable energy integration [58]. Thermal energy storage (TES) can decrease the overall cost of energy systems by accumulating the excess thermal energy produced at a certain moment when the heat-generation equipment works at its optimal operation point, and releasing it at another moment when the demand exceeds the capacity of heaters. According to [59], the main purpose of TES optimization in literature is to minimize the operational cost of the system in which they are integrated.

Several studies devoted to energy hub optimization have considered the inclusion of TES. Maroufmashat et al. [14] developed a general method for the optimization of networks, in which energy storage units are also considered in order to minimize simultaneously operational cost and GHG emissions, using the weighted-average sum method. Brahman et al. [26] assessed the savings provided by the use of TES and electric vehicles. Electric vehicles were used as a form of electrical energy storage. The 24-hour based analysis revealed that the cost could be decreased by 28 to 40% when both electrical and thermal storages are considered, compared to the cases in which they were both unavailable. Coupling electric vehicles and TES has also been found to be financially efficient in [60]. Through a cost minimization in which CO2 emissions were also taken into account as a cost, three scenarios were studied, and their optimal costs were compared. The uncertainty on future electricity price has also been included in that research. The step-by-step addition of multiple modules of electric energy storage and TES, as well as CHP and heat pump units into an energy hub was investigated by Chen et al. [61]. They depicted the differences in the configuration of the energy hub would be under different combinations of heating and electrical loads, while minimizing the total cost of the system as the objective function. The effect of ice storage on the operational cost of energy hubs is investigated in [62], where the hub includes TES, CCHP and renewable energy sources (wind and photovoltaic). The authors illustrated that ice storage within the energy hub can reduce the operational cost of the energy system by 0.37 to 1.29%, based on 4 case studies in which different energy conversion and storage technology were utilized. An operational cost reduction of up to 29.5% was obtained in [63] through the use of compressed-air energy storage in an energy hub comprising CHP unit, natural gas boiler, compressed-air energy storage system, TES and an heat pump. Note that the capacity of the facilities were constant in [62], [63]. The analysis in [64] revealed that TES can reduce operational cost by 0.8%, based on 24-hour load data for an energy hub consisting of natural gas boiler, wind turbine, CHP units, electrical and thermal energy storage systems

Although the inclusion of TES in energy hub models has been considered in several studies, there is still a number of challenges and open questions to be addressed. Literature has revealed the optimal size and operation of energy hubs with TES under different heating and electricity loads. However, the optimal configuration of such system for a combined heating and cooling network has not been covered so far. Furthermore, the optimal capacity of the TES in energy hubs is strongly dependent on its unit purchase cost, and this effect is not precisely addressed in the literature. Finally, from the practice engineers' point of view, there is a need for design charts for many loads from which one could obtain information on the potential financial benefits resulting from the installation of TES within a given energy hub, in particular in the predesign stage. The main objective of this work is to determine the benefits and optimal design and operation of thermal storage within a combined heating and cooling network for a wide range of scenarios. Section 2.4 presents the modeling approach for the implementation of TES within the energy hub model of such systems. Then, in Section 2.5, different scenarios will be generated to investigate the sensitivity of the minimized cost to some key parameters.

The scenarios are defined by their load profiles and by a set of parameters characterizing the hub (e.g., cost of energy, efficiency, etc.). Section 2.6 compares the optimization results with the integration into a combined heating and cooling hub of heat pumps alone, TES units alone and both of them simultaneously. In Section 2.7, TES units are integrated in hubs for which existing components (i.e., chillers or boilers) are too small for satisfying instantly the thermal loads. Finally, the conclusion is presented.

2.4 Implementation of thermal energy storage within energy hub

2.4.1 Modeling of the system

The energy hub that is investigated is shown in Fig. 2.1. It is the schematic view of a thermal grid inspired by that of the campus of Université Laval (Québec City, Canada). Chillers ("CH" in Fig. 2.1) supply the required chilled water to the cooling network. The heat is absorbed by the cooling loop and is ultimately rejected into the environment. A hot water or vapor network, i.e. a second loop, meets the heating demand of the buildings. Two types of boilers (i.e., a natural gas or fuel boiler ("FB" in Fig. 2.1) and an electric heater ("EH" in Fig. 2.1)) are considered.

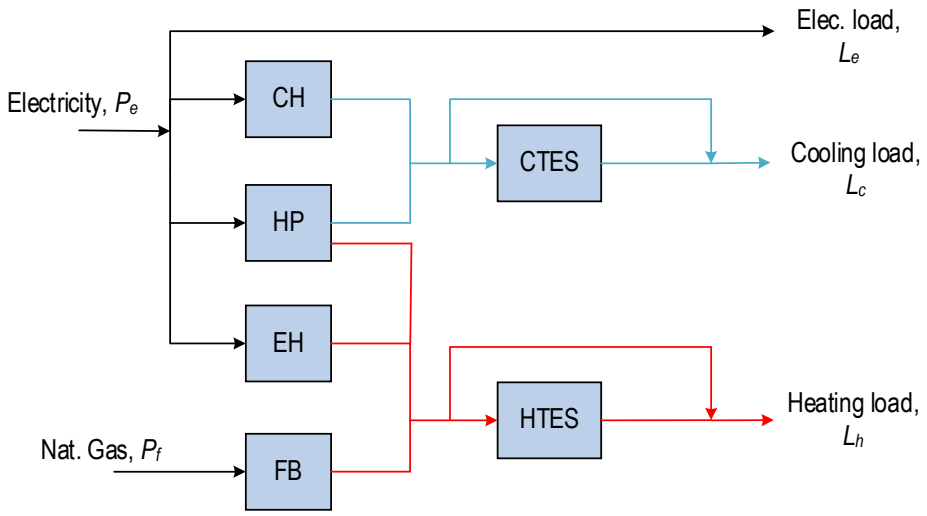

Figure 2.1. Hub representation of the integrated thermal networks including TES [65].

Depending on the design, these two networks (e.g., cold and hot) can be either independent (i.e., no direct interactions) or integrated (i.e., with systems connecting them, for example to recover waste heat from the cold

loop). In an integrated network, heat pump units ("HP" in Fig. 2.1) can be used to provide simultaneous heating and cooling. In this paper, we assume that the energy system with independent heating and cooling loops already exists. Then, the challenge becomes that of identifying the best opportunities for the installation of thermal energy storage units while coupling the thermal networks with heat pumps. CTES and HTES indicate cold and hot thermal energy storages, respectively.

As shown in Fig. 2.1, the cooling load L_c is met by the chillers and heat pumps, and the heating load L_h, by the boilers (EH, FB) and heat pumps. The hot thermal storage allows to store excess heat produced by the heat pump, fuel boiler and electric heater, or to use previously accumulated heat to supply the heating load. The cold thermal storage works in a similar way by storing excess cold produced by the heat pump and the chiller or using the stored cold to satisfy the cooling load. In the end, the various loads indicated in Fig. 2.1 (i.e., L_h , L_e and L_c) pull the energy from the two available resources, i.e. from the electric power grid (i.e., Pe) and from natural gas (i.e., P_f). Note that because L_h , L_e and L_c are time-dependent, so are P_f and P_e.

At a given time, the aggregate load L+P_{ES} (the summation of the loads and the charging power of the TES) is related to the energy resource vector P:

$$\underbrace{\begin{pmatrix} L_e \\ L_c + P_{CTES} \\ L_h + P_{HTES} \end{pmatrix}}_{\mathbf{L}(t)+P_{ES}(t)} = \underbrace{\begin{pmatrix} C_{ee} & C_{fe} \\ C_{ec} & C_{fc} \\ C_{eh} & C_{fh} \end{pmatrix}}_{\mathbf{C}} \underbrace{\begin{pmatrix} P_e \\ P_f \end{pmatrix}}_{\mathbf{P}(t)} \tag{2.1}$$

where P_{CTES} and P_{HTES} indicate the amount of cold and heat supplied to the TES units, respectively. C is the coupling matrix containing the conversion coefficients associated with the technologies of the energy hub.

In this work, since natural gas is not used to satisfy the cooling load, nor the electric demand, the coefficients C_{fc} and C_{fe} are zero. As mentioned above and illustrated in Fig. 2.1, the total electricity consumption, P_e, is the summation of four separate electricity consumptions:

$$P_e = P_{e,EH} + P_{e,HP} + P_{e,CH} + L_e \tag{2.2}$$

i.e. electric heaters ($P_{e,EH}$), heat pumps ($P_{e,HP}$), chillers ($P_{e,CH}$), and other end-uses (L_e). Both thermal loads can be expressed by:

$$\begin{pmatrix} L_c + P_{CTES}^{ch} - P_{CTES}^{dis} \\ L_h + P_{HTES}^{ch} - P_{HTES}^{dis} \end{pmatrix} = \begin{pmatrix} COP_{ec}^{CH} & \left(COP_{eh}^{HP} - 1\right) & 0 & 0 \\ 0 & COP_{eh}^{HP} & \eta_{eh}^{EH} & \eta_{fh}^{FB} \end{pmatrix} \begin{pmatrix} P_{e,CH} \\ P_{e,HP} \\ P_{e,EH} \\ P_f \end{pmatrix} \quad (2.3)$$

where *c*, *h*, *eh*, and *ec* indicate cold, heat, electricity to heat, and electricity to cold, respectively. P_{TES}^{ch} and P_{TES}^{dis} symbolize, respectively, the charging and discharging powers of the TES units. As can be seen, the charging and discharging powers are now expressed by two separate terms, which will facilitate the use of different efficiencies for the charging and discharging processes (as will be shown below). In Eq. (2.3), the loads L_h , L_c , and L_e are assumed to be given at all time steps, as well as the various efficiencies of the equipment, whereas the components of *P* (i.e., the contribution of each equipment in the satisfaction of the heat and cold demands) are to be determined at each time step.

The η-values are the efficiency of each piece of equipment in the energy hub. In this investigation, these efficiency values are held constant. It should be noticed that COP_{eh}^{HP} is defined as the coefficient of performance of the heat pump based on the heating mode, whereas ($COP_{eh}^{HP} - 1$) is the coefficient of performance of the heat pump based on the cooling mode (COP_{ec}^{HP}). Typical magnitudes of COP_{ec}^{HP} are equal to 3-5 for water-to-water heat pumps [33].

For the energy hub model to be physically sound, it is required to invoke additional constraints. First, all power values have to be equal or larger than zero at each time step, i.e.:

$$P_{e,CH}, P_{e,HP}, P_{e,EH}, P_f, P_{CTES}^{ch}, P_{CTES}^{dis}, P_{HTES}^{ch}, P_{HTES}^{dis} \geq 0 \quad (2.4)$$

The amount of energy stored in the thermal storage units at a given time step is equal to:

$$\begin{aligned} M_{HTES}(t) &= \left(1 - \varepsilon_{loss}\right) M_{HTES}(t-1) + P_{HTES}^{ch}(t)\eta_{ch}^{TES}\Delta t - \left(P_{HTES}^{dis}(t)/\eta_{dis}^{TES}\right)\Delta t \\ M_{CTES}(t) &= \left(1 - \varepsilon_{loss}\right) M_{CTES}(t-1) + P_{CTES}^{ch}(t)\eta_{ch}^{TES}\Delta t - \left(P_{CTES}^{dis}(t)/\eta_{dis}^{TES}\right)\Delta t \end{aligned} \quad (2.5)$$

where *M(t)* and ε_{loss} stand for the energy stored in the unit at time *t* and the loss rate coefficient (self-discharge), respectively. The TES units are charged or discharged with the efficiencies of η_{ch}^{TES} and η_{dis}^{TES}, respectively. In order to avoid TES to accumulate heat over the course of each day, we assumed that the initial and final states of the TES units were the same, i.e.

$$M_{HTES}(N_{24}) = M_{HTES}(N_{24} - 23)$$
$$M_{CTES}(N_{24}) = M_{CTES}(N_{24} - 23) \tag{2.6}$$

Furthermore, each energy convertor possesses a limited capacity owing to the sizing of each equipment, which translates as:

$$\begin{aligned} COP_{ec}^{CH} P_{e,CH} &\le Q_{CH,\max} \\ \left(COP_{eh}^{HP} - 1\right) P_{e,HP} &\le Q_{HP,\max} \\ \eta_{eh}^{EH} P_{e,EH} &\le Q_{EH,\max} \\ \eta_{fh}^{FB} P_f &\le Q_{B,\max} \\ M_{HTES} &\le M_{HTES,\max} \\ M_{CTES} &\le M_{CTES,\max} \end{aligned} \tag{2.7}$$

where, $Q_{CH,max}$, $Q_{EH,max}$, $Q_{B,max}$, $M_{HTES,max}$, $M_{CTES,max}$, and $Q_{HP,max}$ symbolize, respectively, the maximum capacities of the chillers, electric heaters, natural gas boilers, hot TES, cold TES, and the maximum cooling capacity of the heat pumps. In this work, the capacity of the TES units ($M_{HTES,max}$ and $M_{CTES,max}$), $Q_{EH,max}$, and $Q_{HP,max}$ are design variables to be optimized. Note that the capacities and the stored energy values have to be positive:

$$Q_{HP,\max}, Q_{EH,\max}, M_{HTES,\max}, M_{CTES,\max}, M_{CTES}(t), M_{HTES}(t) \ge 0 \tag{2.8}$$

Because the charging and discharging power of TES units must be limited, the following constraints are applied:

$$\begin{aligned} 0 \le P_{HTES}^{ch}(t) &\le \alpha_{HTES}^{ch}(t) P_{HTES}^{\max,ch} \\ 0 \le P_{HTES}^{dis}(t) &\le \alpha_{HTES}^{dis}(t) P_{HTES}^{\max,dis} \\ 0 \le P_{CTES}^{ch}(t) &\le \alpha_{CTES}^{ch}(t) P_{CTES}^{\max,ch} \\ 0 \le P_{CTES}^{dis}(t) &\le \alpha_{CTES}^{dis}(t) P_{CTES}^{\max,dis} \end{aligned} \tag{2.9}$$

where $P_{TES}^{max,ch}$ and $P_{TES}^{max,dis}$ indicate the maximum charging and discharging powers of the TES devices. In this study, $P_{HTES}^{max,ch}$ and $P_{HTES}^{max,dis}$ at each moment are fixed to 20% of the heating load magnitude at that moment. The same assumption is applied to $P_{CTES}^{max,ch}$ and $P_{CTES}^{max,dis}$ as they are fixed to 20% of the cooling load. In order to avoid simultaneous charging and discharging TES units, the binary variables α are introduced into the optimization:

$$\begin{aligned}\alpha_{HTES}^{ch}(t)+\alpha_{HTES}^{dis}(t)\le 1\\ \alpha_{CTES}^{ch}(t)+\alpha_{CTES}^{dis}(t)\le 1\end{aligned} \tag{2.10}$$

2.4.2 Objective function and optimization problem

The objective function of the optimization problem is the total cost of the energy hub. It is calculated by summing the levelized annual operational cost, C_{op}, and the purchase cost of the new pieces of equipment (heat pump and/or storage) added to the already existing system:

$$C_{tot}=C_{init}^{TES}+C_{init}^{HP}+C_{init}^{EH}+\frac{(1+i)^n-1}{i(1+i)^n}C_{op} \tag{2.11}$$

where *i* denotes the interest rate and *n*, the lifetime of the project. In line with many studies [30], [66]–[68], the same value for *i* was used to calculate the present value of natural gas and electricity operational costs. As mentioned above, we assumed that the natural gas boilers and chillers are already available and operating at the site. Thus, only the purchase cost of the TES units, heat pump, and electric heaters are considered. The unit purchase cost of the devices can be estimated with:

$$\begin{aligned}C_{init}^{HP}&=\phi_{HP}\,Q_{HP,\max}\\ C_{init}^{EH}&=\phi_{EH}\,Q_{EH,\max}\\ C_{init}^{TES}&=\phi_{TES}\left(M_{HTES,\max}+M_{CTES,\max}\right)\end{aligned} \tag{2.12}$$

where ϕ-symbols stand for the unit purchase cost of each device. As portrayed in Tables 2.1, 2.2, the initial costs are estimated using constant unit purchase cost separately for each facility. In this equation, it is assumed that the unit purchase cost of the cold and hot TES units are the same. Although this might not be a correct assumption for all types of thermal storage technology, we considered here that tanks would serve as both hot and cold TES and therefore, that their unit costs would be similar. For instance, sensible heat TES with water as the storage medium could be good options here, as Ayyappan et al. [69] and Sarbu et al. [70] presented.

Next, the operational cost is related to the consumption of electricity and of natural gas,

$$C_{op}=C_{op,e}+C_{op,f} \tag{2.13}$$

where the fuel consumption cost is the aggregate product of the fuel consumption rate and its unit cost:

$$C_{op,f} = \frac{\lambda_f v_f}{LHV_f} \sum_{t=1}^{N} P_f(t)\Delta t \tag{2.14}$$

with λ_f as unit fuel cost, v_f as specific volume, and LHV_f as the lower heating value of the fuel. The operational cost of electricity is the summation of the cost associated with the electricity consumed and the one related to the peak demand of each month:

$$C_{op,e} = \lambda_{e,energy} \sum_{t=1}^{N} P_e(t)\Delta t + \lambda_{e,peak} \sum_{month=1}^{12} \max\left(P_e(t)\right) \tag{2.15}$$

The optimization problem can be formulated as: Minimize C_{tot} (Eq. (2.11)) with respect to 8N+4 decision variables (i.e., $P_f(t)$, $P_{e,CH}(t)$, $P_{e,EH}(t)$, $P_{e,HP}(t)$, $P_{CTES}(t)$, $P_{HTES}(t)$, $M_{CTES}(t)$, $M_{HTES}(t)$, $M_{CTES,max}$, $M_{HTES,max}$, $Q_{HP,max}$, $Q_{EH,max}$), 2N binary variables, 4N+6 equality constraints (Eqs. (2.3), (2.5), (2.6)), and 20N+4 inequality constraints (Eqs. (2.4), (2.7)-(2.10)). N stands for the number of time steps.

The optimization model in this investigation is non-linear owing to the cost of the electricity monthly peaks appearing in Eq. (2.15). This problem can be transformed into a Mixed-Integer Linear Problem (MILP) by introducing $K(t)$, a binary variable [39] which is always zero, except at the time step in each month at which the peak of the electricity demand occurs (in which case K=1). Consequently, monthly electricity peak, $P_{e,peak}$, becomes a new decision variable to replace $max(P_e)$ in Eq. (2.15). Therefore, the nonlinearity of the model can be eliminated at the cost of adding the following constraints to the optimization problem:

$$P_{e,peak} \geq P_e(t) \tag{2.16}$$

$$P_{e,peak} \leq P_e(t) + G\left(1 - K(t)\right) \tag{2.17}$$

$$\sum_{t}^{month} K(t) = 1 \tag{2.18}$$

G stands for a large number, which is at least greater than the difference between the highest and lowest magnitudes of $P_e(t)$. Eq. (2.16) ensures that $P_e(t)$ is always lower than $P_{e,peak}$. Then, at the time t when the peak demand occurs, K = 1 and Eq. (2.17) forces $P_{e,peak}$ to be precisely equal to $P_e(t)$. In this project, because monthly peak cost is charged once per month, 12 $P_{e,peak}$ variables exist.

The code was tested in several limiting cases to verify that the expected solution was obtained. For instance, the scenario in which the cooling load is zero must result in no operation of the chiller, heat pump, nor CTES.

For the case with no heating load, the heater and HTES should not participate in the energy hub. Cases with extremely high purchase cost of the heat pump and of the TES should lead the solver not to employ them. In the limits where the purchase cost of the TES technology approaches to zero, enormous TES units would be chosen. When the unit cost of the monthly electricity peak is increased to high values, all electricity consumers tend to lower their consumption, thus requiring the natural gas boiler to provide as much heat as possible, the heat pump to supply the highest amount of cold feasible, and the TES units to discharge their maximum possible stored energy.

2.5 Generation of different scenarios

As the optimization problem defined above requires the load to be known, synthetic load functions were adopted in this research:

$$L_x = \beta_{mx} A_{mx} + A_{dx} \sin\left(2\pi \frac{t}{\tau_d} + \theta_{dx}\right) \tag{2.19}$$

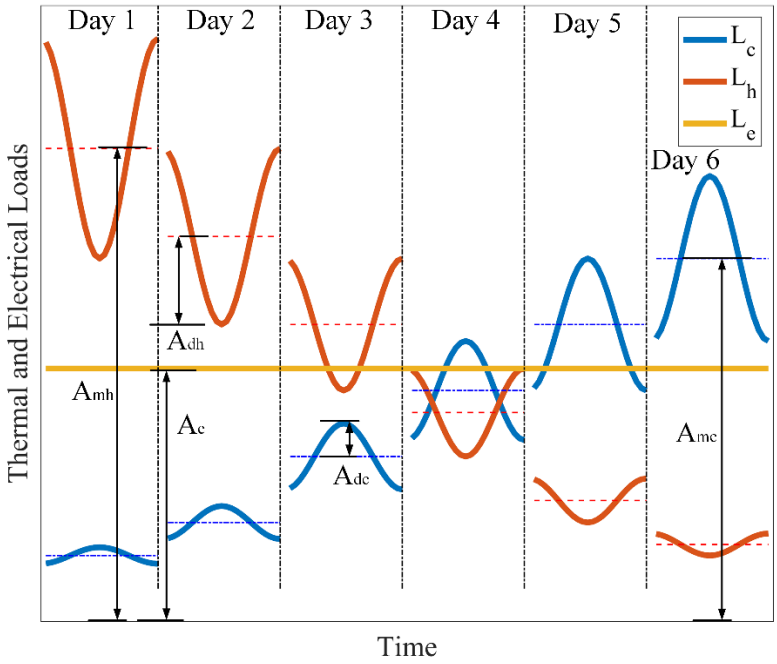

Figure 2.2. Schematic representation of the heating, cooling and electricity loads.

where x is replaced by either c for the cooling load or h for the heating load. τ_d denotes the number of hours in a day, i.e. 24 hours. Each load is characterized by four parameters A_{mx}, A_{dx}, β_{mx}, θ_{dx}. The first two indicate the

maximum amplitude over a year-horizon, and the daily load amplitude, respectively. In this work, we have chosen 6 sample days to estimate the performance of the entire year. It is considered that each day represents a month, and that thermal loads are symmetrical with respect to time, so that the first 6 months are repeated over the subsequent 6 months. The yearly performance is obtained by summing the performance of each characteristic day multiplied by the number of days in that month. In this regard, the amplitude conversion factor, β_{mx}, is introduced in order to adjust the value of the load amplitude each month, as a fraction of its associated maximum yearly amplitude. Also, θ_{dx} denotes the phase shift of the daily load. The synthetic loads of Eq. (2.19) are acceptable approximations of real loads and they comply with the general trends of typical thermal demands. An advantage of synthetic loads is that they facilitate the study of the hub in a wide range of possible load scenarios.

As shown in Fig. 2.2, the cooling load is minimal at the beginning of the year when heating demand is at its peak. As the middle of the year approaches, the cooling load increases while the heating need declines. It should be noted that the electricity cost corresponding to L_e is fully independent of the thermal loads because no power-generating equipment is used in the energy hub (see Fig. 2.1). Consequently, for the sake of simplicity, L_e is assumed to be constant in this study for the whole year, as shown in Fig. 2.2. As mentioned above, L_e is the portion of the electric load dedicated to contributions other than heating and cooling. It thus includes loads such as plug loads, lighting, etc., which do not vary as much as heating and cooling over the year. In that sense, the load L_e uses here can be seen as the non-HVAC electricity baseline load. That way, as the model optimizes the system, the electricity peaks that are generated are caused by the heating and cooling equipment and not by the baseline load L_e. As long as this is the case, the results of the optimization will not be affected by the exact profile of L_e.

Table 2.1 depicts the values of fixed parameters used in this article. Note that the values of the charging/discharging efficiency that we found in literature varied between 0.9 and 0.98. For example, [16], [17], [71] used 0.9, [26], [62] used 0.98 and [63], [64] used 0.95. Based on literature, it was thus decided to use a value of 0.95 in the present study.

Table 2.1. Values of the constant parameters in this work.

Parameter	Description	Constant value	Unit
η_{fh}^{FB}	Nominal efficiency of FB	0.85	
η_{eh}^{EH}	Nominal efficiency of EH	0.95	
cop_{ec}^{HP}	Nominal efficiency of HP in cooling mode	5 [33]	
cop_{ec}^{CH}	Nominal efficiency of CH	5 [72]	

$\eta_{ch}^{HTES}\ \eta_{ch}^{CTES}$ $\eta_{dis}^{HTES}\ \eta_{dis}^{CTES}$	Charging and discharging efficiencies of TES units	0.95	
i	Interest rate	0.05	
n	Life time	10	Years
ϕ_{HP}	Unit purchase cost of HP	230 [33]	CAD/kW
ϕ_{EH}	Unit purchase cost of EH	217.5 [73]	CAD/kW
ε_{loss}	Loss rate of TES per hour	4.38E–3	
$\lambda_{e,energy}$	Unit price of electricity consumption	0.0328 [36]	CAD/kWh
$\lambda_{e,peak}$	Unit price of electricity peak	12.90 [36]	CAD/kW
λ_f	Unit price of natural gas	0.15 [35]	CAD/m^3
$Q_{CH,max}$	Chiller's capacity	Unlimited	MW
β_{mc}	Cooling load amplitude conversion factor	[0.1, 0.2, 0.4, 0.6, 0.8, 1] × A_{mc}	
β_{mh}	Heating load amplitude conversion factor	[1, 0.8, 0.6, 0.4, 0.2, 0.1] × A_{mh}	
A_{dh} , A_{dc}	Daily load amplitude	0.25 × A_{mh} , A_{mc}	MW

Table 2.2. Default values and possible range of parameters investigated in this work.

Parameter	Description	Default value	Range	Unit
A_{mh} , A_{mc}	Maximum yearly amplitude	40	0-40	MW
γ_{FB}	Relative maximum capacity of fuel boiler	100	20-100	%
ϕ_{TES}	Unit purchase cost of TES	4 [74]	0-8	CAD/kWh

Table 2.2 reports the default value and the possible range of different parameters used in the optimization presented later in this study.

To study the effect of TES implementation into this energy hub, a series of examinations was performed. The scenarios that we studied are as follows:

- In Section 2.6, the addition of heat pumps or TES or both (i.e., TES and heat pumps at the same time) into the energy hubs are compared for all possible load profiles defined in Table 1, keeping the other parameters to their default values;

- In Section 2.7, the benefits of introducing TES into undersized hub (e.g., due to an increase of the loads over time which surpass the current equipment capacity or to an equipment being down or to a design choice) is studied. This is accomplished by varying the relative capacity ratios of the natural gas boilers and chillers for different load profiles.

2.6 Comparison between reference system and hubs including heat pumps, TES or both

As presented above, we are interested to include two devices (i.e. TES and heat pump) to an existing energy system. It is thus worth to investigate how each technology affects the profitability of the project. For this purpose, the energy hub was optimized: (i) without any new technology, (ii) with TES units only, (iii) with heat pumps only, and (iv) with heat pumps and TES units at the same time. This was repeated for different yearly load amplitudes. Minimized costs are reported in Fig. 2.3 and the optimal capacity of TES and heat pumps, in Fig.2.4. It should be remembered that each "pixel" in these figures is the result of a full optimization.

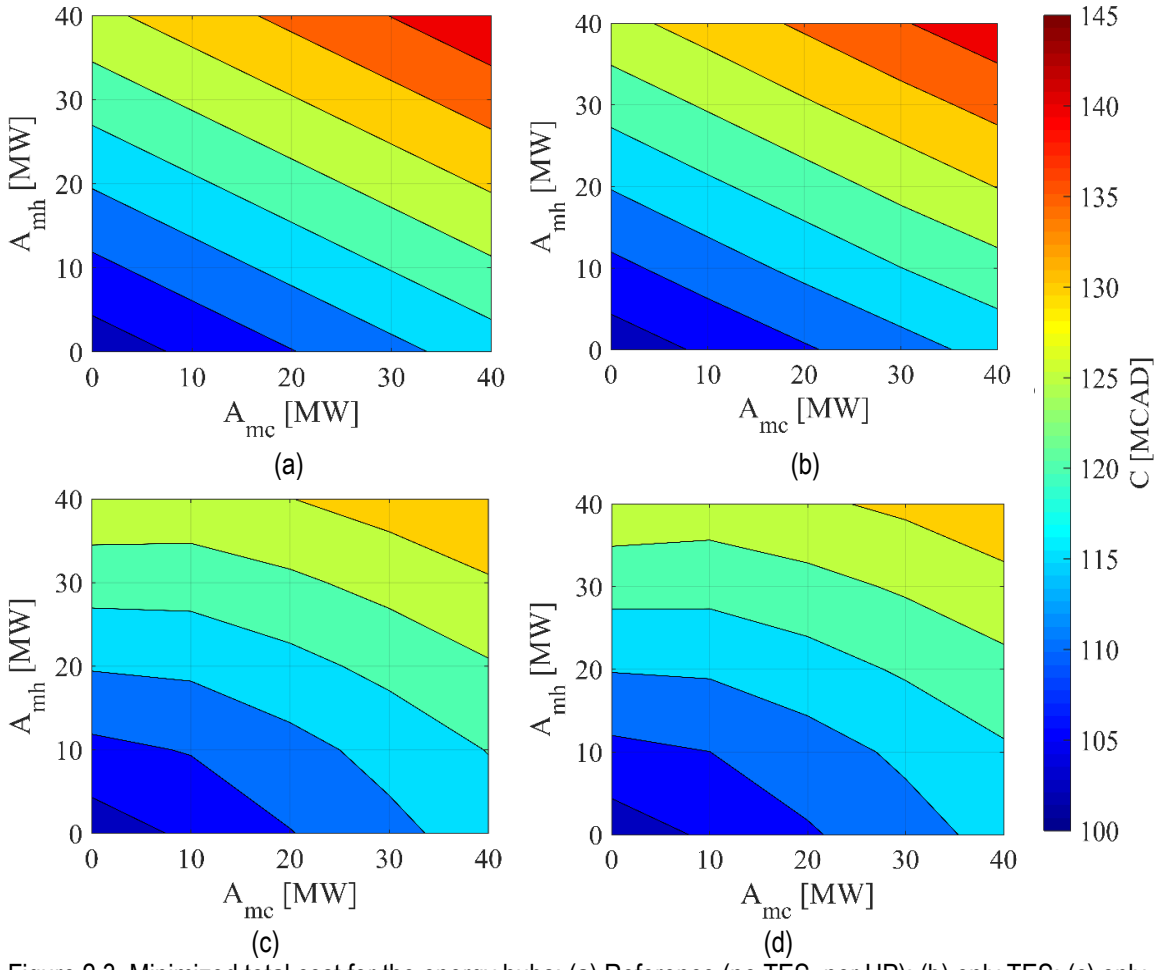

Figure 2.3. Minimized total cost for the energy hubs: (a) Reference (no TES, nor HP); (b) only TES; (c) only HP; (d) both TES and HP.

Figures 2.3a and 2.3b allow a cost comparison between the reference case (i.e., without any new technology) and the case where only TES units would be introduced. It is clear that the benefit of adding TES (i.e., results of

Fig. 2.3b minus those of Fig. 2.3a) is essentially independent of the heating load amplitude A_{mh}. Such behavior originates from the fact that the optimization algorithm did not use any HTES unit. Since natural gas is not charged for peak demand, heat from fuel is available at the same cost in high demand periods. However, this is not the case with electricity. Since it has to be used to produce cold and since its billing depends on peak demands, high cooling load values A_{mc} ask for larger CTES units in order to limit peaks. This can be seen in Fig. 2.4a, which shows the optimized CTES capacity as a function of the loads, when only TES are integrated in the system. The use of CTES units is thus an opportunity to reduce costs by better managing the cooling load.

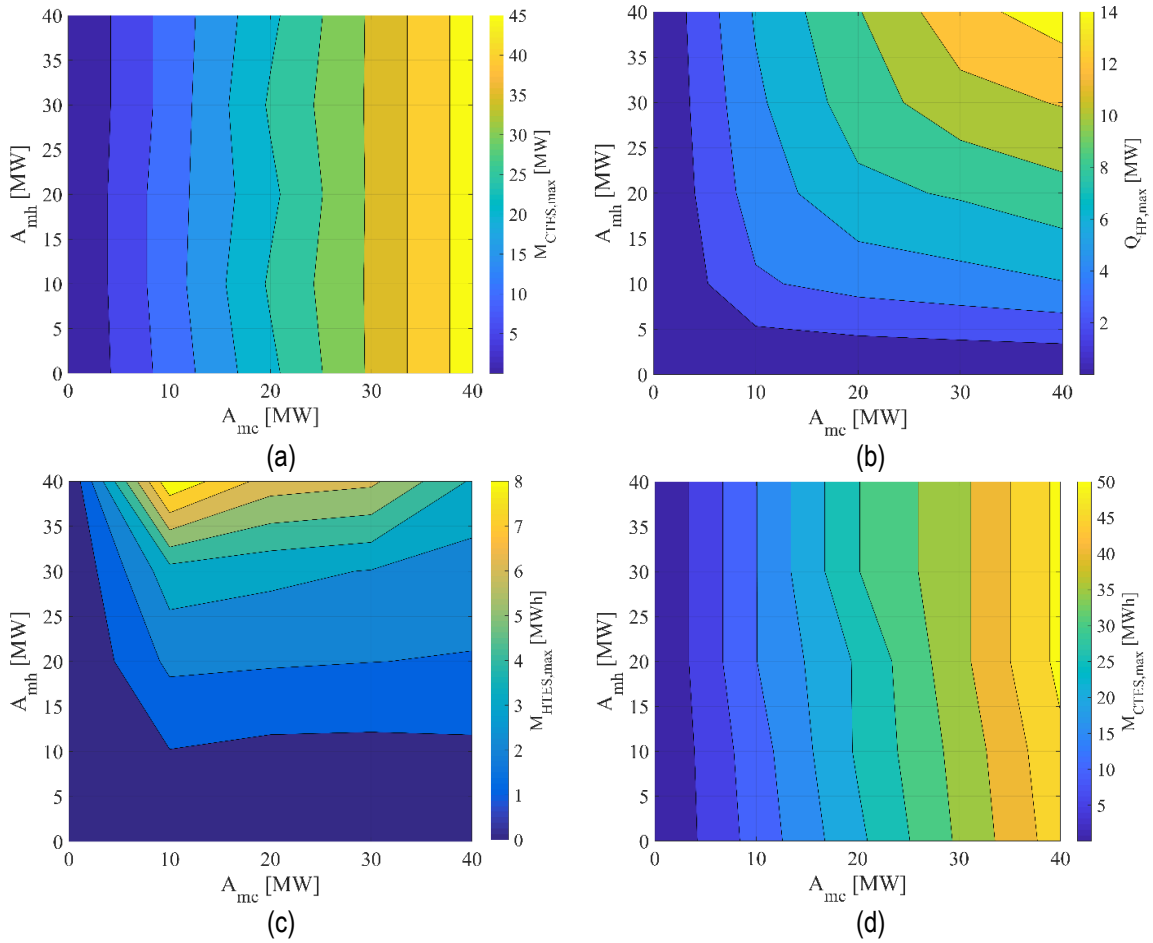

Figure 2.4. Optimal capacity of: (a) CTES for the hub with only TES; (b) HP for the hub with only HP; (c)-(d) HTES and CTES for the hub with both TES and HP.

Next, a comparison is made between the case where only TES units are introduced in the hub and the case where only heat pumps are included. Fig. 2.3b and Fig. 2.3c illustrate the minimized cost in these situations as a function the load amplitude. First, it should be noted that based on the cost comparison, it is always better to include only heat pumps than only TES units. As shown in Ref. [4], heat pumps (without TES) are more beneficial

when simultaneous heating and cooling loads are present. That explains the shape of Fig. 2.4b, which reports the optimized heat pump capacity: when A_{mh} and A_{mc} are too dissimilar, the savings generated by the use of heat pumps go down significantly, and so does the optimal heat pump capacity.

Finally, Fig. 2.3d reports the minimized cost when both TES and heat pumps are introduced into the hub. When comparing the results to the situation where only heat pumps are introduced in the hub, it can be seen that the system benefits from the use of both technologies together. However, more savings are generated from introducing heat pumps only (with respect to the reference scenario), than when introducing TES in a hub with heat pumps (i.e., with respect to the scenario with heat pumps only). Figures 2.4c and 2.4d illustrate respectively the optimal capacity of the HTES and CTES units when both heat pumps and TES are introduced in the hub. One can see that HTES is used less in the optimized hub than CTES, especially for lower A_{mh} values. As for the CTES optimal capacity in Fig. 2.4d, it is essentially independent on the A_{mh}.

The Sankey diagrams displayed in Fig. 2.5 present the annual energy flows in each four energy hub designs discussed above. The energy flows in the TES represent the thermal energy entering and leaving the units over the course of the year, the difference between both being cause by self-discharge. These graphs correspond to the points [A_{mh}, A_{mc}] = [40,40] of Figs. 2.3 and 2.4. Again, as can be observed in Fig. 2.5a, the reference case uses no HP nor TES units. As mentioned above, because there is no peak penalty on natural gas consumption, no HTES is required when only TES are introduced in the hub (Fig. 2.5b), but the use of CTES is visible to reduce electricity peak demand when useful. If only HP is added to the reference energy hub (Fig. 2.5c), the energy flows allow to visualize the part of the loads assumed by the heat pumps and not by the chillers and boilers anymore. Finally, when both HP and TES are implemented into the reference energy hub (Fig. 2.5d), both CTES, and HTES units help the system to lower the cost. The capacity of TES units in this case, correspond to those shown in Figs. 2.4c-d.

Figure 2.5. Sankey diagram illustrating the annual energy flows in MWh in the hubs when A_{mh} = A_{mc} = 40 MW: (a) Reference (no TES, nor HP); (b) only TES; (c) only HP; (d) both TES and HP.

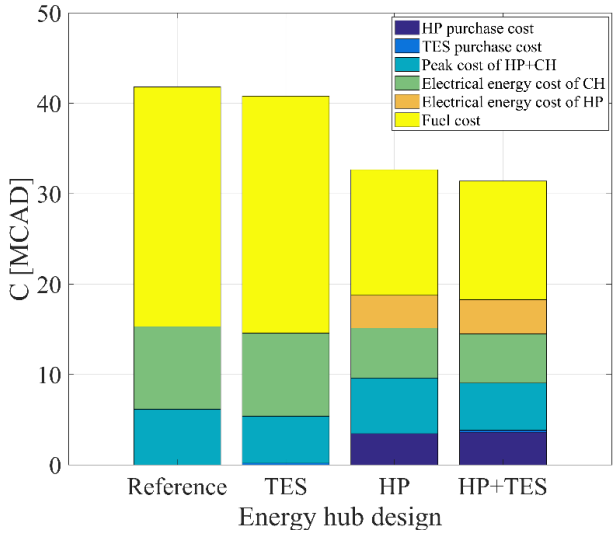

Figure 2.6. Cost breakdown in the reference energy hub, with TES alone, with HP alone and with both HP and TES for the thermal load A_{mh} = A_{mc} = 40 MW (note that the cost to satisfy L_e is not included in the figure).

Figure 2.6 reports the cost breakdown for a selected load profile for the reference hub, as well as for the hubs with TES units only, with HP only and with both of them. This cost is equal to the entire cost of the energy hubs presented in Figs. 2.3a-d minus the cost associated with L_e, which is nearly 103 MCAD and the same for all cases. As evident in this figure, the introduction of HP alone remarkably lowers the total cost by decreasing the operational costs of the chillers and boilers. Another cost-reducing factor that is apparent in this figure is the decrease of the electricity peak demand cost by introducing TES units to both the reference energy hubs and the hub with TES. Finally, TES purchase costs, which are mostly due to CTES (see Figs. 2.4a, and 2.4c-d), are not significant in comparison with other costs. In sum, the total cost was reduced respectively by 0.48%, 6.37%, and 7.25% with addition of only TES, only heat pumps, and both.

2.7 Influence of TES in undersized hubs

This section investigates the potential of TES units to help meeting the demand in hubs with limited boiler capacity (Section 2.7.1) and limited chiller capacity (Section 2.7.2). As demonstrated in Section 2.6, TES units become particularly useful to reduce cost when combined with heat pumps, since they allow the heat pumps to operate even in the absence of simultaneous heating and cooling loads. Therefore, we will study the benefits of introducing TES units in hubs with heat pumps (but again, with limited boiler or chiller capacities). The following cost difference will thus be used below:

$$\Delta C = C_{HP} - C_{HP+TES} \tag{2.20}$$

where C_{HP} is the total cost of the hub optimized with heat pumps only, and C_{HP+TES}, the total cost of the energy hub optimized when both heat pumps and TES are used simultaneously. These costs will be determined for different levels of under-sizing of the boilers and chillers.

2.7.1 Impact of TES units with undersized natural gas boiler

This section investigates the extent to which TES can help to meet the required loads in cases where the capacity of the natural gas boiler varies. For example, these scenarios can represent situations in which the heating load has increased over the years up to a point where current equipment do not have enough capacity or enough redundancy at certain moments. The maximum capacity of the natural gas boiler was thus varied between 20 and 100% of the heating load amplitude (i.e., γ_{FB} = 20-100%), as shown in Table 2.2. The natural gas boiler capacity in a given scenario, $Q_{B,max}$, is then

$$Q_{B,\max} = \gamma_{FB}\, A_{mh} \tag{2.21}$$

As mentioned above, for each set of natural gas boiler capacity and load profiles, the hub was optimized with and without TES units in order to determine the influence of TES on the system design and operation. For the sake of simplicity, we assumed $A_{mc} = A_{mh}$.

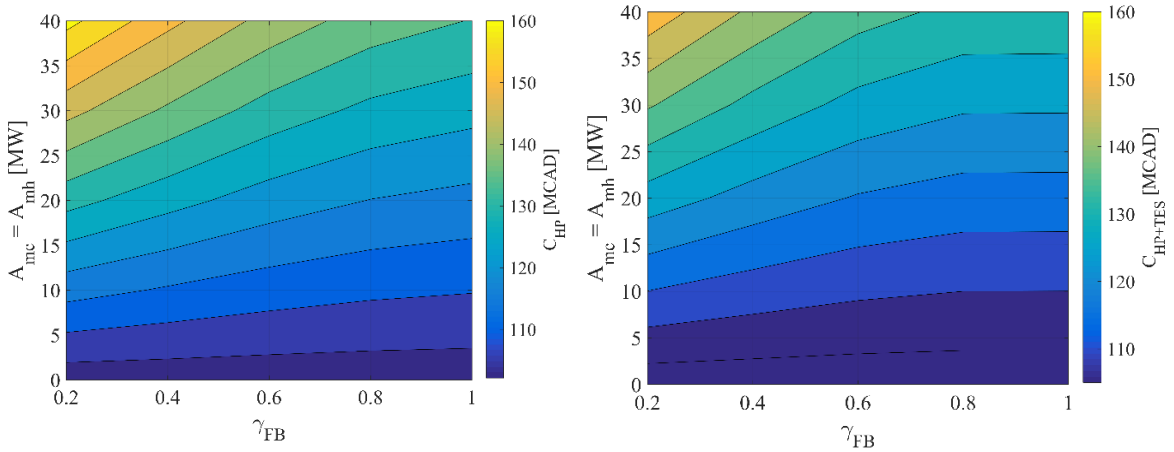

(a) (b)

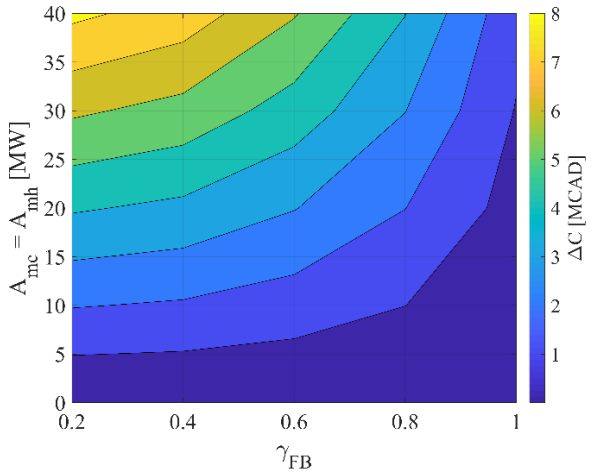

(c)

Figure 2.7. Impact of the thermal load amplitudes and FB size on the optimized energy hub: (a) Minimized total cost with only HP and (b) with both HP and TES; (c) Maximized savings ΔC due to using both HP and TES.

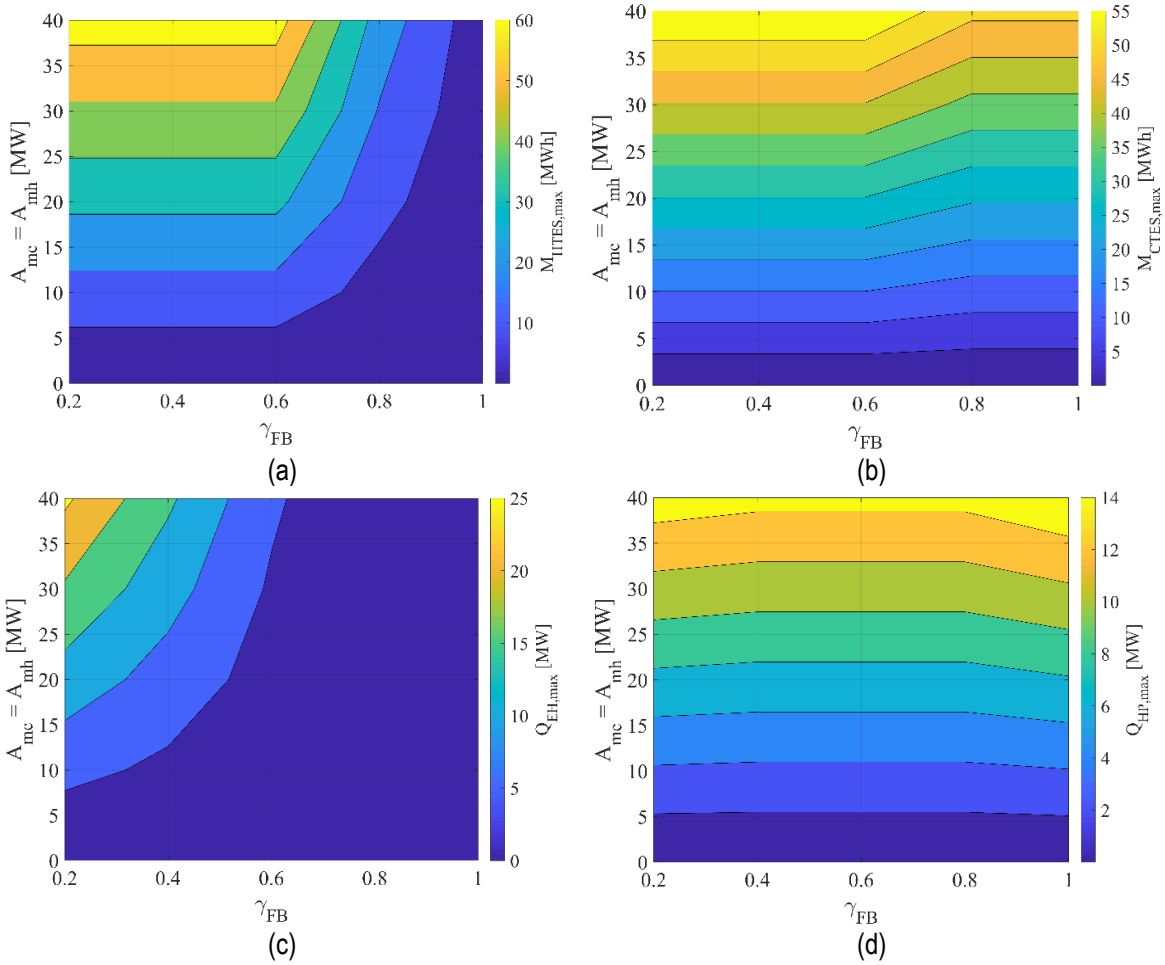

(a) (b) (c) (d)

Figure 2.8. Impact of the thermal load amplitudes and FB size on the optimized energy hub: (a) Optimal HTES capacity; (b) Optimal CTES capacity; (c) Optimal EH capacity; (d) Optimal HP capacity.

Figures 2.7 and 2.8 show how the capacity of the natural gas boiler and the thermal load amplitudes affect the relevance of introducing TES in the studied energy system. Again, each "pixel" in these figures is the result of an optimization run. The total cost of the energy hubs including only HP, both HP and TES, and the cost difference between them are portrayed in Fig. 2.7. The total costs shown in Figs.2.7a and 2.7b are only weakly sensitive to γ_{FB} except for high loads. By subtracting Fig. 2.7b from Fig. 2.7a, Fig. 2.7c can be achieved, from which it is apparent that when the thermal loads are high and the natural gas boiler is undersized (upper left corner), the system relies heavily on both hot and cold TES units (see Figs. 2.8a-b), and it is where the maximum benefit is achieved from implementing TES into the energy hub (see Fig. 2.7c). The explanation is provided in Fig. 2.8c, where it can be seen that a large electric heater capacity must be used to satisfy the heating load when the boiler is undersized. Such a large electric heating (EH) capacity requires larger HTES devices, as depicted in Fig. 2.8a, so that the electricity peak demands resulting from a higher use of EH are shaved.

A fraction of the heat will also be supplied by the heat pump. As discussed above, the HP capacity is determined by both cooling and heating loads. Nevertheless, undersized boiler does not change the design of the cooling network. This is why the optimal HP capacity does not considerably change with respect to γ_{FB} as illustrated in Fig. 2.8d. This also justifies that the CTES capacity is not influenced by the undersized boiler, as exhibited in Fig. 2.8b. When γ_{FB} increases, the contribution of the electric heater diminishes drastically (see Fig. 2.8c), while the heat pump keeps working in the network as an ideal (multi-generation) equipment. This is where the importance of TES appears by helping the energy hub to benefit from heat pumps compared to the case where only heat pumps (without TES) are added to the energy system. On the other hand, as seen in Figs. 2.8a and 2.8c, when the boiler operates with capacities close to their maximal required size, no electric heater is employed, making the optimization model choose smaller HTES, regardless of the load amplitudes.

In Figure 2.9, Sankey diagrams illustrate the role played by TES units when natural gas boilers are undersized (γ_{FB} = 20%), for thermal load amplitudes of [A_{mh}, A_{mc}] = [40,40] MW. Energy flows in the reference hub (Fig. 2.9a), in the hub with only TES (Fig. 2.9b), in the hub with only HP (Fig. 2.9c) and finally, in the hub with both HP and TES (Fig. 2.9d) are reported. As observable in this figure, in all four situations, the electric heater has to heavily be employed in order to meet the heating load.

When introducing TES alone (Fig. 2.9b), the chiller and electric boiler are operated more during off-peak periods, storing excesses in TES units for further usage, which helps to reduce costs in the case of cold production and meet the demand in the case of heat production. The HP in Fig. 2.9c helps to reduce the energy consumption of all pieces of equipment (chiller and boilers) by producing simultaneous heating and cooling, and adding TES (Fig. 2.9d) allows to use even more the HP. Note that for this specific case, the addition of TES units only lowered

the total cost by ~7 MCAD, the addition of HP only by ~22 MCAD, and of both HP and TES units at the same time by ~30 MCAD.

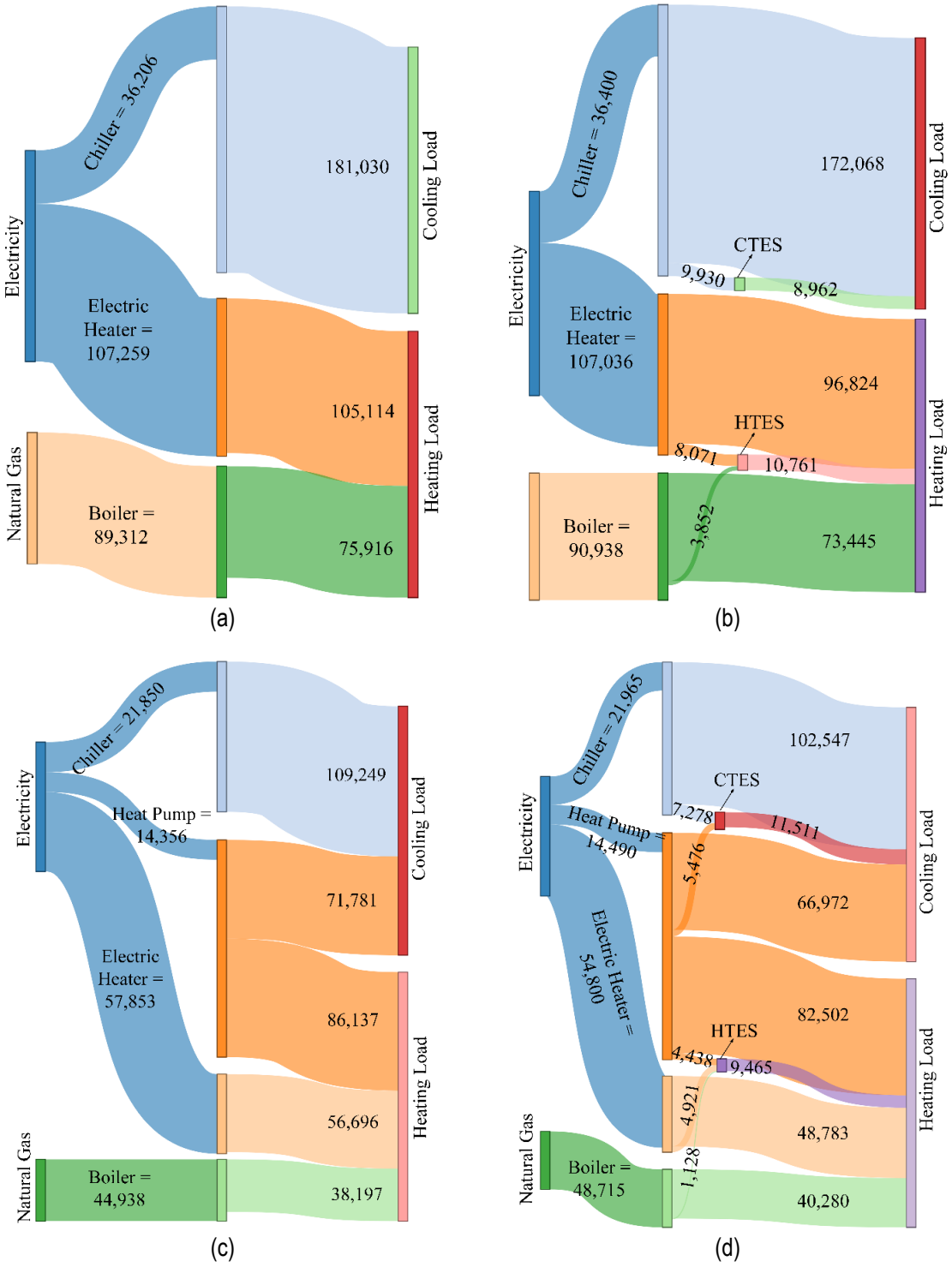

Figure 2.9. Sankey diagram for the energy hubs for undersized boiler of γ_{FB} = 20%: (a) Reference; (b) only TES; (c) only HP; (d) both TES and HP.

Finally, the influence of the TES unit purchase cost ϕ_{TES} on the financial benefit of adding storage units in the hub was studied. Figure 2.10a shows the impact of ϕ_{TES} for different boiler capacity for the load profile corresponding to A_{mh} = A_{mc} = 40 MW. As can be expected, the TES is particularly helpful when the natural gas boiler is highly undersized and when the TES unit purchase cost is low. For all cases tested, TES were always beneficial, i.e. ΔC is larger than 0. In fact, one can observe that the ΔC is more dependent on the boiler sizing than on the TES purchase cost as the isolines in Fig. 2.10a are essentially vertical. When the boiler is highly undersized, the hub can rely on large and cheap TES units, particularly when ϕ_{TES} is small, as evident from Fig. 2.10b.

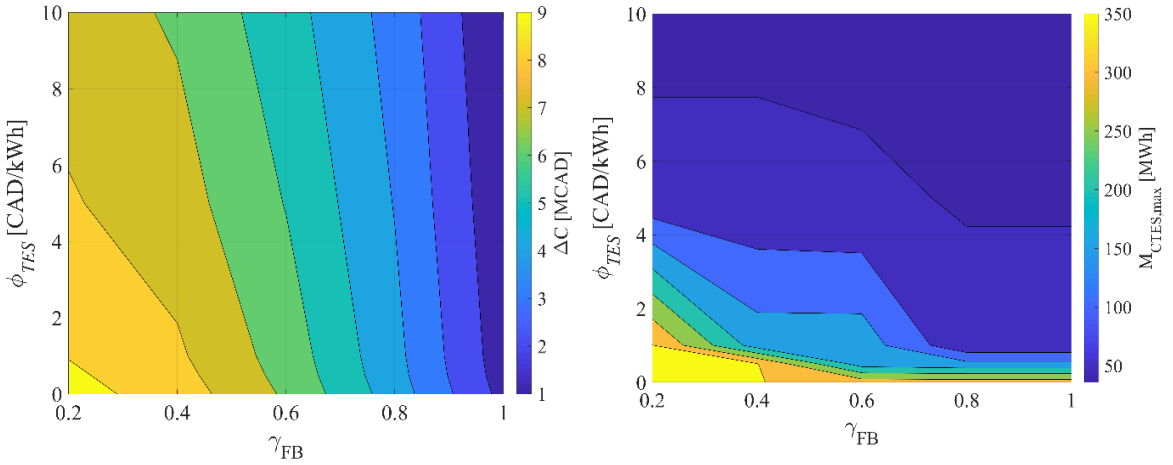

Figure 2.10. Impact of the TES unit purchase cost and FB size on the optimized energy hub when A_{mh} = A_{mc} = 40 MW: (a) Maximized savings due to using TES; (b) Optimal CTES capacity.

2.7.2 Impact of TES units with undersized chiller

Finally, this section analyzes the effect of using TES units in an energy hub in which the chiller might be undersized. It should be considered that the efficiency of the HP and chiller are the same in this study (see Table 2.1). However, only the chillers are supposed to be already available in the hub, and the HP units have to be purchased. As stated above, both devices use only electricity, for which both electricity peak and consumption must be paid for. Moreover, the maximal cold demand occurs during day 6 (see Fig. 2.2), which dictates the required chiller capacity. As a matter of fact, since the peak cold demand occurs simultaneously with the lowest heating demand, the use of HP is difficult in that case without TES units. Furthermore, the charging and discharging power values of TES units was limited to 20% of the peak demand (see Section 2.4.1). Therefore, a limited back-up of 20% could be available from TES for each device operating on undersized mode. A wide range of undersized natural gas boiler and HP situations could be assessed in the previous sub-section, with relative capacities ranging from 0 to 100%, taking into account the support that the electric heater and the chiller

can provide. In contrast, the investigation of hubs with undersized chillers is limited to a narrow range of possible relative capacity (γ_{CH}), because the CTES units can only provide 20% of the cold peak demand and there is no other equipment than the chiller to provide cold during the peak period. The chiller capacity in a given scenario, $Q_{CH,max}$, is

$$Q_{CH,\max} = \gamma_{CH}\ A_{mc} \tag{2.22}$$

According to the discussion above, we decided to investigate the hub performance only on the day 6, which is the bottleneck in scenarios with undersized chillers. A comparison will be provided between the scenario with γ_{CH} = 0.77 and γ_{CH} = 1 (no under-sizing). The first scenario is the minimal chiller under-sizing limit for which a solution existed, due to the constraints invoked above. Again, for the sake of simplicity, we assumed A_{mc} = A_{mh} = 40 MW.

Figure 2.11 shows how the cooling demand is satisfied in the energy hub, and in particular, the role played by the CTES for the two relative capacity values of the chiller. The instantaneous cold production by the chiller and heat pumps are respectively ($COP_{ec}^{CH}\ P_{e,CH}$) and ($COP_{ec}^{HP} - 1$) $P_{e,HP}$ in the figures. The cold charged in or discharged from the CTES units is ($P_{CTES}^{ch} - P_{CTES}^{dis}$), with positive values in the figure corresponding to charging and negative, to discharging. The curve identified by ($L_c + P_{CTES}^{ch} - P_{CTES}^{dis}$) thus represents the actual instantaneous cold production that is required from the chillers and heat pumps. For both chiller capacity ratios, the CTES units help to flatten the required production of cold over time (i.e. purple curves) to satisfy the cooling load L_c (blue curves).

By comparing the upper and lower frames of Fig. 2.11, one can observe that the plateau of cold production by the chillers is slightly lower in Fig. 2.11a (γ_{CH} =0.77) than in Fig. 2.11b (γ_{CH} =1). In the case with γ_{CH} =1, even though the chiller capacity is 50 MW, it is in fact never fully used at full capacity in the optimized hub as part of the cold is produced by the heat pump, yielding an actual peak cold production value from the chiller of ~40 MW. It is only when the chiller capacity is reduced below that value that changes occur in the hub, as is the case with γ_{CH} =0.77 which corresponds to a capacity of 38.5 MW. In that case, in order to compensate the lack of instantaneous cold production by the chiller, the HP and CTES units are more solicited. However, the use of the CTES is limited by the constraint on the discharge rate which is 20% of the cold demand (i.e. 10 MW), and the use of the HP is limited by the heating demand (all the heat need is satisfied by the HP without any usage of the boiler). When γ_{CH} =0.77, the maximal discharge of the CTES is almost reached, making a further reduction of the chiller capacity impractical. Overall, the total cost with the undersized chiller is slightly higher than with the full chiller, since larger HP and CTES are needed. Accordingly, the case with γ_{CH} = 0.77 costs 133.54 MCAD, which is 0.03 MCAD more expensive than the case γ_{CH} = 1.

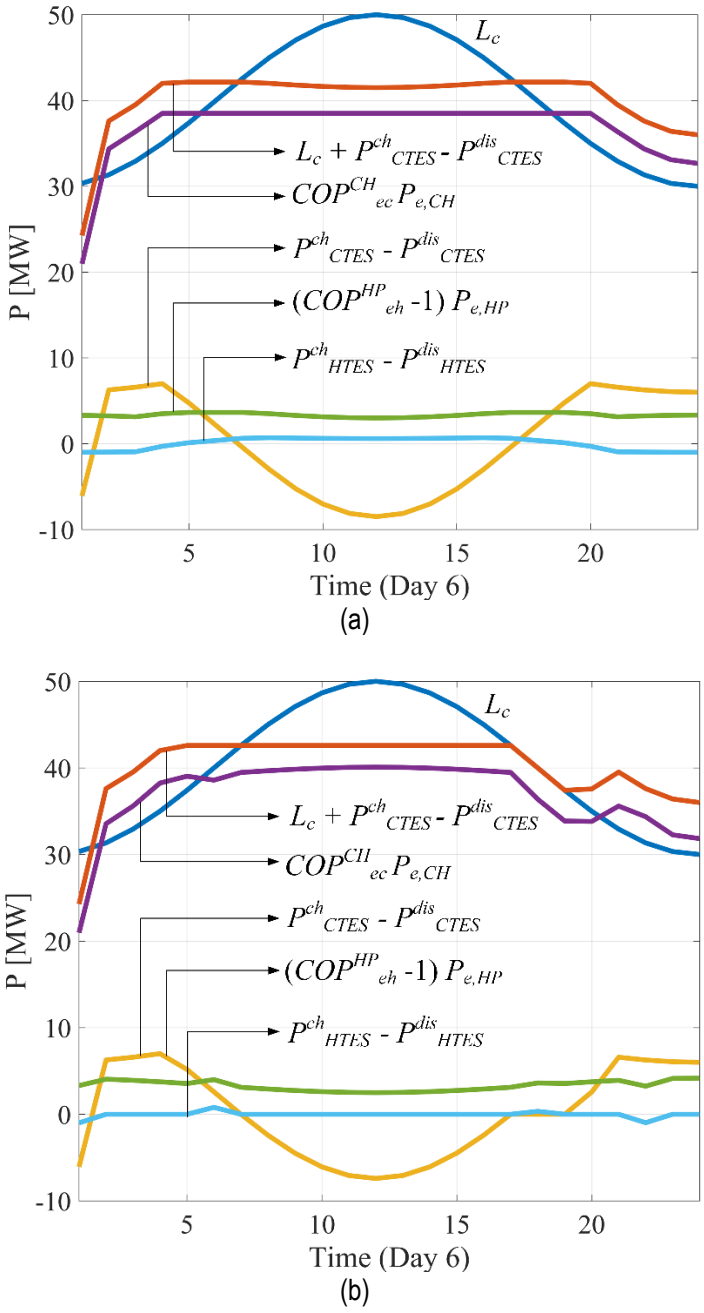

Figure 2.11. Heat transfer rates as a function of time in the energy hub for satisfying the cold demand with two relative chiller capacities: (a) γ_{CH} = 77% (b) γ_{CH} = 100%.

2.8 Conclusions

In this paper, different scenarios were considered to evaluate the usefulness of TES units. First, energy hubs with TES units, with heat pumps and with a combination of both were compared to a reference hub for a wide range of load profiles. Second, TES units were introduced into systems with boilers and chiller having too small a capacity to meet the instantaneous thermal demand. In each case, the optimization model was used to determine the best hub design and operation in order to minimize the total cost. TES units were found to be financially profitable when working with heat pumps in all above-mentioned cases, but some parameters of the scenarios were more influential than others on the benefits generated by TES. For example, the thermal load combination and the cost of energy had a strong influence, whereas the cost of the TES units themselves did not appear to be influential. The different figures that were presented in the paper can be used to evaluate at a glance the potential of using TES in a given situation.

This study allows to make some recommendations regarding the design and operation of integrated heating and cooling networks in the studied context, which can help the designers and operators of such systems. When no thermal integration is intended (i.e. no heat pump is used), TES units are not effective to reduce the total cost. When heat pumps are used to thermally integrate networks, TES units lower the lifetime cost since they allow a certain manipulation of the thermal demands. The most important cost reduction due to the TES in the cost breakdown is on the electricity peak cost, which makes the use of TES particularly useful when such tariff structure exists. Furthermore, TES can also decrease the total cost when used to counteract a lack of capacity of natural gas boilers, preventing the use of electricity heaters.

In this work, the efficiency of the different parts of the energy hub were kept constant. In future work, it would be interesting to consider the impact of part-load operation and climate on efficiency. That would allow to introduce scheduling into the optimization model, i.e. choosing when to operate a series of chillers and boilers that would be available. Furthermore, other objective functions could be introduced into the problem, such as greenhouse gases emissions, robustness of the hub in case of equipment failure, percentage of renewable energy on the supply side, etc. Finally, it is worth to mention that some of the numerical values in the model (e.g., cost structure of electricity and natural gas, etc.) apply only to the context under study and might be different in other situations. Further studies could determine the extent to which the conclusions that we presented hold true in other economic contexts by relying on the proposed model, but with an adjustment of these values.

Acknowledgments

This work was supported by the Natural Sciences and Engineering Research Council of Canada (NSERC).

Chapitre 3 COMBINED HEATING AND COOLING NETWORKS WITH PART-LOAD EFFICIENCY CURVES: OPTIMIZATION BASED ON ENERGY HUB CONCEPT

3.1 Résumé

Les réseaux de chaleur et de refroidissement se retrouvent dans des applications à différentes échelles, allant des bâtiments aux villes. Les modèles de hub énergétiques peuvent être utilisés pour optimiser leur conception, leurs opérations et leur intégration énergétique globale. Dans la pratique, l'efficacité à charge partielle des équipements tels que les refroidisseurs, les chaudières et les pompes à chaleur peut fortement affecter leurs performances globales. Cependant, les modèles de hub énergétiques considèrent généralement des efficacités constantes pour leurs convertisseurs d'énergie en raison du défi de la mise en œuvre de l'efficacité à charge partielle (PLE) dans de tels modèles. Ceci, à son tour, introduit des erreurs dans les résultats. Même si les formulations NLP et MILP ont été introduites dans la littérature pour optimiser les hubs avec des dispositifs PLE, elles se concentrent généralement uniquement sur les coûts opérationnels. De plus, la manière dont les appareils PLE affectent les réseaux combinés de chauffage et de refroidissement pour un large éventail de profils de charge possibles n'est pas documentée. Par conséquent, dans ce travail, le coût à vie (exploitation + achat) d'un tel système a été minimisé sur la base d'un hub énergétique dans lequel les appareils PLE (chaudières à gaz naturel, radiateurs électriques, refroidisseurs électriques et pompes à chaleur) ont été simulés sous de nombreuses combinaisons différentes de charges thermiques. Le modèle a été linéarisé pour réduire le temps de calcul et améliorer la capacité du solveur à trouver des solutions. Pour déterminer l'impact des efficacités à charge partielle, chaque appareil est examiné individuellement tandis que l'efficacité des autres appareils reste constante. L'erreur résultant de l'hypothèse d'un rendement constant est ensuite calculée sur la base d'un hub de référence avec des rendements constants. Les résultats indiquent une erreur maximale sur le coût total de 1,85 %, 0,6 % et 0,16 % en supposant un rendement constant pour les chaudières, les refroidisseurs et les pompes à chaleur respectivement. Les charges pour lesquelles ces erreurs maximales se produisent sont ensuite choisies pour optimiser le hub avec tous les appareils modélisés avec une courbe d'efficacité à charge partielle. Les erreurs ont augmenté à 1,9 %, 0,71 % et 1,49 %, respectivement.

3.2 Abstract

Heating and cooling networks are found in applications of different scales, ranging from buildings to cities. Energy hub models can be used to optimize their design, operations, and overall energy integration. In practice, part-load efficiency of equipment such as chillers, boilers and heat pumps can strongly affect their overall performance. However, energy hub models typically consider constant efficiencies for their energy convertors due to the challenge of implementing part-load efficiency (PLE) in such models. This, in turn, introduces errors in the results. Even though NLP and MILP formulations have been introduced in literature to optimize hubs with PLE devices, they typically focus solely on operational costs. Furthermore, how PLE devices affect combined heating and cooling networks for a wide range of possible load profiles is undocumented. Therefore, in this work, the lifetime cost (operation + purchase) of such system was minimized based on an energy hub in which PLE devices (natural gas boilers, electric heaters, electric chillers, and heat pumps) were simulated under many different combinations of thermal loads. The model was linearized to reduce computational time and improve the capability of the solver to find solutions. To determine the impact of part-load efficiencies, each device is individually examined while the efficiency of other devices remains constant. The error resulting from assuming a constant efficiency is then calculated based on a reference hub with constant efficiencies. The results indicate a maximum error on the total cost of 1.85%, 0.6%, and 0.16% by assuming constant-efficiency for the boilers, chillers and heat pumps respectively. The loads for which these maximum errors occur are then chosen to optimize the hub with all devices modeled with a part-load efficiency curve. The errors increased to 1.9%, 0.71%, and 1.49%, respectively.

3.3 Introduction

Nowadays, “energy hubs” are widely used for the modeling and optimization of complicated energy systems. This concept defines a framework in which the energy resources available in an area can be linked to the end-users’ thermal and electrical demands. Accordingly, the energy hub consists of three main sections: (i) energy resources, (ii) energy conversion devices, and (iii) loads.

Recently, energy hubs were found to be quite useful for optimizing the design and operation of integrated heating and cooling networks [4], an important category of applications which is the topic of interest in the present work. Such networks can be seen as thermal grids satisfying the heating and cooling needs of buildings, campuses, districts or cities. They are found abundantly, at different scales, and throughout the world. Providing optimization and decision-making tools, design guidelines and operational best practices for a wide range of possible load

configurations thus offers an opportunity for reducing significantly energy consumption and costs for many end-users.

As in any energy hub optimization problem, the assumptions regarding the efficiency of the energy convertors can strongly affect the results and the computational time. Even though the literature using energy hub modeling for optimizing specifically integrated heating and cooling networks is scarce, recent work related to energy hubs are instructive in that matter and will be examined here. A closer look at current literature revealed that almost systematically, a constant efficiency (CE) is assumed in hub models. For example, Brahman et al. [26] used constant efficiencies for photovoltaic units, Combined Cooling, Heating and Power (CCHP) equipment, absorption chillers, and electric chillers while minimizing both cost and CO_2 emissions of a residential energy hub. Moghaddam et al. [16] defined a comprehensive model for an energy hub in which the Coefficient of Performance (COP) of an absorption chiller and heat pump, and the boiler's efficiency were constant. In a study focusing on minimizing total annual cost and environmental impact of twenty buildings combined in five energy hubs [75], unit purchase costs, maintenance costs, and efficiencies were all held constant. A complex of cooperative energy hubs was optimized in [76] with the assumption of constant efficiencies. Recently, constant efficiencies were also used to optimize a district energy system with demand response [77], a smart energy hub considering users' uncertain behavior [78], and a multi-energy system with nodal energy prices [79], among others. In all these examples and many others, constant efficiencies have the advantage of being easy to implement and fast to solve (by preserving linearity in the models), and can often provide a fair estimate of the optimal design and/or operation of a system.

However, it is well known that a system's performance can be strongly affected by the part-load efficiency (PLE) of the different devices that it contains. Manufacturers often provide curves of the efficiency as a function of the part-load ratio (PLR) for different pieces of equipment. Typically, the efficiency tends to drop as one moves away from the optimal operating point of the device. Considering these PLR efficiency curve in hub optimization creates non-linearities in the model, and thus makes the problem more challenging. However, the inclusion of PLR-based efficiencies could remarkably change the design of energy hubs compared to cases in which the impact of PLR on efficiency is ignored [80]. In order to solve such problems, two main types of formulations have been found in literature: NLP (i.e. using a non-linear solver) and MILP (i.e., linearizing the model and then solving it). Note that in most cases reported in literature, the number of time steps analyzed is limited to 24, i.e. the 24 hours in a day.

The first category of formulations (NLP) including PLE accounts for the majority of the publications. Several studies devoted to energy hub optimization have developed NLP methods to consider part-load efficiencies (PLE). Fabrizio et al. [81] used PLR-basis efficiencies to model an Organic Rankine Cycle (ORC) in an energy

hub template. The life cycle cost of an energy hub including PLR-based efficiency of equipment was minimized by Deng et al. [82] using Mixed-Integer Nonlinear Programming (MINLP) in MATLAB. In their approach, they first optimized the capacities of the constant-efficiency devices, and then performed the operational optimization. Their energy hub included gas turbine, gas boiler, absorption chiller, electric chillers, and heat recovery steam generator. The same approach was chosen in [83] where the daily operational cost was to be minimized. In their analyses, the authors considered a PLE curve for one device at a time while other devices functioned on a constant-efficiency basis in the model in order to determine the influence of PLR-based efficiency of each part. Sequential Quadratic Programming (SQP) was employed by Mu et al. [71] considering PLR-based efficiencies for CHP, HP, and gas boiler. In contrast to the approach of [82], [83], the one introduced in [71] optimized the design in the first step with the total annual cost as the objective function. The operational characteristics were then optimized by considering operation and maintenance cost as the objective function in order to reevaluate the efficiencies. Different non-linear solving approaches were recently compared by Li et al. [84], including a proposed improved tunicate swarm algorithm, in order to solve theoretical benchmark dynamic economic emission dispatch problems. Operational cost and emissions were minimized while the relation between fuel consumption and power output included non-linearities that could represent part-load behaviors.

In the second category of formulations, the problem is linearized, which tends to make the implementation more tedious, but the convergence faster. Fewer papers have used that approach. As detailed in [85], the first studies that presented Mixed-Integer Linear Programming (MILP) for optimization of PLR-based efficiencies of energy systems were performed by Yokoyama et al. [86], [87]. Then, Voll et al. [88] used the approach elaborated by Yokoyama to emphasize not only the optimal solution, but that the near-optimal region is important for energy systems. As will be demonstrated later in the present work, the transformation from NLP to MILP via piece-wise linearization method necessitates the introduction of some breakpoints on the curve of the nonlinear function. The greater the number of those points, the higher the computational time, as evident in [89]. The NLP-to-MILP transformation may also be performed using Karush-Kuhn-Tucker (KKT) conditions [90]–[92], as illustrated in [93] where the maximization of revenue is the objective function.

The recent work of Huang et al. [94] offers an interesting summary of the advantages and disadvantages of different ways to consider PLR efficiency curves. They modeled a hub including combined heating and power, compression electric refrigerator, heat pump, auxiliary boiler and thermal storage, and they compared three ways to account for efficiency variations: using constant efficiencies, introducing part-load efficiency curves into an NLP formulation and linearizing the problem with part-load efficiency curves into a MILP formulation. For their problem, they showed that the computational time was smaller with the constant efficiency than with the other formulations, but that it introduced an error close to 14% (compared to the most exact case). Furthermore, even though the associated error was smaller with the NLP formulation, its computational time was much longer (293

s vs 0.43 *s* for the constant efficiency case). The linearization introduced in the MILP formulation allowed to keep both the computational time (0.47 to 3.39 *s*) and errors (0 to 8%) within reasonable limits. However, only the operational cost was considered. Sizing the hub components through the optimization model makes the problem even more complex as the part-load ratio appearing in efficiency curves involves precisely the component size (which would then be a design variable).

Table 3.1. Overview of publications that considered part-load ratio efficiencies when optimizing energy hub.

Method used	Algorithm used	Objective function	Number of time steps (h)	Calculation time (s)	Equipment in energy hub*	Ref.
NLP	SQP in fmincon	operational costs	24	292.73	CHP, CERG, HP, AB, TES	[94]
	Genetic Algorithm	annual benefit	12	NA	CH, AC, AB, ORC, PM	[67]
	MATLAB optimization	operational costs	6*30*24	NA	ORC, WB, OB, TES	[81]
	MATLAB MINLP	life cycle cost	3*24	NA	GT, HRSG, FB, AC, CH, HEX	[82]
	BARON in GAMS	daily operational costs	24	12.34	GT, HRSG, AC, CH, PV, EES, HEX	[83]
	PSO	relative annual benefit	12	NA	GE, CH, AC, AB, CCHP	[95]
	SQP in SNOPT	annual total cost	3*24	15.18	HP, EES, PV, CHP, FB, TES	[71]
MILP	GUROBI	operating costs	24	0.47-3.39	CHP, CERG, HP, AB, TES	[94]
	CPLEX	operating costs	24	6.08-34.50	CHP, HP, TES	[96]
	MATLAB *IBM* CPLEX	CO_2 emissions	7 & 14	14.30	HP, FB, TES, PV	[89]
	N/A	revenue	24	NA	AC, CH, GT, FB, TES, HRSG, HEX	[93]
Proposed in this work	CPLEX in GAMS	total lifetime cost (Op.+ Cap.)	6*24	8.50-60.22	HP, FB, CH, EH	

**CERG: compression electric refrigerator group; AB: auxiliary boiler; CHP: combined heating and power; CCHP: combined cooling, heating and power; PHEV: plug-in hybrid electric vehicles; AC: absorption chiller; CH: electric chiller; WS: water storage; PM: prime mover (diesel engine, gas turbine and gas engine); GT: gas turbine; GE: gas engine; DE: diesel engine; EES: electrical energy storage; ORC: organic Rankine cycle; WB: wood biomass boiler; OB: oil boiler; HRSG: heat recovery steam generator; HEX: heat exchanger; FB: natural gas boiler; EH: electric heater; HP: heat pump; TES: thermal energy storage.*

Table 3.1 presents a summary of papers that have included PLR efficiencies in their hub model. It reports the optimization algorithm, objective function, number of time steps, calculation time and pieces of equipment in the hub. Different limits and gaps in literature can be highlighted, such as:

The majority of the studies reported in Table 3.1 focus on minimizing daily operational costs (in particular for MILP formulations for which no sizing optimization was found). When designing a new system or refurbishing an existing system, device capacities become additional decision variables. However, these capacities also appear in the PLE relations, increasing the non-linearity and overall complexity of the model. There is thus a need to develop a formulation (in particular MILP, which tend to be faster to solve) capable of minimizing lifetime cost, i.e. capable of sizing equipment with PLE curves and of simulating more than one day.

The impact of PLR efficiency on the optimization of integrated heating and cooling networks has not been investigated. As mentioned above this class of system is particularly important due to its omnipresence. From a practical point of view, it would be useful to provide a model specific to that important application and to show the relevance (or not) to use PLR efficiency versus CE in the model in that application. Above all, guidelines regarding the best design and operational practices are needed for different load scenarios to help practice engineers design and manage these systems.

Finally, in the publications of Table 3.1, the PLR-based efficiency profiles were evaluated by polynomials using pre-defined regression coefficients between the efficiency and the PLR value, which can constrain the device selection and limit the optimization. Furthermore, the linearization of these curves can influence significantly the computational time, even increasing it to the point where the problem becomes longer than with an NLP formulation when many breaking points are used [94]. Developing flexible and generalized ways to account for efficiency curves could facilitate the resolution of the problem.

In this work, we introduce a MILP formulation for minimizing the lifetime cost of integrated heating and cooling networks while considering PLR efficiency. We show the error introduced by assuming a constant efficiency and the impact of using PLR efficiency on the results. The performance of the system was tested for an extensive range of thermal load combinations.

The paper is organized as follows. Section 3.4 presents the modeling approach of the energy hub in which the energy convertors operate on PLR-based efficiency. Then, in Section 3.5, representative loads are introduced. The methodology is discussed in Section 3.6. Optimization results are discussed in Sections 3.7 and 3.8.

3.4 Energy hub optimization model

In this section, the energy hub for which the current study is performed is introduced, and the related governing equations are listed. The optimization problem is then developed, and the objective function, constraints, and decision variables are presented. The linearization methods are explained. Lastly, there is a discussion on how near-optimum efficiency profiles can be achieved while optimizing both design and operation of the energy hub.

3.4.1 Modeling of the system

Figure 3.1 represents a thermal network inspired by the energy hub of the campus of Université Laval (Québec City, Canada). In this thermal grid, fuel boilers and an electric heater ("FB" and "EH" in Fig. 3.1, respectively) supply the required heat transfer fluid to the heating loop. The chillers ("CH" in Fig. 3.1) provide chilled water to the cooling loop to absorb the rejected heat from buildings. This heat is eventually dissipated into the environment via cooling towers. To improve the overall performance of the system, heat pump units ("HP" in Fig. 3.1) are integrated to couple the two thermal networks. They capture the rejected heat from the cold loop, and generate simultaneous cooling and heating. This integration is well explained in [4]. The PLR-based efficiency of the different devices introduced above is the subject of this research.

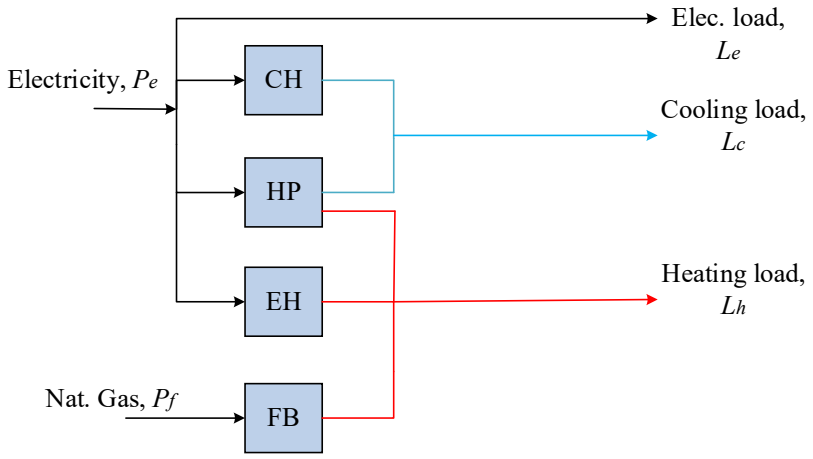

Figure 3.1. Hub representation of the integrated thermal networks [97].

In this model, four types of electricity uses are highlighted: chiller, heat pump, electric heater, and the rest of local electricity consumers (indicated by L_e in Fig. 3.1). No power-generation device is defined in this energy hub, since electricity from the grid is very clean, cheap and abundant in the context under study (Quebec, Canada). Therefore, the entire electricity has to be supplied by the power grid. As depicted in Fig. 3.1, the chiller

and heat pump supply the cooling demand L_c, and the electric heater, fuel boiler, and heat pump feed the heating load L_h. No thermal storage unit is included in this energy hub. Therefore, each load exhibited in Fig. 3.1 (i.e., L_h , L_e and L_c) asks for one or the two available energy resources, i.e. natural gas (i.e., P_f) and electric power grid (i.e., P_e). It is important to note that the time-dependency of L_h, L_e and L_c makes P_f and P_e vary in time as well.

At each time step, the load matrix, L, is related to the energy resource vector, P, via the coupling matrix, CM, as represented by

$$\underbrace{\begin{pmatrix} L_e \\ L_c \\ L_h \end{pmatrix}}_{\mathbf{L}(t)} = \underbrace{\begin{pmatrix} C_{ee} & C_{fe} \\ C_{ec} & C_{fc} \\ C_{eh} & C_{fh} \end{pmatrix}}_{CM} \underbrace{\begin{pmatrix} P_e \\ P_f \end{pmatrix}}_{\mathbf{P}(t)} \tag{3.1}$$

where CM includes all the conversion factors corresponding to the hub components. P indicates the power consumption from each energy resource. The subscripts of the coefficients in CM denote the conversion/transformation type and direction. The first letter represents the energy resource and the second, the end-user. In this regard, e, f, h, and c show electricity, fuel, heating, and cooling, respectively. For example, C_{fh} indicates the factor for the fuel-to-heating conversion. Since no cooling or electricity is produced from natural gas, the coefficients C_{fc} and C_{fe} are equal to zero.

According to what is stated above, the total electricity supplied from the grid is distributed into four principal electricity consumers:

$$P_e = P_{e,EH} + P_{e,HP} + P_{e,CH} + L_e \tag{3.2}$$

i.e. heat pumps ($P_{e,HP}$), electric ($P_{e,EH}$), chillers ($P_{e,CH}$), and other end-users (L_e). All P and L values are in W in this study. Therefore, the energy conservation of the energy hub can be rewritten as

$$\begin{pmatrix} L_c \\ L_h \end{pmatrix} = \begin{pmatrix} COP_{ec}^{CH} & COP_{ec}^{HP} & 0 & 0 \\ 0 & \left(COP_{ec}^{HP}+1\right) & \eta_{eh}^{EH} & \eta_{fh}^{FB} \end{pmatrix} \begin{pmatrix} P_{e,CH} \\ P_{e,HP} \\ P_{e,EH} \\ P_f \end{pmatrix} \tag{3.3}$$

where η denotes the efficiency of each device. In Eq. (3.3), the loads and nominal efficiencies of the equipment must be known and introduced as model inputs. However, since the efficiencies are power dependent, their magnitudes must be determined by optimization, along with the optimal power values. “Power”, in this case,

refers to the contribution of each device at a given time to satisfy the thermal loads in the energy hub. It is important to note that COP_{ec}^{HP} indicates the coefficient of performance of the heat pump with respect to the cooling mode. That justifies the use of the factor $(COP_{ec}^{HP} + 1)$ for the electricity-to-heating conversion of the heat pump. Typical nominal magnitudes of COP_{ec}^{HP} equal 3-5 for water-to-water heat pumps [33].

The energy hub model must invoke other constraints to be feasible. First, at each time step, the power of each equipment has to be equal or greater than zero, i.e.

$$\begin{pmatrix} P_{e,CH} \\ P_{e,HP} \\ P_{e,EH} \\ P_f \end{pmatrix} \geq 0 \tag{3.4}$$

In addition, since each device owns a limited capacity, one has:

$$\begin{aligned} COP_{ec}^{CH} P_{e,CH} &\leq Q_{CH,\max} \\ COP_{ec}^{HP} P_{e,HP} &\leq Q_{HP,\max} \\ \eta_{eh}^{EH} P_{e,EH} &\leq Q_{EH,\max} \\ \eta_{fh}^{FB} P_f &\leq Q_{FB,\max} \end{aligned} \tag{3.5}$$

where, $Q_{EH,max}$, $Q_{CH,max}$, $Q_{B,max}$, and $Q_{HP,max}$ indicate the maximum capacities of the electric heater, chiller, natural gas boilers, and the maximum cooling capacity of the heat pump, respectively (all in W).

To model the power dependence of the efficiencies associated with each equipment of the energy hub, we used a 2nd order polynomial:

$$\eta = a\left(\frac{P}{P_{max}}\right)^2 + b\left(\frac{P}{P_{max}}\right) + d \tag{3.6}$$

In this equation, *P* denotes the energy input in the device at a given time step (see Eq. (3.4)), and *a*, *b,* and *d* represent the regression coefficients of the polynomial. Based on published PLR-efficiency curves and on manufacturers data [71], [82], [95], it was found that the parabolic shape of Eq. (3.6) was adequate to represent several types of boiler, chillers and heat pumps such as those considered in the present study. In order to relate the coefficients in Eq. (3.6) to the characteristic curve of a device, the following conditions were used:

$$
\begin{aligned}
&P = 0 \Rightarrow \eta = 0 \\
&P = P_x \Rightarrow \eta = \eta_{nom} \\
&P = P_x \Rightarrow \frac{d\eta}{dP} = 0
\end{aligned}
\tag{3.7}
$$

where P_x (in W) indicates the power consumption at which the equipment functions at its nominal efficiency, η_{nom}. Applying the aforementioned conditions into Eq. (3.6) yields the following form of the part-load efficiency which was used here:

$$
\eta = \eta_{nom}\left(\frac{2P}{P_x} - \left(\frac{P}{P_x}\right)^2\right) \tag{3.8}
$$

It can be seen that the efficiency is now characterized by only two parameters, namely P_x and η_{nom}. Both these parameters are specified by manufacturers. Eq. (3.8) is valid for values of P between 0 and P_{max}, where P_{max} (in W) is the maximum possible power consumption corresponding to the capacity of the equipment. Figure 3.2 illustrates the part-load efficiency profile for two values of P_x/P_{max}, according to Eq. (3.8). Note that Eq. (3.8) could apply for all the hub's components: heat pumps, chillers, electric boilers and fuel boilers, for which P would mean respectively the electric power (HP, CH, and EH), and the natural gas power (FB) required for thermal energy generation of the devices. Each device would have its own relation with specific values of P_x and η_{nom}.

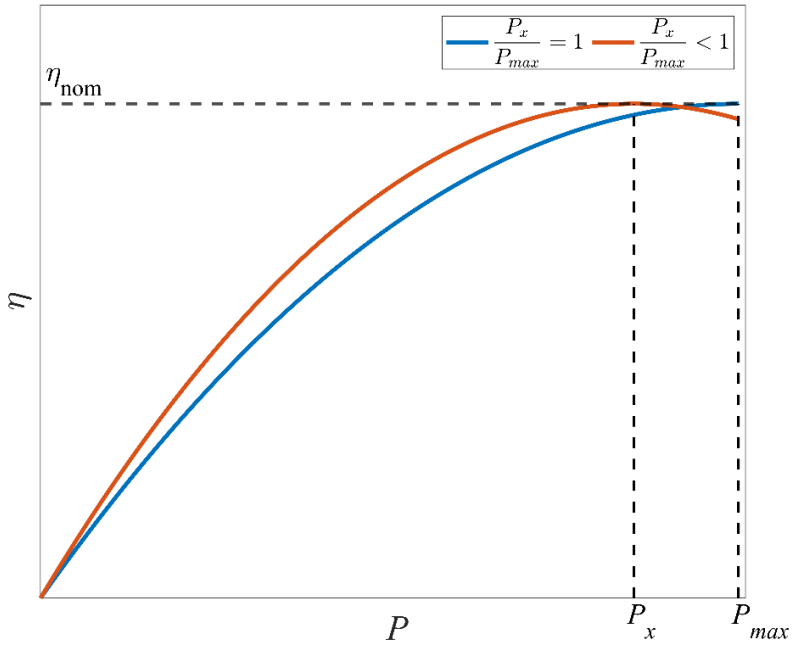

Figure 3.2. Schematic representation of the part-load efficiency profile for two values of P_x/P_{max}.

3.4.2 Objective function and optimization problem

In this research, we aim at minimizing the total cost of the energy hub. The definition of this cost is

$$C_{tot} = C_{init}^{FB} + C_{init}^{CH} + C_{init}^{HP} + C_{init}^{EH} + \frac{(1+i)^n - 1}{i(1+i)^n} C_{op} \tag{3.9}$$

and comprises the levelized annual operational cost, C_{op}, and purchase cost of the devices. In this context, C_{init}^{FB}, C_{init}^{HP}, C_{init}^{EH}, and C_{init}^{CH} represent the purchase cost of the natural gas boiler, heat pump, electric heater, and chiller (all in CAD) while the letters *i* and *n* indicate the interest rate and the lifetime of the system, respectively.

The purchase costs of the units are calculated via the following equations

$$\begin{aligned} C_{init}^{FB} &= \phi_{FB}\, Q_{FB,\max} \\ C_{init}^{CH} &= \phi_{CH}\, Q_{CH,\max} \\ C_{init}^{HP} &= \phi_{HP}\, Q_{HP,\max} \\ C_{init}^{EH} &= \phi_{EH}\, Q_{EH,\max} \end{aligned} \tag{3.10}$$

where the *f*-symbols denote the unit purchase cost of each device (all in CAD/W). As stated in 3.3, the initial costs are estimated using a constant unit purchase cost.

Next, the annual operational cost accounts for both electricity ($C_{op,e}$) and natural gas ($C_{op,f}$):

$$C_{op} = C_{op,e} + C_{op,f} \tag{3.11}$$

where the operational cost associated with natural gas can be calculated using

$$C_{op,f} = 3600 \frac{\lambda_f \nu_f}{LHV_f} \sum_{t=1}^{N} P_f(t) \Delta t \tag{3.12}$$

with λ_f being the unit fuel cost (in CAD/m^3), v_f, the specific volume (in m^3/kg), and LHV_f, the lower heating value of the fuel (in J/kg). The multiplication by 3600 is because *P* magnitudes are reported usually based on hourly rate. The electricity cost itself has two terms; one associated with the electricity consumption, and the other with the peak demand for each individual month:

$$C_{op,e} = \lambda_{e,energy} \sum_{t=1}^{N} P_e(t)\Delta t + \lambda_{e,peak} \sum_{month=1}^{12} \max\left(P_e(t)\right) \quad (3.13)$$

where $\lambda_{e,energy}$ (in CAD/Wh) and $\lambda_{e,peak}$ (in CAD/W) indicate the unit electricity costs for consumption and peak, respectively.

In sum, the decision variables of the optimization are the power consumption of the different pieced of equipment in Fig. 1 along with their efficiencies and capacities, i.e. $P_{e,HP}$, $P_{e,EH}$, $P_{e,CH}$, P_f, COP_{ec}^{HP}, η_{eh}^{EH}, COP_{ec}^{CH}, η_{fh}^{FB}, $Q_{HP,max}$, $Q_{EH,max}$, $Q_{CH,max}$, $Q_{B,max}$. The constraints of the optimization problem are summarized in Equations (3.2)-(3.5), in order to minimize the total cost shown in Eq. (3.9). There are also two other sets of constraints that will substitute Eq. (3.8) and (3.13) by Eqs. (3.15) and (3.16) respectively in order to linearize the problem.

3.4.3 Linearization

As observed in Eqs. (3.8) and (3.13), the model has two types of nonlinearities. The first one, which is reported in Eq. (3.8), is related to each equipment's part-load efficiency, which leads to a 3rd power of *P* in the problem formulation when used in combination with Eq. (3.3). The second nonlinearity comes from the max(*P*) function in Eq. (3.13). There are two main approaches to solve the model: using a nonlinear solver or linearize the model. In nonlinear optimization, it is a significant issue to find a global optimal solution while the linearized form of the same problem could help to obtain an approximated global optimal solution [98]. Although linearization introduces several additional constraints, binary and continuous variables, it tends to reduce computational time compared to the nonlinear model [94]. Therefore, the second approach is selected in this research, and is described below. In fact, we performed optimization runs with the proposed model and with an NLP solver, and found that the NLP solver was very slow and often did not converge at all. An example of such results is shown in Table 3.2 for a specific heating and cooling load profile (these are detailed below in Section 3.5). For the sake of comparison, the minimized cost and computational time assuming constant efficiency is also reported.

Table 3.2. Example of minimized cost and computational time for different formulations (NLP versus MILP versus constant efficiency), device with PLR efficiency and with $A_{mh} = A_{mc} = 40$ MW.

Method used	PLR efficiency	Cost (MCAD)	Calculation time (s)
Constant efficiency	-	144.59	0.73
NLP	boiler	145.80	635.31
	chiller	Not Converged	NA
	heat pump	144.71	542.75
	all	Not Converged	NA
MILP (Proposed in this work)	boiler	145.89	25.82
	chiller	144.96	9.82
	heat pump	144.70	12.26
	all	146.65	60.22

Linearization of the multiplication of power and PLE

As stated above, a 3rd order function is obtained by replacing the part-load efficiency profile of Eq. (8) into Eq. (3). Such function, $f(P)$ can be represented by

$$f(P) = \eta P = \eta_{nom}\left(\frac{2P^2}{P_x} - \frac{P^3}{P_x^2}\right) \tag{3.14}$$

To linearize this function, the first piece-wise linearization methods presented in [98] may be used. The basic concept of these methods is to break the nonlinear continuous function into a few pieces based on a sole variable, and then to approximate each piece by a separate linear function. It should be mentioned that P_x is not a decision variable as will be explained in Section 3.4.4. To begin the linearization, P is split into s breakpoints, $z_1 < z_2 < \cdots < z_s$. Then, the formulation of the linearization method used here is developed as

$$\begin{aligned}
&L(f(P)) = \sum_{j=1}^{s} f(z_j)\,\omega_j = \sum_{j=1}^{s} \eta_{nom}\left(\frac{2z_j^{\,2}}{P_x} - \frac{z_j^{\,3}}{P_x^{\,2}}\right)\omega_j \\
&P = \sum_{j=1}^{s} z_j\,\omega_j\,,\ \sum_{j=1}^{s}\omega_j = 1,\ \sum_{j=1}^{s}\gamma_j = 1 \\
&\omega_1 \le \gamma_1\,,\ \omega_s \le \gamma_{s-1} \\
&\omega_j \le \gamma_{j-1} + \gamma_j \ \ \forall\, j = 2,3,...,s-1
\end{aligned} \tag{3.15}$$

where $L(f(P))$ denotes the linearized form of the function $f(P)$. The linearized form is evaluated by an aggregate of the values of the nonlinear function in each breakpoint, z_j, multiplied by a new variable, ω_j, which is related to

P, as shown in this equation. This procedure involves s new binary variables, γ_1, γ_2 … γ_s. The computational time of the optimization depends heavily on s as in each linearization process, and for each time step, 7s constraints, s positive variables, and s binary variables are added to the optimization. If all four thermal machines are going to be PLE-based, for N number of time steps, 28s×N constraints, 4s×N positive, and 4s×N binary variables will be added to the optimization.

Linearization of max function

In this section, another binary variable, $K(t)$ [39], is defined to be non-zero when the peak demand of the electricity occurs (where K=1) once a month. It is zero for the remaining time steps of each month. Accordingly, we replaced $max(P_e)$ in Eq. (3.13) with a new decision variable, $P_{e,peak}$, which is a monthly-based variable, using

$$\begin{aligned} & P_{e,peak} \geq P_e(t) \\ & P_{e,peak} \leq P_e(t) + G\left(1 - K(t)\right) \\ & \sum_{t}^{month} K(t) = 1 \end{aligned} \tag{3.16}$$

by which the inferiority of $P_e(t)$ compared to $P_{e,peak}$ is always guaranteed. G denotes a large number, greater than the difference between the two extremes (highest and lowest) of $P_e(t)$ magnitudes. Hence, the nonlinearity of the problem is eliminated by introducing additional variables and linear constraints. To be precise, if N_m months and N time steps are to be used, 2N inequality constraints (the first and second equations of Eq. (3.16)), N_m equality constraints (last equation of Eq. (3.16)), N binary variables ($K(t)$), and N_m continuous variables ($P_{e,peak}$) are added to the optimization.

3.4.4 Overall calculation procedure and determination of P_x

This section describes how the model presented in Sections 3.4.1 and 3.4.2 is used to optimize the energy hub schematized in Fig. 3.1. Such modeling approach is illustrated in Fig. 3.3. The solution algorithm starts with all input constants and parameters. Then the right-hand side term of Eq. (3.13) is linearized using the method formulated in Eq. (3.16). Afterwards, we optimized the energy hub on a constant-efficiency basis so that the optimal capacities (Q_{max}), power $P(t)$ for chiller, boiler, and heat pump for all time steps, and P_{max} of each device over time were obtained. These capacities are used as the first guess for the iterative method detailed below. Next, the total number of devices of each type, α_{max}, was fixed. This value is achieved by dividing Q_{max} of each

device by the capacity of a single unit of that type. These unit capacities can be chosen as 10 MW FB, 10 MW CH, 1 MW HP units, and 1 MW EH units. These α_{max} values do not change over time.

Prior to performing the optimization, the ratio P_x/P_{max} is specified and remains fixed, thus characterizing the shape of the part-load efficiency curve for the equipment considered. In order to determine the efficiency at each time step from Eq. (3.8), it is necessary to know P_x alone, thus requiring the value of P_{max} to isolate P_x from the specified ratio P_x/P_{max}. However, P_{max} is a design variable (capacity of the equipment) resulting from the optimization. Therefore, we introduced an iterative method to handle this issue (the loop in Fig. 3.3). The value of P_x was then first guessed (P_{x1}), and the required number of devices in operation of each equipment at a given time, α(t), was obtained based on its maximum power consumption.

These initial values allowed us to run the PLE-hub optimization. To do so, it is first needed to linearize the 3rd order polynomial in Eq. (3.14) using Eq. (3.15). Since the number of devices in operation and the power magnitudes change over time, so does the PLE. Then the model is run to optimize the operational and design variables. The resulting optimal capacity (P_{max}) is used to update the value of P_x based on the initially specified ratio (P_x/P_{max}). This new P_x value is identified by P_{x2} in Fig. 3.3. The procedure is repeated by using this new P_x value until the error becomes small between two consecutive iterations, i.e. until $|P_{x2} - P_{x1}|$ becomes less than a definite threshold, δ, which is considered as 1 kW in this paper.

The CPLEX solver was used to solve the model. The typical computational time of optimization for the hub including only one part-load efficiency device was approximately one minute. The computer used had a CPU Core i7-10700T with 2.00 GHz and 16 GB of RAM.

To ensure the validity of the model, we tested the code under different conditions, particularly for cases in which the optimal solution was obvious. For example, the absence of a heating load should result in inactivity of FB, EH, and HP, while a similar effect is observed for CH, and HP in the case of zero cooling load. The cases with extremely high initial cost of HP and EH result in them not being selected. Large unit purchase cost of CH and FB leads to the highest practically possible capacities of HP. In the limits where $\lambda_{e,peak}$ increases, lower electricity consumption of all devices are predicted. Thus, HP tends to contribute as much as possible to cooling satisfaction while FB contributes to the heating supply.

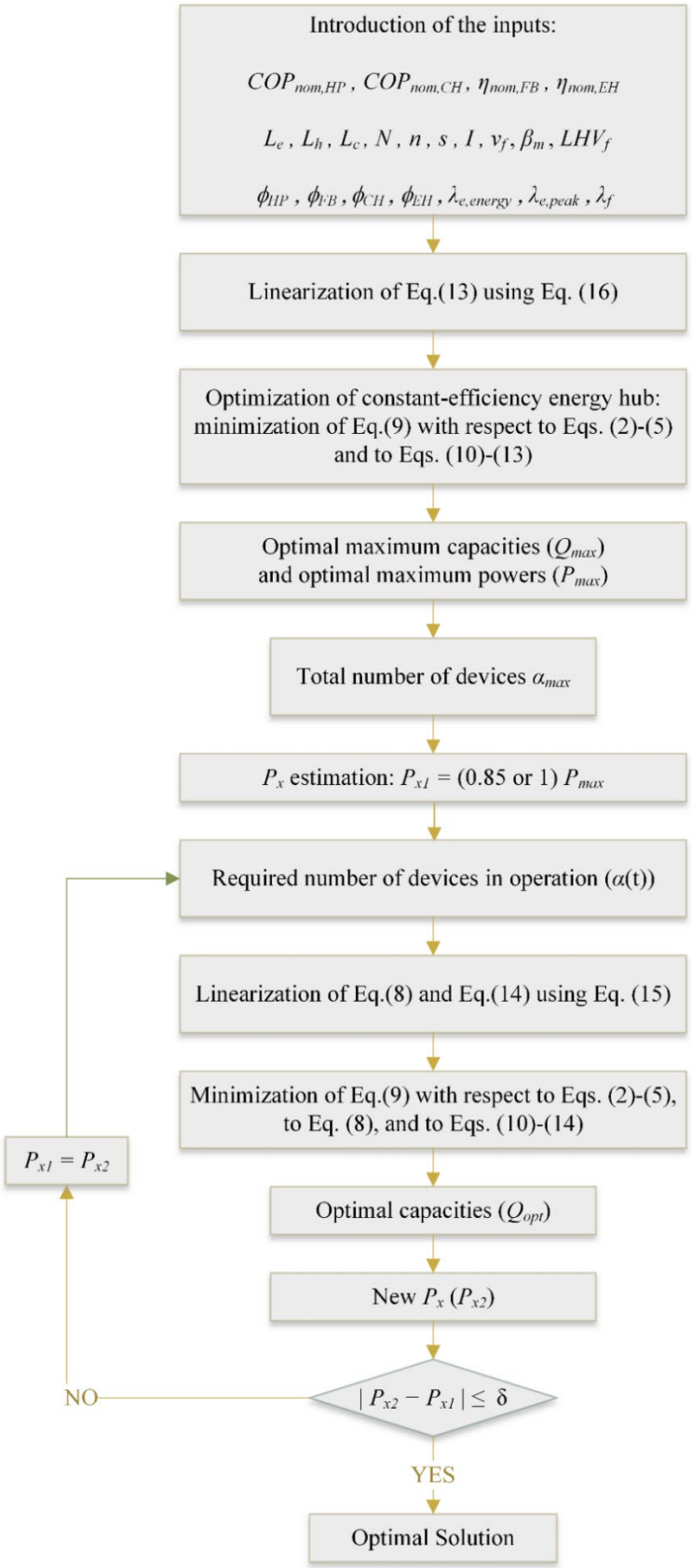

Figure 3.3. Flowchart diagram illustrating the entire modeling procedure, including the determination of P_x.

3.5 Load definition

Since the loads need to be known to run the optimization, we adopted a synthetic load function in this article:

$$L_x = \beta_{mx} A_{mx} + A_{dx} \sin\left(2\pi \frac{t}{\tau_d} + \theta_{dx}\right) \tag{3.17}$$

where x is replaced by either c for the cooling load or h for the heating load. τ_d denotes the number of hours in a day, i.e. 24 hours. Each load is characterized by four parameters A_{mx}, A_{dx}, β_{mx}, θ_{dx}. The first two indicate the maximum amplitude over a year-horizon, and the daily load amplitude, respectively.

In this work, we have chosen 6 sample days to estimate the performance of the entire year. Approximating yearly performance of energy systems using representative days is a simplification used vastly in the literature in order to reduce computational time. For instance in [71], [82], authors have evaluated the entire year operation of their system by three typical days (transition season, winter, and summer). One representative day of each season is used in [99]. In [100], only a typical day is chosen to verify the model, while in [78], 12 days are considered to represent the entire year (one day per month). Other studies using sample days for their modeling can be found in [17], [101]–[103].

Here, it is considered that each day represents a month, and that thermal loads are symmetrical with respect to time, so that the first 6 months are repeated over the subsequent 6 months. The yearly performance is obtained by summing the performance of each characteristic day multiplied by the number of days in that month. In this regard, the amplitude conversion factor, β_{mx}, is introduced in order to adjust the value of the load amplitude each month, as a fraction of its associated maximum yearly amplitude. Also, θ_{dx} denotes the phase shift of the daily load. The synthetic loads of Eq. (3.17) are acceptable approximations of real loads and they comply with the general trends of typical thermal demands. An advantage of synthetic loads is that they facilitate the study of the hub in a wide range of possible load scenarios. As shown in Fig. 3.4, the cooling load is minimal at the beginning of the year when heating demand is at its peak. As the middle of the year approaches, the cooling load increases while the heating need declines. Fig. 3.4 illustrates a case where A_{mh} is greater than A_{mh}, but different values can be chosen, as depicted in Table 3.3. It should be noted that the electricity cost corresponding to L_e is fully independent of the thermal loads because no power-generating equipment is used in the energy hub (see Fig. 3.1). Consequently, for the sake of simplicity, L_e is assumed to be constant in this study for the whole year, as shown in Fig. 3.4.

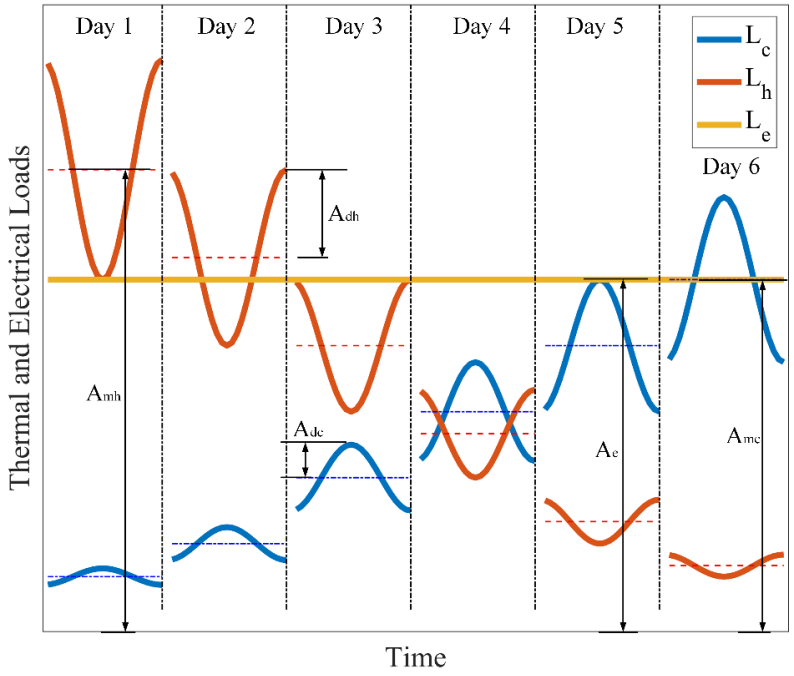

Figure 3.4. Schematic representation of the synthetic heating, cooling and electricity loads.

Table 3.3. Values of the fixed parameters in this work.

Parameter	Description	Constant value	Unit
N	Number of time steps	6×24 = 144	
η_{nom}^{FB}	Nominal efficiency of FB	0.85	
η_{nom}^{EH}	Nominal efficiency of EH	0.95	
$cop_{nom}^{HP,ec}$	Nominal efficiency of HP	5 [33]	
cop_{nom}^{CH}	Nominal efficiency of CH	5 [72]	
v_f	Specific volume of the fuel	1.4615	m^3/kg
LHV_f	Lower heating value of the fuel	48.949	MJ/kg
i	Interest rate	0.05	
n	Life time	10	Years
s	Number of breakpoints	6	
$\mathbb{Z}_{HP}$	Unit purchase cost of HP	230 [33]	CAD/kW
$\mathbb{Z}_{EH}$	Unit purchase cost of EH	217.5 [73]	CAD/kW
$\mathbb{Z}_{CH}$	Unit purchase cost of CH	114 [104]	CAD/kW
$\mathbb{Z}_{FB}$	Unit purchase cost of FB	88 [73], [75]	CAD/kW
$\lambda_{e,energy}$	Unit price of elec. consumption	0.0328 [36]	CAD/kWh
$\lambda_{e,peak}$	Unit price of elec. peak	12.90 [36]	CAD/kW
λ_f	Unit price of natural gas	0.15 [35]	CAD/m^3
A_{mh}, A_{mc}	Maximum yearly amplitude	0 to 40	MW
β_{mc} β_{mh}	Amplitude conversion factor	[0.1, 0.2, 0.4, 0.6, 0.8, 1] × A_{mc} [1, 0.8, 0.6, 0.4, 0.2, 0.1] × A_{mh}	
A_{dh} A_{dc}	Daily load amplitude	0.25 × β_{mh} 0.25 × β_{mc}	MW

3.6 Simulation procedure and simulation plan

In this section, we describe the methodology that was used to study the influence of the part-load efficiency profiles on operational parameters and cost. First, the impact of the part-load efficiency profile was studied one equipment at a time, keeping the efficiency of the other devices constant (i.e., not varying with load) and equal to their nominal values from Table 3.3. In each case, the optimization of the energy hub was performed for various combinations of the heating and cooling loads by varying their amplitudes (i.e., A_{mh} and A_{mc}). These amplitudes were both varied between 0 and 40 MW, by increment of 10 MW, and every possible combination was considered. The daily heating and cooling load amplitudes were maintained at 25% of A_{mh}, and of A_{mc}, respectively. Consequently, for each scenario, the hub was optimized for the 25 possible load profiles, yielding the optimal operational and financial parameters is each case. This procedure can be repeated for different ratios of P_x/P_{max}. Here, we considered two ratio values, i.e. 0.85 and 1. To observe the importance of using a part-load efficiency in the energy hub, we made a comparison between hubs optimized by using part-load efficiency curves and hubs optimized by assuming a constant efficiency (here called the reference energy hub or REH). In the REH, all energy convertors contribute to the thermal load satisfaction while operating at their nominal efficiencies. The result from the hub model with constant efficiencies can be seen as those that would be obtained from typical current models. Considering the 25 load combination scenarios, two P_x/P_{max} values, and three devices investigated (i.e., heat pump, fuel boiler and chiller) plus the reference hub (with constant efficiencies), more than 150 simulations were performed. Again, the value of the main parameters used for the simulations are listed in Table 3.3.

3.7 Impact of each PLE curve in the hub model

3.7.1 Fuel boiler

First, the impact of considering the part-load efficiency curve of the fuel boiler is studied by keeping the other efficiency values constant. Fig. 3.5 shows the resulting cost difference over 10 years introduced by the consideration of the part-load effiency curve of the boiler in the model for two values of the ratio $P_{f,x}/P_{f,max}$ (i.e., 0.85 and 1). Again, the comparison is against the reference energy hub in which the efficiencies are all held constant and is reported for various load combinations. In other words, the cost difference presented in Fig. 3.5 is represented by an “error” caused by assuming a constant boiler efficiency rather than a part-load curve in the hub model. Such error for the device *i* (i.e., fuel boiler, heat pump or chiller) is defined as

$$Error_i = \frac{C_{PLE,i} - C_{REH}}{C_{PLE,i}} \times 100 \tag{3.18}$$

where $C_{PLE,I}$ and C_{REH} stand for the total cost of the energy hub including the device *i* modeled with a PLE curve and the total cost of the REH.

It is apparent from Fig. 3.5 that this error is more sensitive to the heating load than to the cooling load. As the boiler capacity increases, the constant efficiency assumption leads to larger errors. Lower cost differences, however, can be observed on the right side of Figs. 3.5a and 3.5b. In principle, simultaneous heating and cooling loads will result in a higher employment of the heat pump [4]. Therefore, a lower capacity of the boiler is preferred by the optimization to allow larger heat pumps to supply a greater share of the thermal load. As discussed above, the lower the optimal boiler size, the lower the cost difference.

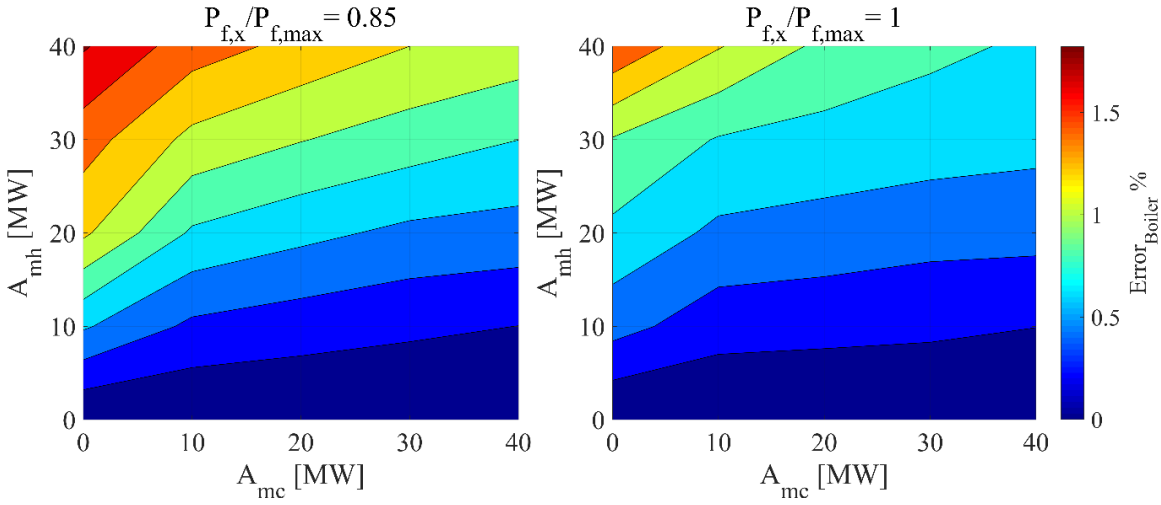

Figure 3.5. Total cost difference between the hub with a part-load efficiency model for the fuel boiler and the reference energy hub (REH) versus thermal load amplitudes for a) $P_{f,x}/P_{f,max}$ = 0.85 and b) $P_{f,x}/P_{f,max}$ = 1.

Neglecting part-load efficiency in the boiler model results in slightly larger errors for lower $P_{f,x}/P_{f,max}$ ratios, as observed by comparing Figs. 3.5a and 3.5b. This is owing to the fact that at peak heating demand where the highest contribution is required of the fuel boiler, its efficiency is not at its maximum for the case of lower $P_{f,x}/P_{f,max}$. If both thermal loads are high, heat pumps could be used to compensate such deficiency. Otherwise, it is electric heaters that have to be used so that the heating peak is satisfied. On the other hand, as can be seen in Fig. 3.2, the boiler tends to be more efficient for most power values when $P_{f,x}/P_{f,max}$=0.85 than when it is equal to 1. As a result, the optimal solution in the former situation requires a slightly smaller boiler and less fuel. Therefore, there are two factors here which act in opposite directions. For instance, the highest error in these two figures occurs at [A_{mh}, A_{mc}]=[40,0]. At that point, the case $P_{f,x}/P_{f,max}$=1 uses fuel boilers costing 0.14 MCAD more to purchase,

and also consume 0.53 MCAD more natural gas while no electric heater is used. The case $P_{f,x}/P_{f,max}$=0.85, nevertheless, needs an electric heater, as discussed above. That costs 0.33 MCAD to purchase, and 1.61 MCAD for electricity. Consequently, the latter is 1.27 MCAD more expensive than the former.

3.7.2 Chiller

The cost difference between the model using PLE chillers and the reference hub are depicted in Fig. 3.6, for $P_{CH,x}/P_{f,max}$ of 0.85 and 1. Contrary to the PLE boiler, the error produced from a constant efficiency assumption for the chiller is more sensitive to A_{mc}. This is because of the use of larger chillers that are required to satisfy higher cooling demands. On the other hand, the error decreases with respect to A_{mh} when A_{mc} is held constant. This is due to the higher contribution of the heat pump to satisfy the cooling load. That also justifies why a lower cost difference is observable for simultaneously high heating and cooling loads.

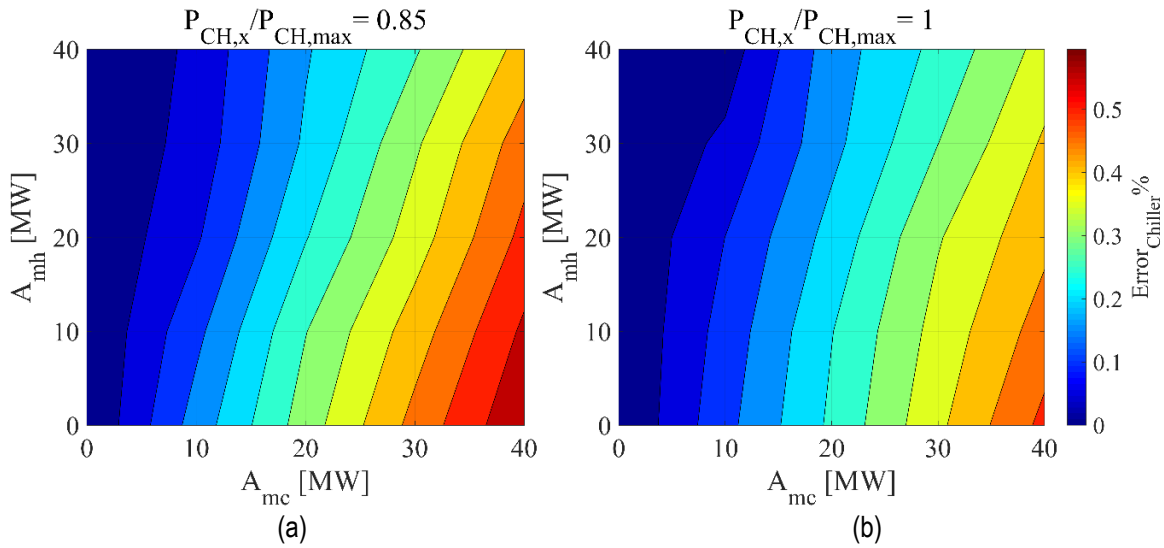

Figure 3.6. Cost difference over 10 years between the hub with a part-load efficiency model for the chiller and the reference energy hub (REH) versus thermal load amplitudes for a) $P_{CH,x}/P_{CH,max}$ = 0.85 and b) $P_{CH,x}/P_{CH,max}$ = 1.

Furthermore, the errors associated with $P_{CH,x}/P_{CH,max}$=1 (right-hand side of Fig. 3.6) are lower than those obtained with $P_{CH,x}/P_{CH,max}$=0.85 (left-hand side of Fig. 3.6). Similarly to what happened with boilers in Section 3.7.1, the chillers tend to be slightly smaller and use less electricity when $P_{CH,x}/P_{CH,max}$=0.85 than when this ratio is equal to 1. However, the former needs to consume higher electricity at cooling peaks since it does not operate with its nominal efficiency during those peak moments. That results in a penalty peak cost of 0.19 MCAD for the case $P_{CH,x}/P_{CH,max}$=0.85 at the point where the maximum error is reported, i.e. [A_{mh}, A_{mc}]=[0,40].

3.7.3 Heat pump

Since the heat pump has been implemented in the energy hub specifically to integrate the cooling and heating networks [4], its optimal capacity increases when both thermal demands increase simultaneously. This explains the behavior of the curves in Fig. 3.7. The larger the heat pump, the bigger the error generated by assuming a constant efficiency. However, the order of magnitude of the error introduced by assuming a constant efficiency for the heat pump is lower than for the boiler or chiller. This is due to lower purchase costs of the heat pump compared to the two other devices. The biggest error occurs at [A_{mh}, A_{mc}]=[40,40] for the heat pump. Again here, although bigger heat pumps are to be used for $P_{HP,x}/P_{HP,max}$=1, lower contributions of chiller and fuel boiler to thermal satisfaction is required. That lowers the total cost of this case by 0.11 MCAD compared to the other.

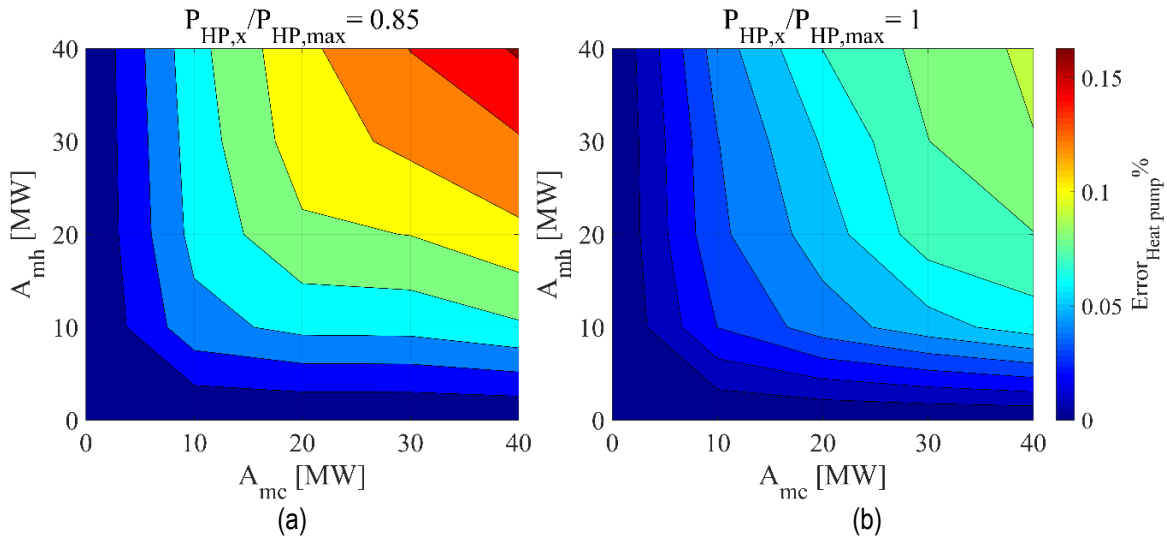

Figure 3.7. Cost difference over 10 years between the hub with a part-load efficiency model for the heat pump and the reference energy hub (REH) versus thermal load amplitudes for a) $P_{HP,x}/P_{HP,max}$ = 0.85 and b) $P_{HP,x}/P_{HP,max}$ = 1.

3.8 Errors resulting from the assumption of PLE curve for all devices

In the previous section, we studied the impact of the part-load efficiency curve of each device one at a time in the hub model. Now, we present results obtained when all the energy convertors in the hub follow a part-load efficiency curve. It should be mentioned that simulating such a hub is quite demanding computationally due to the high number of decision variables resulting from the linearization of the problem. Hence, it was decided to

perform the optimization of the hub in that case only for the three aforementioned load scenarios for which the errors were maximal (i.e., [A_{mh}, A_{mc}] = [40,0], [0,40], and [40,40] respectively when the influence of the fuel boiler, chiller and heat pump PLE curves were studied in Section 3.7). The cases that were tested are listed in Table 3.4. The default value for P_x/P_{max} was set to 1 for all devices. Additionally, we tested scenarios in which P_x/P_{max} was 0.85 for specific pieces of equipment, while the other parts used PLE profiles corresponding to P_x/P_{max}=1. The total cost difference was calculated as previously, by comparing results to the REH (i.e., hub optimized with constant efficiency).

Table 3.4. Scenarios considered to optimize the hub with all equipment with PLE curves.

Load, MW [A_{mh}, A_{mc}]	P_x/P_{max} value for boiler	P_x/P_{max} value for chiller	P_x/P_{max} value for heat pump
[40,0]	0.85 and 1	1	1
[0,40]	1	0.85 and 1	1
[40,40]	1	1	0.85 and 1

3.8.1 Fuel boiler

The load [A_{mh}, A_{mc}] = [40,0] yielded the largest error when the boiler was modeled with a constant efficiency rather than a part-load efficiency (See Section 3.7.1). As mentioned above, this specific load was thus retained in this section but this time, assuming all devices operating with a PLE. Figure 3.8a shows the optimal PLE value at the different hours (and days) of operation, and Fig. 3.8b indicates the fuel consumption versus time for which the efficiency of the boilers is represented by different colors at each hour. Since higher heating demand is needed in the first day (see Fig. 3.4), higher fuel consumption is observed (Fig. 3.8b). Therefore, the first day requires all boiler units to be in operation (in this case 10 boilers of 5MW capacity), while the following days call for fewer units to function as the heating demand decreases, i.e. 8, 6, 4, 2, and 1 boilers respectively, for both ratios. Using several units of the same device allows the optimization to keep the efficiency of the equipment high even for the low demand periods, as can be seen in Fig. 3.8a.

Based on the results of Section 3.7.1, the boilers with $P_{f,x}/P_{f,max}$=0.85 uses less natural gas for the same load. The total cost of the energy hub corresponding to the curve of $P_{f,x}/P_{f,max}$=0.85 & 1 is 135.55, and 134.21MCAD. If compared to the cost of REH with these loads (132.90 MCAD), a cost difference (error) of 2.56 MCAD appears or 1.9% for the ratio of 0.85. This is nearly the same error observed when only the boiler was modeled with PLE (1.85%) in Section 3.7.1. The case with $P_{f,x}/P_{f,max}$=1 results in an error of 1.31 MCAD or 0.97%. The dashed circles displayed in Fig. 3.8b show the regions where the boilers possessing $P_{f,x}/P_{f,max}$=0.85 cannot supply the

required heating load, and since no heat pump can be used (as no cooling load is demanded), the system has to rely on electric heaters during these moments.

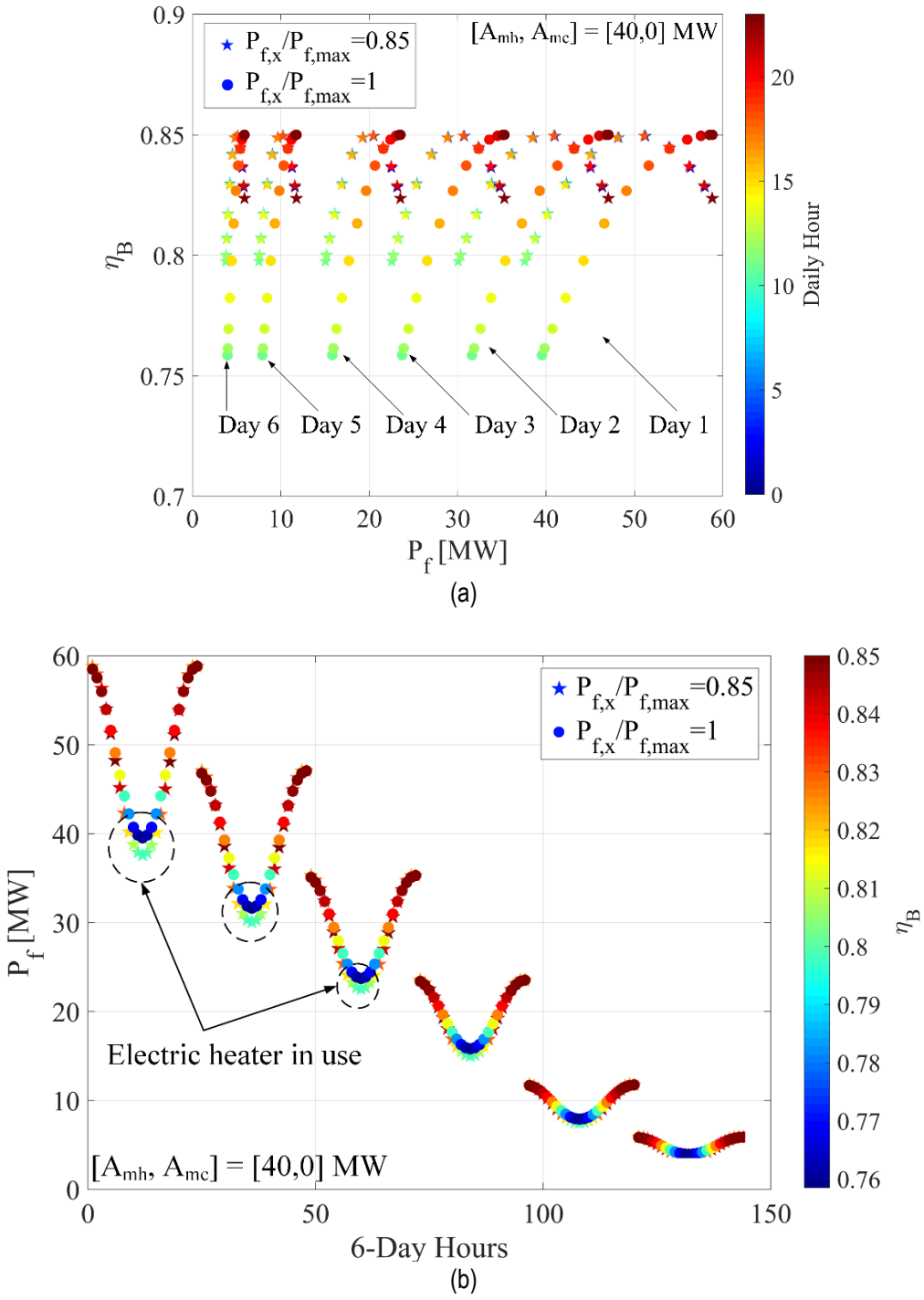

Figure 3.8. Boiler's part-load efficiency for two different values of $P_{f,x}/P_{f,max}$ versus a) fuel power consumption and b) time.

3.8.2 Chiller

The other worst case load scenario, [A_{mh}, A_{mc}]=[0,40] MW, is when the hub using only PLE chillers would generate the largest error. For this load with all part-load efficiency devices, the optimized PLE of the chillers is illustrated in Fig. 3.9. In contrast to Fig. 3.8, lower power magnitudes correspond to the first days, and vice versa, as expected from Fig. 3.4. The first days, therefore, need the minimum number of chillers in operation (1 chiller of 5MW capacity), and the following days use 2, 4, 6, 8, and 10 chillers, for both $P_{CH,x}/P_{CH,max}$ values.

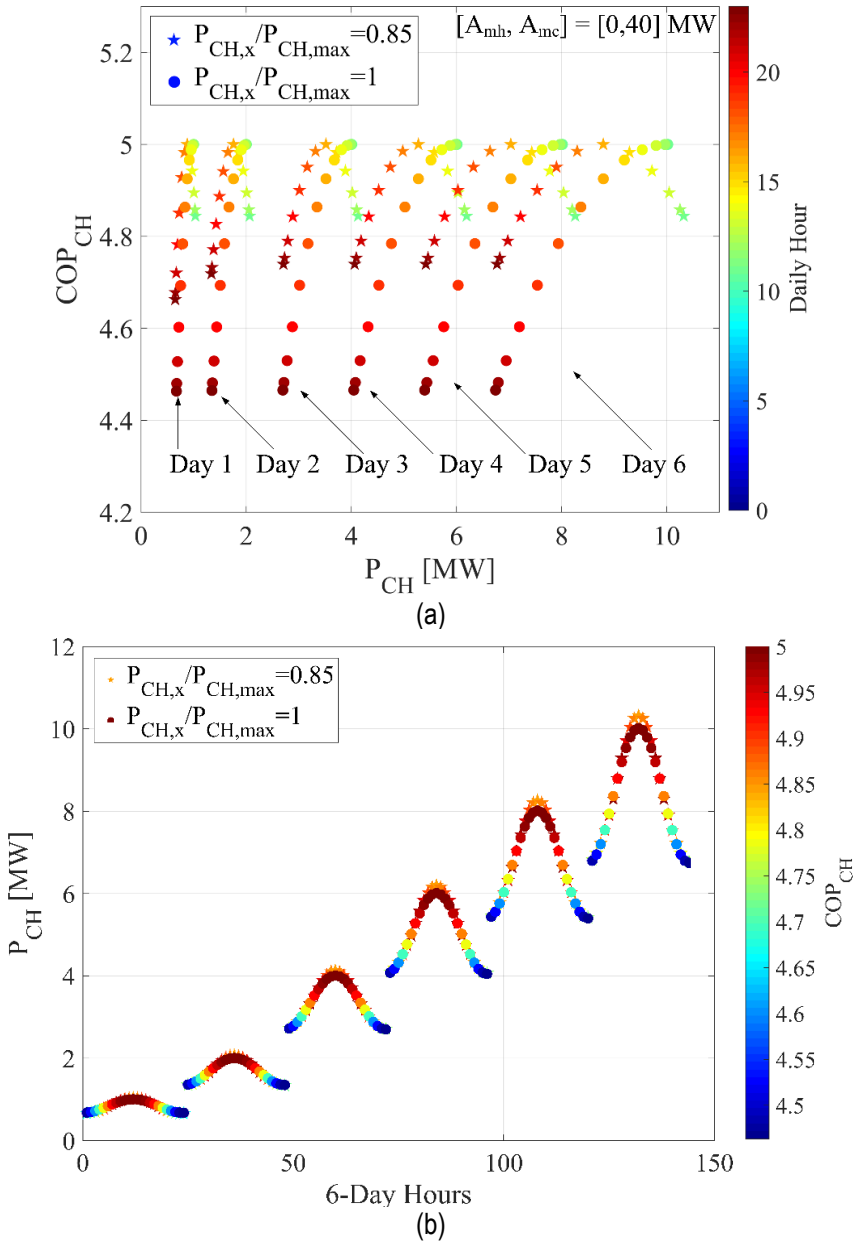

Figure 3.9. Chiller's part-load efficiency for two different values of $P_{CH,x}/P_{CH,max}$ versus a) electric power consumption of the chiller and b) time.

The minimized total cost for the case $P_{CH,x}/P_{CH,max}$=0.85 is 123.83 MCAD, which leads to errors of 0.71% if compared to the cost of REH with these loads (122.95 MCAD). The error in the case $P_{CH,x}/P_{CH,max}$=1 is 0.63 MCAD or 0.51%. These values reveal that the error generated by considering only the chillers as a PLE equipment (0.6%) is close to that of the PLE energy hub.

3.8.3 Heat pump

Finally, the maximum error of the PLE heat pump was reported for the load [A_{mh}, A_{mc}]=[40,40] MW. If all energy convertors of the energy hub function on a PLE basis, the PLE heat pump behaves according to what is indicated in Fig. 10. Here, from the first to the last day, there are respectively 1, 2, 3, 3, 2, and 1 heat pumps in operation with a 5MW capacity.

As discussed above, the performance of the heat pump depends heavily on the simultaneous existence of both thermal loads. This explains the reason for higher power values occurring on days 3, 4 and lower ones on days 1, 6 (see Fig. 3.4). The contribution of heat pumps in the thermal supply is always limited to the minimum of the cooling and heating loads [4]. Considering the load profiles in Fig. 3.4, this explains why the highest efficiency occurs during day 3 (see Fig. 3.10a). This is also why the profiles of days 1 and 2 resemble the cooling load and the ones of days 4, 5, and 6 mimic the heating load. Therefore, the dashed circles in Fig. 3.10b, represent the power consumption of the heat pumps where maximum heating and minimum cooling (minimum electricity) are demanded. Since the heat pump cannot function with high power and efficiency at those points, the electric heater has to supply a portion of the heating demand.

With the load [A_{mh}, A_{mc}]=[40,40] MW, 146.65 MCAD is the minimized total cost for the case $P_{HP,x}/P_{HP,max}$=1, and 146.52 MCAD is the cost associated with $P_{HP,x}/P_{HP,max}$=0.85. Comparing the total cost with that of the REH (144.5 MCAD), and evaluating the error yields approximately 1.49%, and 1.4%, respectively for the ratios of 1 and 0.85. These are considerably higher than the 0.16%, and 0.1% value that resulted from optimizing the energy hub with only PLE heat pumps.

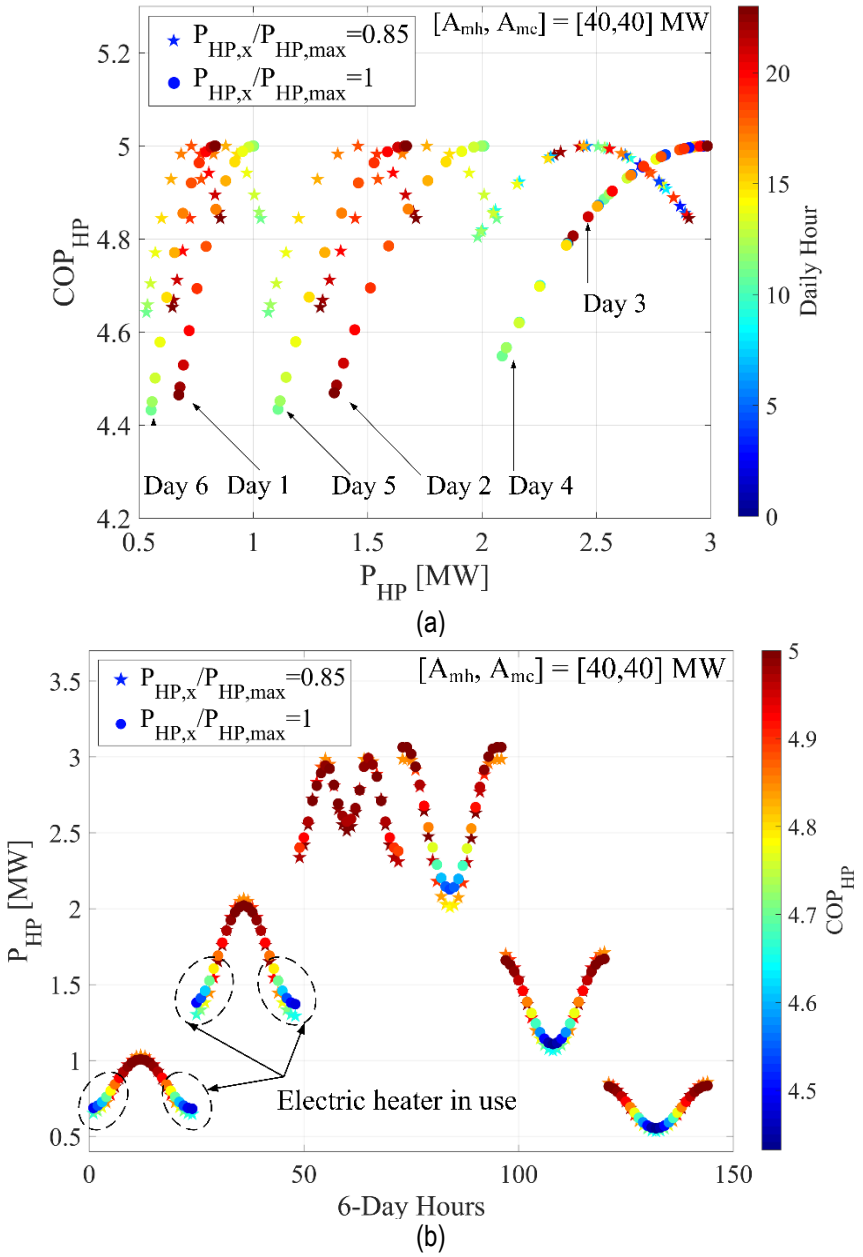

Figure 3.10. Heat pump's part-load efficiency for two different values of $P_{HP,x}/P_{HP,max}$ versus a) electric power consumption of the heat pump and b) time.

3.9 Interpretation of errors

As explained before, there are neither TES nor electricity-generation units in the energy hub studied in this chapter. In addition, L_e is assumed constant in this work. Therefore, the errors can also be computed when both cost values in Eq. (3.18) exclude the cost of L_e. Here, to better understand the significance of the error values, a comparison of the errors is made in Table 3.5. These errors are measured with respect to different cost basis.

If the errors are calculated based on thermal-satisfaction (HVAC) cost, they have higher magnitudes since the HVAC cost calculation does not include the cost of L_e.

Table 3.5. Error magnitudes based on Total and HVAC costs.

Variable Efficiency	$[A_{mh}, A_{mc}]$	P_x/P_{max}	Error based on Total cost (%)	Error based on HVAC cost (%)
Only fuel boiler (Figure 3.5)	[40,0]	0.85	1.85	7.71
		1	1.35	4.05
Only chiller (Figure 3.6)	[0,40]	0.85	0.60	2.6
		1	0.51	1.91
Only heat pump (Figure 3.7)	[40,40]	0.85	0.16	0.85
		1	0.10	0.61
All equipment with PLE curves with a focus on fuel boiler (Figure 3.8)	[40,0]	0.85	1.91	7.66
		1	1.40	4.05
All equipment with PLE curves with a focus on chiller (Figure 3.9)	[0,40]	0.85	0.71	3.25
		1	0.51	2.08
All equipment with PLE curves with a focus on heat pump (Figure 3.10)	[40,40]	0.85	2.60	7.03
		1	3.05	9.73

As expected, all values of errors calculated based on HVAC cost are considerably higher than those based on the total cost. Nevertheless, it is hard to conclude whether these errors are high or low. This depends on the application and required level of modeling accuracy. Nevertheless, they can be compared to one another or can just be considered as hints for pre-design stage so that one could estimate the probable errors of considering constant-efficiency devices in the energy hubs of synergetic heating and cooling systems.

3.10 Conclusions

In this article, we proposed a framework to minimize the total cost of an integrated cooling and heating network equipped with devices characterized by part-load efficiency curves. To this end, an iterative method was developed in order to optimize not only the design and operational characteristics of the hub, but also the efficiency profile under various combinations of thermal loads. The energy hub comprised natural gas boilers, chillers, electric heaters, and heat pumps. Its behavior was studied under different combinations of thermal loads. Looking back at Table 1 which summarized several recent publications, it can be seen that the method used in this work to consider PLE curves is comparable to other MILP approaches in terms of computational time, but

with the advantage of including more time steps and considering purchase costs of new devices added to the hub.

The model allowed to document how the PLE curves affect the design, performance and integration of combined heating and cooling network systems, a specific class of systems which is marginally present in Table 1. First, the influence of considering each device part-load efficiency curve on operation was investigated while the other components were functioning at constant efficiency. For each device, this study revealed which thermal load combinations would result in the largest error as a consequence of the assumption of a constant efficiency. The constant efficiency boiler, chiller, and heat pump led to maximum errors of 1.85%, 0.6%, and 0.16% with loads of [A_{mh}, A_{mc}]=[40,0], [0,40], [40,40] MW, respectively, compared to models with PLE curves. These conclusions can be used by modelers to decide on how to model device efficiency in heating and cooling networks, depending on the required precision and load profile considered. The large range of load profiles tested in this paper allows to assess the impact of PLE curves on the performance of combined heating and cooling networks straightforwardly with the figures provided.

These thermal demand combinations were then chosen to examine the case in which all convertors operate with a PLR efficiency. The errors augmented to 1.9%, 0.71%, and 1.49% this time. It may be concluded that the consideration of constant-efficiency operation under simultaneous high thermal demands could result in errors of approximately 1.49%, while the errors are higher if heating and cooling loads do not occur at the same time, due to the presence of heat pumps connecting the hot and cold loops. Again, these errors can guide the development of future models of combined heating and cooling networks in terms of how to account for PLE curves in accordance with the purpose of the model.

The model that was developed relies on a series of assumptions, which are important to recall since they can affect the results presented here. For example, although the variation of efficiency due to part-load operation was included, the impact of environmental conditions (e.g., outdoor temperature [105]) on the efficiency of chillers could also be integrated in future models. Transient variations of efficiency due to fouling, wear and tear, leakage, stop/start commands, etc., could also be considered in the future. Even though the number of time steps in the models was higher than in most studies with similar computational times, it is still a challenge to simulate large numbers of time steps (e.g., 8760 hours of the year) without a sharp increase of the computational time. The synthetic load profiles and efficiency curves allowed to analyze the behavior of the system in a large number of scenarios, but it would also be interesting to test the method with real data.

As previously explained, combined heating and cooling networks or thermal grids being so widely used in practice, they are an appealing system to optimize and integrate thermally in order to have a strong environmental and economic impact for multiple users. In future work, it would be interesting to develop other

integration strategies than the use of heat pumps. Literature presents many studies of highly complex hubs, generally with electricity production and several interconnected devices forming a large-scale system. Thermal grids are often smaller-scale systems, but their integration into a larger energy system, when physically possible, could also be looked at. In that context, the present model could be tested with more and more devices to better assess its limits in terms of computational times and convergence as the hub gets more complex.

Acknowledgments

This work was supported by the Natural Sciences and Engineering Research Council of Canada (NSERC).

Conclusions

Cooling and heating networks are among the most widely used energy systems. Thermally integrating them with heat pump is a practical way to improve their energy efficiency. The challenge to properly design such a system for it to be economically viable and yield as much GHG emission reduction as possible is quite complex and there is a lack of tools to do so in practice. In this work, we introduced an energy hub model to optimize the design and operation of a synergetic cooling and heating network. For simultaneous heating and cooling targets where electricity generation is not required (cheap electricity from grid), the utilization of heat pump was studied. The system included a chiller, an electric heater, a natural gas boiler and heat pumps. Specifically, we focused on the waste heat recovery provided by the heat pumps. The objective functions that were considered are the total cost and the CO_2 emissions. After that, the optimal implementation of heat and cold storage units in the same energy hub was studies. A model simulating its operation determined how different thermal load profiles should be satisfied by the different pieces of equipment to minimize the total cost. It also finds the optimal size of the thermal storage units and of the heat pump. Next, we assessed the impact of part-load operation of the energy hub's facilities, individually or collectively, on the total cost of an energy hub. The boiler, chiller, and heat pump's performance on constant-efficiency basis led to the maximum errors of 1.85%, 0.6%, and 0.16% corresponding to $[A_{mh}, A_{mc}]$=[40,0], [0,40], [40,40] MW, respectively, compared to their constant-efficiency operation. We introduced a MILP formulation for minimizing the lifetime cost of integrated heating and cooling networks while considering PLR efficiency. We show the error introduced by assuming a constant efficiency and the impact of using PLR efficiency on the results. The performance of the system was tested for an extensive range of thermal load combinations. In the end, for an industrial workshop with slightly higher temperatures than residential or commercial sectors, the feasibility of using absorption chiller, local heating, and local hot water production were examined.

The contributions of this investigation can be briefly summarized as follows:

- The energy hub concept was successfully adapted for the optimization of combined cooling and heating networks with heat pumps. We were able to achieve a linear model that solved relatively fast and that could provide a significant insight on the optimal features of the system;

- In the different scenarios investigated, the use of heat pumps to recover heat from the cooling loop always proved to be beneficial in terms of both cost and emissions. The heat pump optimal capacity is around 80% of the thermodynamic maximal value based on the load analysis.

- A theoretical analysis of the system was performed and was able to provide the correct order of magnitude for the optimal sizing of the heat pump. By comparing the analysis to the formal optimization results, we obtained correlations that can be used to easily size the heat pump system.

- The results were shown to be in line with current literature and help to fill the lack of knowledge on optimized synergetic heating and cooling networks. The figures and correlations that have been developed in this work can serve as straightforward design tools for practice engineers to properly size and operate such systems.

- The weighted sum average method allowed generating a Pareto front when minimizing simultaneously cost and GHG emissions. A relatively sharp transition between two families of solutions was noted at the point when electricity becomes more viable an option than gas for heating in the combined objective function as more emphasis is put on CO_2 than on cost.

- Different scenarios were considered to evaluate the usefulness of the TES units by varying the load amplitudes, capacity of the boilers and chillers, and purchase cost of TES units. TES units were found to be financially profitable when working with heat pumps in all cases, but some parameters of the scenarios were more influential than others on the benefits generated by TES. The different figures that were presented in chapter 2 can be used to evaluate at a glance the potential of using TES in a given situation.

- A framework is proposed to minimize the total cost of an integrated cooling and heating network equipped with devices characterized by part-load efficiency curves. I this regard, an iterative method was developed in order to optimize not only the design and operational characteristics of the hub, but also the efficiency profile under various combinations of thermal load.

As for every research, this one is also based on some simplifying assumptions and limitations that could be addressed in future work:

- The energy hub here, is comprised of natural gas-fired and electric boilers, electric chillers, heat pumps, and TES units. However, integrating renewable energy (PV, etc.) or geothermal energy could be taken into account in order to reveal a more general view of combined thermal networks modeled via energy hub concept.

- TES operation as a member of integrated thermal network, and its benefits was solely studied for the energy hubs under constant efficiency. Although the effect of PLE curves was estimated for the combined cooling and heating energy hub in the 3rd article, TES was absent in that network. Therefore, such assessment could also be performed while PLE curves of TES are considered.

- The thermal integration in this network was only executed via heat pumps. In future works, it would be interesting to develop integration strategies other than the use of heat pumps. Literature presents many studies of highly complex hubs, generally with electricity production and several interconnected devices forming a large-scale system. Thermal grids are often smaller-scale systems, but their integration into a larger energy system, when physically possible, could also be looked at. In that context, the present model could be tested with more and more devices to better assess its limits in terms of computational times and convergence as the hub gets more complex. For instance, the inclusion of CCHP, battery storage units, absorption chillers, etc. could be considered.

- The workshop introduced in APPENDIX A can be used as a case study for future work focusing on energy hubs benefitting from thermal network integration. The energy hub method could be employed for modeling and optimization of the energy systems detailed in section 4 while minimizing cost, CO2 emission, or other parameters.

- The general equation used to model PLE curves of devices in the 3rd paper was a 2nd order polynomial. Although the comparisons made between this approach and the relevant pieces of research in literature affirmed its capability of being PLE representative, other general mathematical formulations could be examined.

- The effect of ambient pressure and temperature on the efficiency of the devices included in the hub have not been evaluated. Future analyses could also take those parameters into account in order to more-precisely model the devices.

APPENDICES

Appendix 1 EVALUATING THE HEAT REJECTION OF THE WORKSHOP OF A MANUFACTURING PLANT AND INTRODUCING WASTE HEAT RECOVERY SOLUTIONS

A1-1 Résumé

Le potentiel de récupération de chaleur perdue (WHR) d'un atelier de fabrication a été évalué. Dans un premier temps, les sources de chaleur résiduelle ont été identifiées et évaluées, ce qui a conduit à la préparation d'une carte de chaleur résiduelle pour l'entreprise. Par la suite, trois principales méthodes WHR ont été choisies pour l'usine, comme suit. Pour les étés, la possibilité de remplacer les refroidisseurs actuels de bureaux par un refroidisseur à absorption simple effet de 52 kW a été étudiée, ce qui coûterait 8,000 CAD de plus que les refroidisseurs actuels sur 20 ans. Pour les hivers, le flux de chaleur résiduelle conditionné peut être utilisé à des fins de chauffage local au lieu d'utiliser les systèmes de chauffage électrique actuellement utilisés, ce qui permettrait d'économiser environ 110,000 CAD sur 20 ans. Pour le reste de l'année, la consommation interne d'eau chaude de l'entreprise peut être fournie en utilisant un chauffe-eau hybride (WHR + électricité), ce qui permettrait d'économiser environ 2,000 CAD sur la même période.

A1-2 Abstract

The waste heat recovery (WHR) potential of a manufacturing workshop was assessed. First, the sources of waste heat were identified and evaluated, leading to preparation of a waste heat map for the company. Subsequently, three main WHR methods were chosen for the plant, as follows. For summers, the possibility of replacing the current office chillers with a 52 kW single-effect absorption chiller was investigated, which would cost 8,000 CAD more than the present chillers over 20 years. For winters, the conditioned waste heat flow can be used for local heating purposes instead of using the electric heating systems currently used, which would save approximately 110,000 CAD over 20 years. For the rest of the year, the internal hot water consumption for

the company can be supplied by using a hybrid (WHR + electricity) water heater, which would save around 2,000 CAD over the same period.

A1-3 Introduction

The industrial sector is the main energy consumer in Quebec, accounting for 38% of all energy consumed. However, studies show that between 20 to 50% of the energy consumed in industry is lost in the form of waste heat. It is therefore an important source of potential energy savings that can be exploited. Although the field of machining has been the subject of some work related to its energy consumption, no study has been listed on the energy integration potential that it offers.

As mentioned, 38% of the annual energy consumption in Quebec is used for industries, making it the most energy-intensive sector compared to transportation, residential and commercial [106]. According to the US Department of Energy, it is estimated that between 20 and 50% of the total energy input in the industrial sector is lost in the form of thermal releases to the environment [107]. The numbers are similar here in Canada. This industrial waste heat represents a huge potential "reservoir" for energy savings and greenhouse gas emissions reduction. Currently, industrial waste heat is often non-exploited. Several factors can explain why: lack of knowledge of the industry on its own waste heat and their potential for recovery, low quality of waste heat, interference with industrial processes, high associated capital cost, etc.

The case study is an avant-garde company specialized in high precision machining. Located in the Parc Technologique de Québec. The main plant of the company occupies about 2000 m^2 and is in full expansion. It will double its area in 2019-2020 as part of an expansion project. The equipment used in the plant generates a lot of heat that for the moment is simply dissipated to the environment.

Although various studies have recently focused on energy in the manufacturing sector, including machining, no study has paid detailed attention to the heat rejection of the computer numerically controlled (CNC) machining process nor to a workshop. In this regard, understanding how much heat is rejected from a manufacturing plant including machining equipment is important since heat rejection is not negligible, especially when the focus is on designing a ventilation system for the plant. Therefore, there is a need for developing the state of knowledge in order to better understand the energy performance of a workshop, the potential use of its heat rejection, and the possibilities of thermal integration and improvements of energy efficiency. Accordingly, the current study addressed the above-mentioned challenges.

To this end, this study aimed to improve the energy performance of a workshop by recovering waste heat. The specific objectives of this report are as follows: (i) Performing a detailed mapping of energy consumption and heat dissipation, (ii) Analyzing heat loss flows in the workshop; (iii) Conducting a feasibility analysis of the WHR potential and its method for the workshop of the company.

A1-4 Methods for calculating the heat rejection of each machine

A1-4-1 Energy budget

The principal energy consumers of a CNC unit are different spindle motors, chiller, ejector, cutting oil refining systems with their associated motors and pumps, control box, lightings, fans, computer, etc., as indicated in

$$\dot{E}_{in} = \underbrace{\dot{Q}_{w,CH} + \dot{Q}_{w,EC} + \dot{Q}_{w,Ej}}_{Waste\ heat} + \dot{E}_{spl} + \dot{E}_{l,\Delta P} + \dot{E}_{l,other} \quad \text{(A1.1)}$$

where E_{in}, $Q_{w,CH}$, $Q_{w,EC}$, $Q_{w,Ej}$, E_{spl}, and $E_{l,\Delta P}$ represent the entire electricity input to the machine, waste energy of the chiller, electric cabin, ejector, power consumption of the spindle, energy loss associated with the cutting-oil pumps, respectively. In addition, $E_{l,other}$ indicates the other sources of energy dissipation within the machine (e.g., lightings, fans, chip removal belt motor, etc.). An illustration of the power breakdown of CNC units is shown in Figure A1.1 based on the introduced items in Eq. (A1.1).

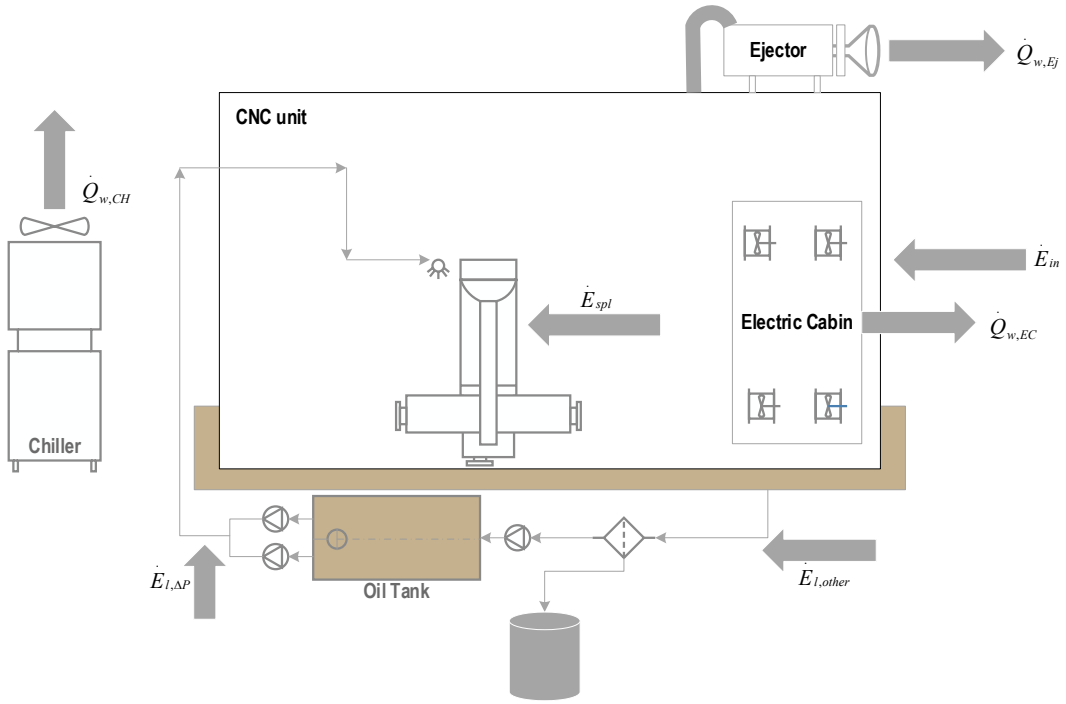

Figure A1.1. Power breakdown of a typical CNC machine according to energy conservation law.

A1-4-2 Calculations

The machine plate depicts the required electricity of the machine. It should be noticed that the electricity written on the plate is the entirely required electricity for the machine operation. Thus, the electricity consumption of the spindle, chiller, and other equipment are included in this number. The waste heat of the chiller can be calculated via:

$$\dot{Q}_{w,CH} = \dot{Q}_{Cooling,CH} + \dot{E}_{el,CH} \tag{A1.2}$$

where $Q_{cooling,CH}$ and $E_{el,\,CH}$ denote the cooling capacity and the electricity usage of the chiller, respectively. The heat dissipation of the electric cabin (the control box) of the CNC unit can be assessed by

$$\dot{Q}_{w,EC} = n\,\dot{V}_{fan}\,\rho_{air}\,C_{p,air}\left(T_{e,air} - T_{i,air}\right) \tag{A1.3}$$

where n and V_{fan} represent the numbers and the volumetric flow rate of each fan. The density, specific heat capacity at constant pressure, the outlet, and inlet temperatures of the air are indicated by ρ_{air}, $C_{p,air}$, $T_{e,air}$, and $T_{i,air}$, respectively.

The volumetric flow rate of each fan is approximately 500 m^3/h for most installed machines. The air density and specific heat capacity can also be estimated as 1.2 kg/m^3, and 1.006 kJ/kg ˚C, respectively. Furthermore, the input and output temperatures are measured as 20-22 and 30-32 ˚C. The results of Eq. (A1.3) are 1.7 and 3.53 kW for the waste heat associated with the electric cabins owning to one or two fan(s), respectively. The ejector waste heat calculation is similar to that of the electric cabin as shown by:

$$\dot{Q}_{w,Ej} = \dot{V}_{Filter}\, \rho_{air}\, C_{p,air} \left(T_{e,air} - T_{i,air} \right) \tag{A1.4}$$

where V_{filter} denotes the volumetric airflow rate passing through the filter of the upper-mounted ejector of the machine and is evaluated by 747 CFM (ft^3/min) or 0.352545 m^3/s [108]. The other parameters of Eq. (A1.4) are the same as those of Eq. (A1.3). Thus, the waste heat of the ejector is estimated to be 3.38 kW.

The pump mechanical power consumption is principally approximated by the product of the pressure difference of the liquid and the flow rate as:

$$\dot{W}_{Mech,pump} = \dot{V}\, \Delta P \tag{A1.1}$$

which must be divided by the mechanical and electrical efficiencies of the pump to yield the real power consumption of the pump, i.e.:

$$\dot{E}_{l,\Delta P} = \frac{\dot{V}\, \Delta P}{\eta_{mech}\, \eta_{elec}} \tag{A1.2}$$

where $E_{l,\Delta P}$ is the parameter that was required for Eq. (A1.1). The nominal volumetric flow rate of each pump can be either found from the plate on it or the technical documents and manuals.

A1-4-3 Analysis of the results

The calculation results of the waste heat out of the entire workshop are illustrated in Figure A1.2. The total amount of the waste heat is estimated to be 288 kW, corresponding to 32% of the total electricity input.

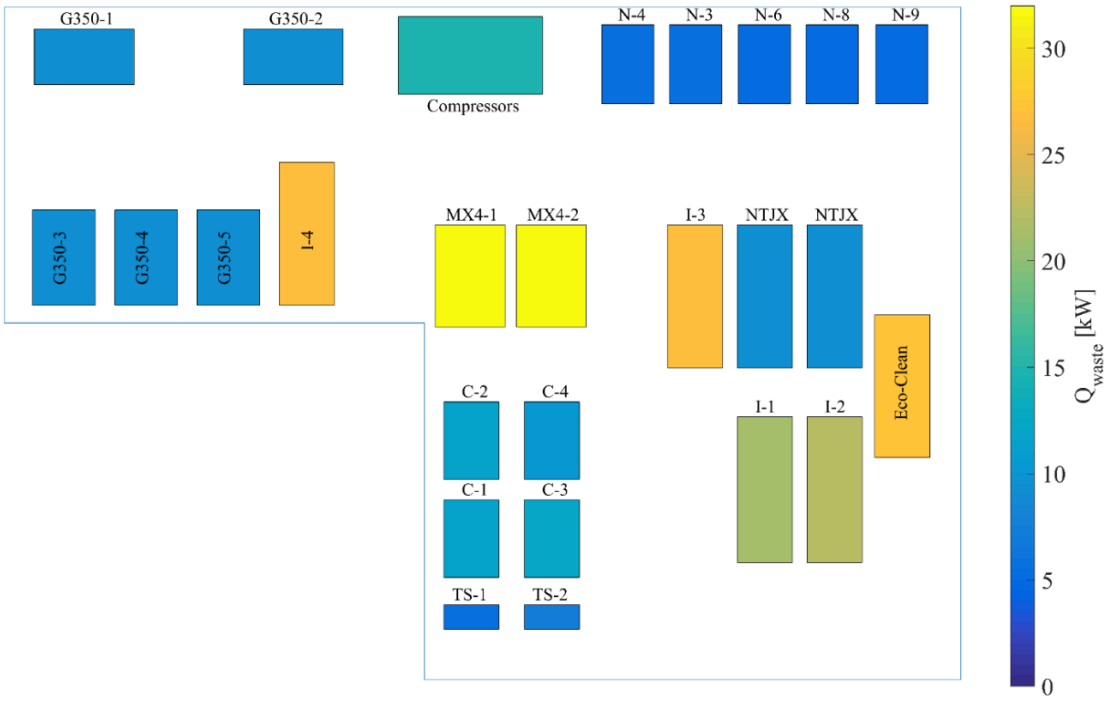

Figure A1.2. Heat dissipation map of each CNC machine at the workshop, considering the heat rejection compressors and electrical transformers.

A1-5 Feasibility study of WHR implementation

The main waste heat sources of the company are machining devices and the compressor room. The suggestable heat recovery method is a system that can catch the generated waste heat in the company without interfering with the performance of the production units nor the ventilation system. Therefore, such a system should be installed where the entire heat of the plant is gathered, which are the central air duct return ports for the ventilation system. As the ventilation system switches from the winter to the summer mode when the outside temperature goes above 14 ˚C, the WHR method can also have two modes of winter/summer to correspond to the ventilation system performance. In the summer mode, the chillers are on-line, cooling the air before it flows into the workshop. After absorbing the heat from the airflow, the chillers discharge the heat to the ambient. However, the chillers are out of order in the winter mode, and the only actual waste heat resource, which is practically recoverable, is that of the compressor room.

A1-5-1 Summer mode

In the summer mode, the outside temperature is permanently more than 14 ˚C. The discharged heat of the chiller can be introduced to the generator of an absorption chiller to satisfy the cooling load of the offices in the company, where another ventilation system is currently working to condition the air. To better illustrate such an idea, the entire proposed WHR system for the summer mode of the ventilation system is outlined in Fig. A1.3.

The third source of waste heat depicted in Fig. A1.3 is the compressor room heat dissipation. To identify how much heat is caught by the cooling air, air velocity and temperature were measured for each of the outlet vents. The larger vent dimension is 715×715 mm^2 and is associated with the compressors of 50 and 60 *hp*. The exhaust air temperature and velocity can reach up to 50-60 ˚C and 8-9 m/s on this vent, respectively. The other vent, which is related to the 30 *hp* compressor, is a round-type vent with a net flow area of 0.212 m^2, the air leaving temperature of nearly 30-40 ˚C, and the velocity of 3-4 m/s. The lower and upper limits of the ambient temperatures correspond to T_{env} = 14 and 25 ˚C, respectively. Their associated waste heat can be calculated by

$$\dot{Q}_{Waste} = \rho_a V_a A\left(h_{a,e} - h_{a,i}\right) \tag{A1.3}$$

where ρ,V, and A denote the air density, velocity and the flow area, respectively. The subscript a stands for air flow. It is revealed accordingly that the amount of waste heat for large and small vents accounts for 158.62 and 10.57 kW, respectively.

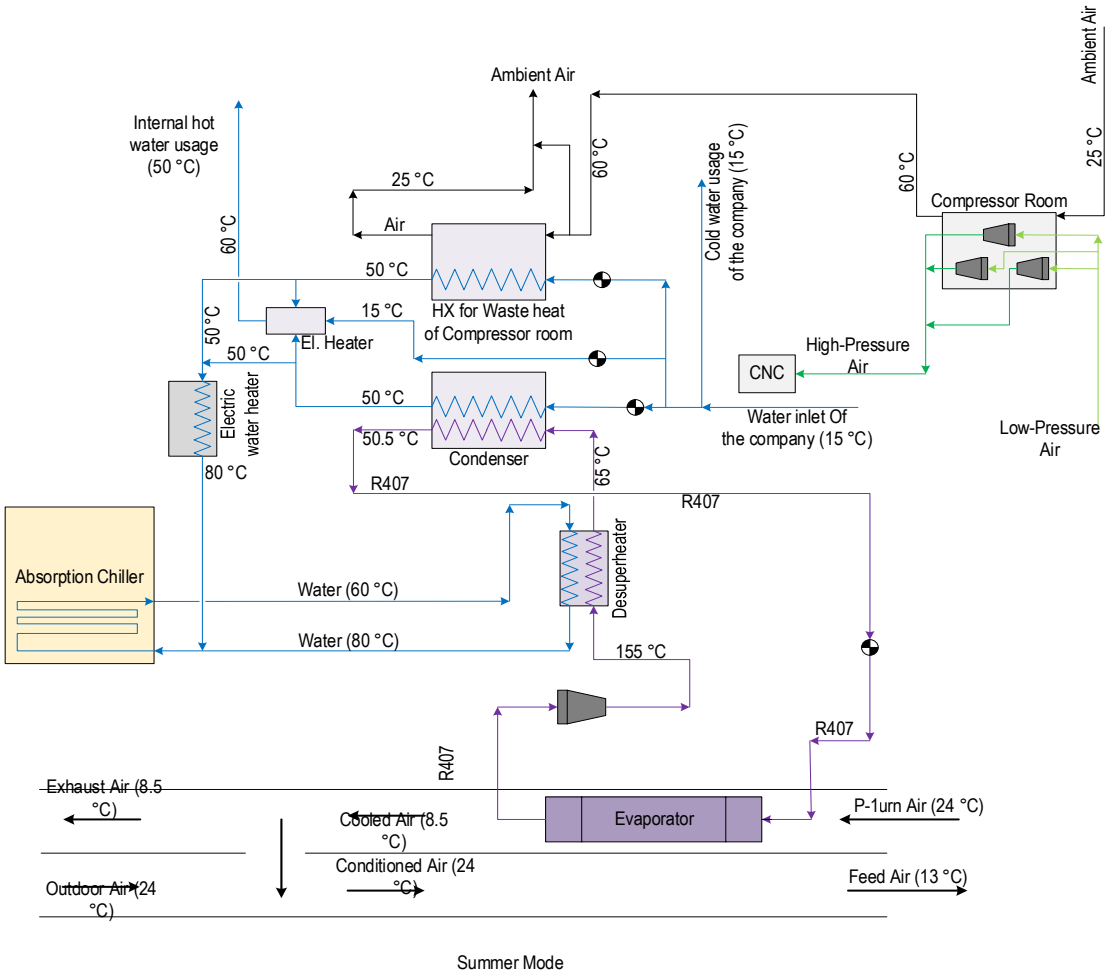

Figure A1.3. WHR system proposed for the summer mode of the ventilation system.

The above-mentioned higher temperature waste heat can release its heat content into a water flow in another heat exchanger at 0.98 kg/s in the case of recovery. Water enters and leaves at 15 and 50 ˚C to conform to the first and second laws, considering a thermal efficiency of 90% for the heat exchanger, respectively. In addition, there is a potential 0.98 kg/s of 50 ˚C hot water that can be used exactly the same way it was explained for the cooling water of the condenser. Accordingly, there is the possibility of generating 0.75 + 0.98 = 1.73 kg/s of 50 ˚C hot water by the WHR of the compressor room and the condenser of the ventilation system of the compressor room.

Cost analysis of the proposed system for the summer

The levelized total cost of the absorption chiller, C_{tot}^{abs} is calculated via:

$$C_{tot}^{abs} = C_{init}^{abs} + \frac{(1+i)^n - 1}{i(1+i)^n}\left(C_{op}^{abs} + C_M^{abs}\right) \quad \text{(A1.4)}$$

with i = 5% and n = 20 years. The unit purchase cost can be estimated by ϕ_{init}^{abs} = 550 €/kW (830.5 CAD/kW) as proposed by Schöpfer [109]. For $\dot{Q}_{cap,cooling}$ = 52 kW, the initial cost is calculated as

$$C_{init}^{abs} = \phi_{init}^{abs}\, \dot{Q}_{cap,cooling} \quad \text{(A1.5)}$$

which accounts for 43,186 CAD. The maintenance cost of the absorption chiller can be estimated as 1% of the purchase costs (C_M^{abs} = 0.01C_{init}^{abs}) for each year [109], [110]. The operational cost of the absorption chiller is actually the electricity cost of its auxiliary equipment for the entire lifetime of the plant. The electricity price for the company is approximated by ϕ_{op}^{abs} = 0.08 CAD/kWh to be used in

$$C_{op}^{abs} = \phi_{op}^{abs}\, E_{elec}^{abs} \quad \text{(A1.6)}$$

Accordingly, the total cost with n = 20 and 3,285 hours of the operation of each year for the absorption chiller is estimated by 70,681 CAD. Further, the total cost for the current electric chiller systems for the same time period, C_{tot}^{curr} can be evaluated using:

$$C_{tot}^{curr} = \frac{(1+0.5)^{20} - 1}{0.05(1+0.5)^{20}}\left((17.11 \times 3285 \times 0.08) + 500\right) = 62287\ CAD \quad \text{(A1.7)}$$

where it is 8,394 CAD less than the absorption chiller. Therefore, the cost analysis shows that the WHR implementation for supplying the cooling load of the offices of the company by an absorption chiller might be more costly compared to when using the current systems.

In this analysis, although the electricity unit cost is supposed to be constant for the entire 20 years, it will probably change though. Additionally, the cost analysis may vary since the electricity consumption of the electric chillers (17.11 kW) is more sensitive to that of the absorption chiller (6.752 kW). On the other hand, the maintenance cost of the absorption chillers for the first 2-3 years can be free given that most suppliers offer remarkable guaranty services, which are not included in Eq. (A1.11). Moreover, the lifetime of the current system may not be necessarily considered 20 years with the same nominal electricity consumption since they have already been used for several years whereas the new absorption chiller will have the presumed lifetime.

A1-5-2 Winter mode and related cost analysis

In this study, the average ambient air temperature and the tap water temperature are assumed to be -10 and 4 ˚C in winter time, respectively. Figure A1.4 depicts a schematic view of the WHR design that is modeled for the winter mode. Considering again the temperature gain of 35 ˚C of the compressor room, its leaving temperature will be approximately 25 ˚C. With the same above-mentioned airflow speed and vent, the magnitude of the available waste heat is evaluated by 158.4 kW. As similarly conducted for summer mode, the mass flow rate and the exhaust temperature of the cooling water are computed as 2.42 kg/s, and 20 ˚C, respectively.

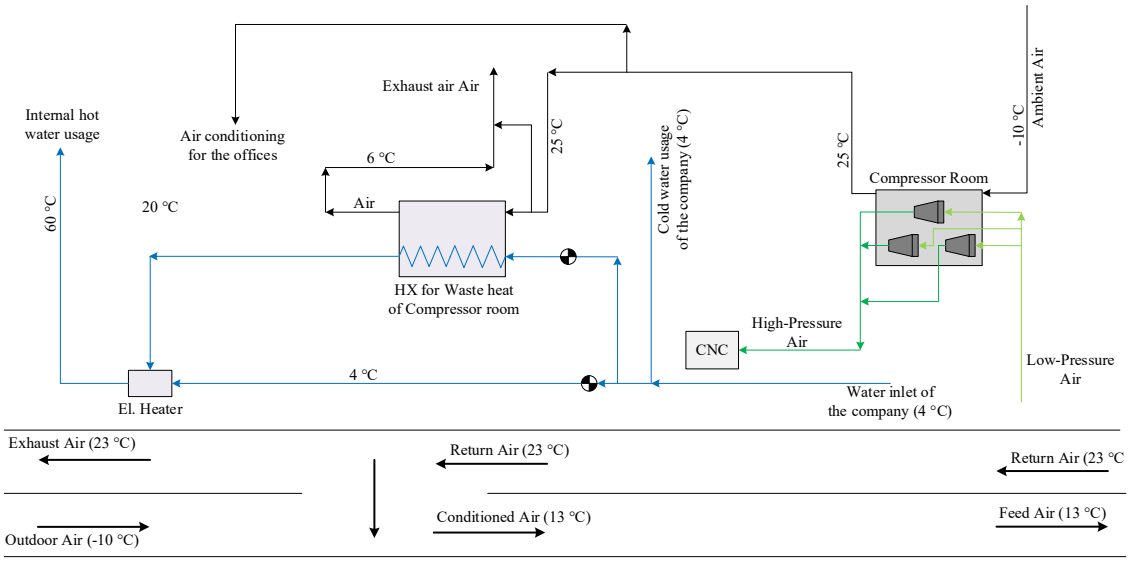

Winter Mode

Figure A1.4. WHR system proposed for the winter mode of the ventilation system.

Here, there is an idea of extracting the waste heat of the compressor room so that to directly filter and send it toward the heat-required places of the company. The total nominal heating capacity of the three ventilation systems, meeting the heating demands of the offices, is 40 kW. The electricity consumption of those electric heaters for providing this nominal 40 kW of heat is also approximately 40 kW. If a fraction of the 25 ˚C air is directed to heat those places, after installing the new duct system, 40 kW of electricity consumption during the entire winter period will represent a decline of 10,512 CAD/year in winter.

The findings of [111] are used to roughly evaluate the cost of ductwork for the proposed WHR method, indicating that the cost is nearly 35-55 USD (45.5-71.5 CAD) per linear foot (including labor and materials). Accordingly, the capital cost for the ductwork is estimated at approximately 11,921-18,733 CAD if 80 m (262 ft.) of ducting is assumed to be necessary. In this study, the average value of 15,000 CAD is chosen for the cost analysis. The analysis results in the total costs of 27,462 and 137,233 CAD if the entire heat is supplied by WHR or by the

current electric heat pumps, respectively. The costs are calculated based on a lifetime of 20 years and 3,285 operating hours of equal to 4.5 months each year.

A1-6 Results

Three main WHR method were selected for the plant as follows:

-The possibility of replacing the current chillers of the offices with a 52 kW single-effect absorption chiller was investigated for the summer mode. The generator of the absorption chiller would utilize the rejected heat of the condenser of the ventilation system associated with the workshop.

-Another WHR method was to recuperate the compressor room waste heat by an air to water plate heat exchanger in order to preheat the required hot water of the complex. This method could be used for both summer and winter modes of the system.

-For the winter, the current heating systems of the offices can go offline and the heated exhaust air of the compressor room can be filtrated, and addressed to the offices using the required ductworks.

Table A1-1 compares these three WHR approaches versus the current devices from an economic standpoint. The absorption chiller and the currently available chillers of the offices are compared in the first two rows. The two succeeded rows indicate the difference between the current electric water heater and the designed hybrid WHR system (water pre-heater). The last two rows investigate the economic benefit of direct heating of the offices using the compressor room return air compared to the present heat pumps. In this Table, *El.*, *WH*, *CAD*, *NA*, *Comp.*, *S*, and *W* represent electricity, waste heat, Canadian dollars, not assigned, compressor, summer, and winter, respectively.

Table A1-1. A summary of the chosen WHR systems in economic comparison with the currently installed equipment [112].

System Mode	WH source	Inlet Temp. of WH (°C)	Outlet Temp. of WH (°C)	Technology	Operating Hours (hour)	Initial Cost (CAD)	El. Cost (CAD/year)	Maintenance Cost (CAD)	Total Cost (CAD)
S	Refrigerant	155	65	Abs. Chiller	3285	43186	1774.5	431	70681
S	NA	NA	NA	Chillers, El.	3285	NA	4496.5	500	62287
S/W	Air from Comp.	S: 60 W: 25	S: 25 W: 6	Water heater, WHR + El.	1300	9000	1230.4	300	28072
S/W	NA	NA NA	NA NA	Water heater, El.	1300	NA	2250.4	150	29914
W	Air from Comp.	25	6	Heating with air at 25 °C	3285	15000	NA	1000	27462
W	NA	NA	NA	Heat pumps, El.	3285	NA	10512	500	137233

Appendix 2 ADDITIONAL SIMULATION RESULTS

This appendix presents additional simulation results that were obtained after the publication of the articles that constitute the main core of this thesis. They have been included here since they can help to better understand some of the findings of this work.

A2-1 Dual-objective optimization

The dual-objective optimization of the energy hub developed in Section 1.8 was performed with an a more powerful computer. As a result, the abrupt variations observed in some curves of Fig. 1.10 almost vanished, as expected, and the updated figure is provided below. This might indicate that the initial version of the solver was stuck in local optima.

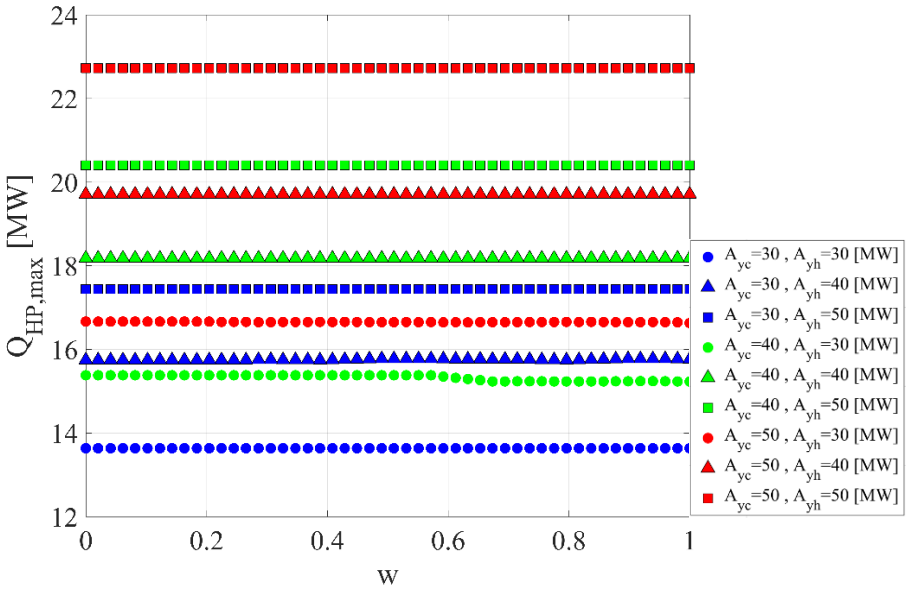

Figure A2.1. Updated heat pump capacity as a function of the weight value w for nine load scenarios.

A2-2 Considering maintenance and space cost

An important economic consideration that was disregarded in the thesis is the maintenance and space cost (C_{MS}). One simple way to account for these costs is to introduce an additional term in operation costs (e.g., Eq. (2.11)) Here, to estimate its influence on the total cost of the energy hub, which is reformulated by

$$C_{tot} = C_{init}^{TES} + C_{init}^{HP} + C_{init}^{EH} + \frac{(1+i)^n - 1}{i(1+i)^n}\left(C_{op,e} + C_{op,f} + C_{MS}\right) \tag{A2.1}$$

we have expressed the maintenance and space cost as a percentage of the purchase cost of each equipment as

$$C_{MS} = \alpha_y \left(C_{init}^{TES} + C_{init}^{HP} + C_{init}^{EH}\right) \tag{A2.2}$$

where α_y is the yearly percentage of the purchase cost of the associated device Values in the interval [0%, 3%, 5%, 8%] were tested The case α_y = 0% is exactly the case we had already seen in Fig. 2.3(d).

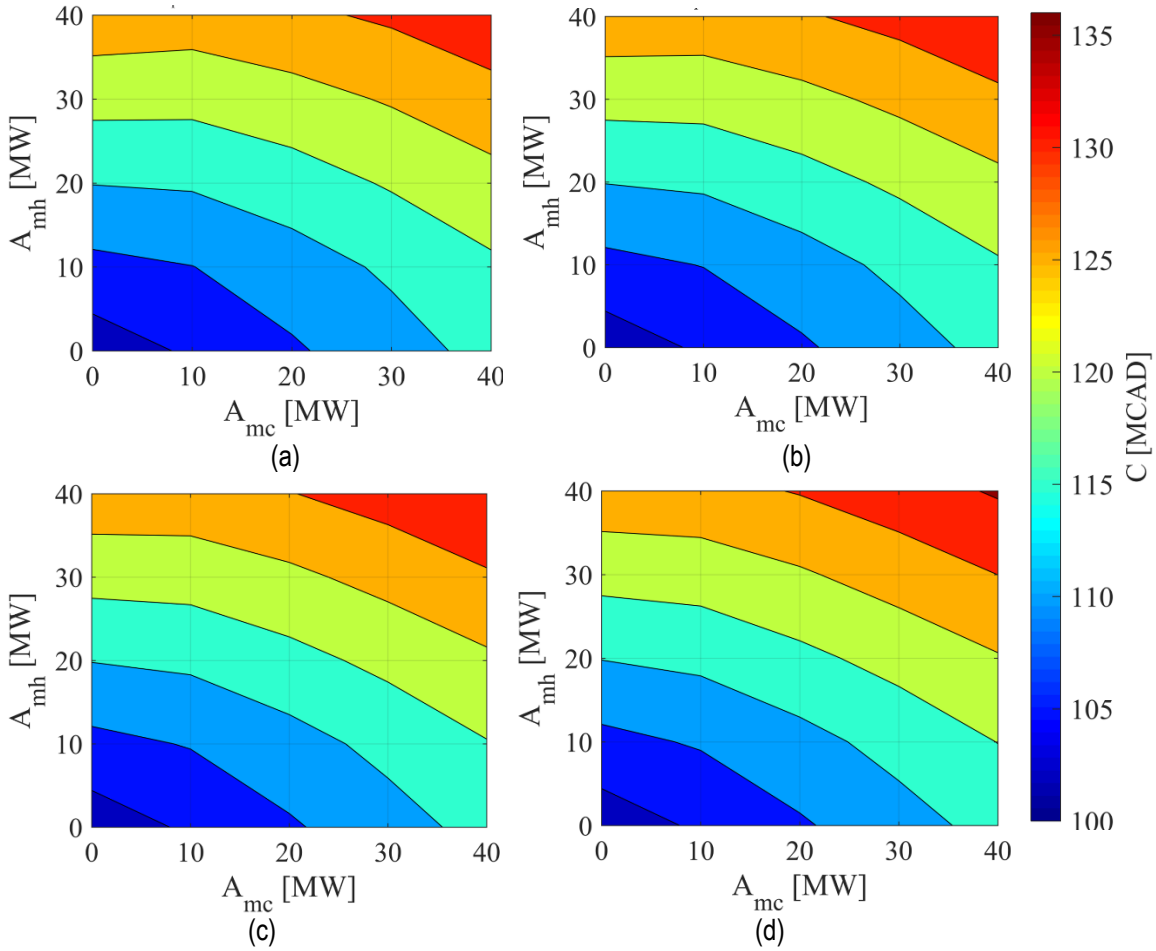

Figure A2.2. Optimal total cost for the energy hub of Figure 2.1 for different magnitudes of α_y; (a) α_y = 0%, (b) α_y = 3%, (c) α_y = 5%, (d) α_y = 8%; (CH and FB already available)

In Fig. A2.2, the total costs considering maintenance and space cost is illustrated with different values of α_y. This figure corresponds to the energy hub including both TES and heat pump with the devices operating with a constant-efficiency basis. For the thermal load of [A_{mh}, A_{mc}] = [40,40] MW, the total cost can increase from 133.26 MCAD for α_y = 0% to 135.53 MCAD for α_y = 8% as obvious in this figure. This accounts for the total difference of 2.27 MCAD over 10 years if C_{MS} is estimated with 8% of the sum of the purchase cost of TES, heat pump, and electric heater, as the case of Section 2, and Fig. 2.3(d). However, if all equipment were to be purchased, i.e., not only TES, heat pumps, electric heaters, but also the chillers and fuel boilers, then considering maintenance cost would have more influence from a financial standpoint, as demonstrated in Fig. A2.3

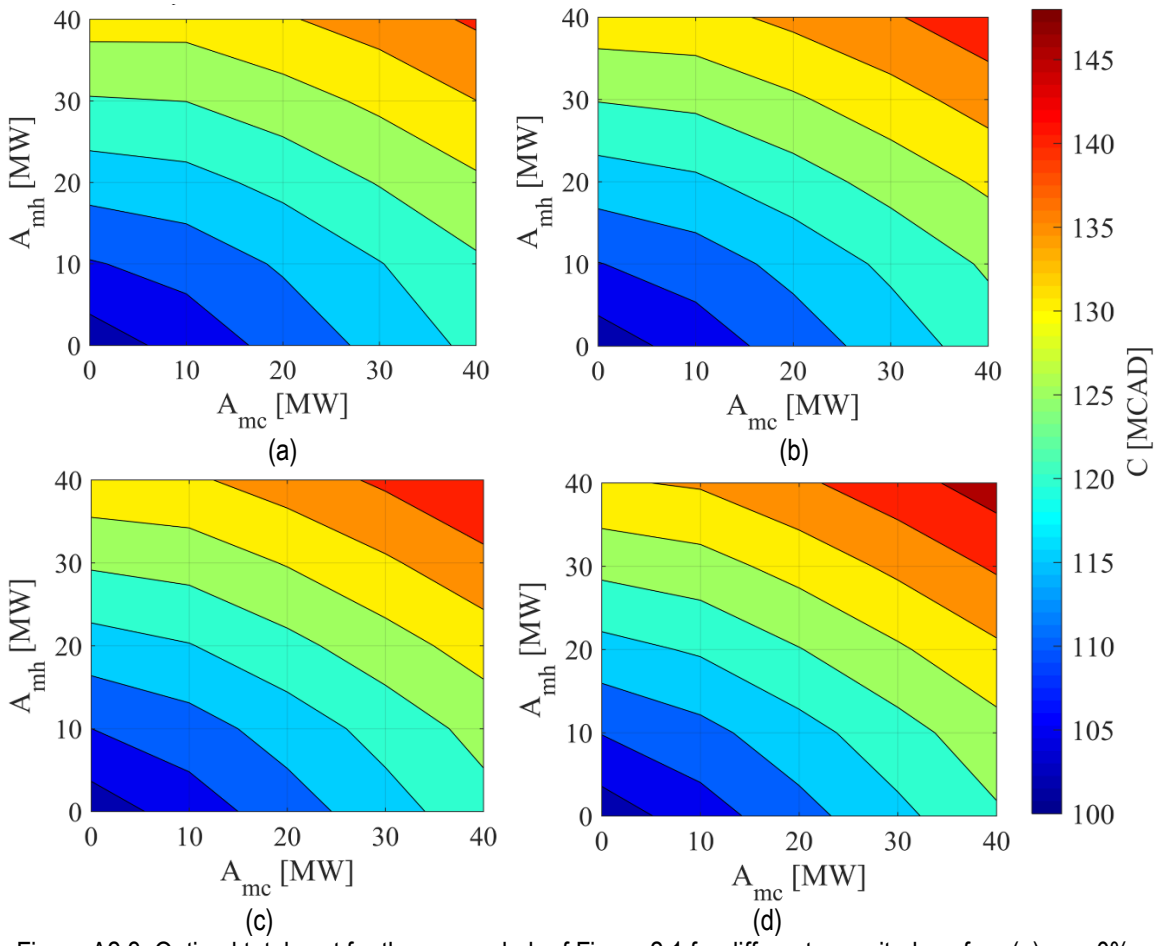

Figure A2.3. Optimal total cost for the energy hub of Figure 2.1 for different magnitudes of α_y; (a) α_y = 0%, (b) α_y = 3%, (c) α_y = 5%, (d) α_y = 8%; (all equipment to be bought)

A2-3 New capacity constraint for the 2nd article

In the second article, Chapter 2, the charging and discharging power magnitudes of the TES units at each moment were limited by 20% of the heating load magnitude at that moment as shown in Eq. (2.9). However, to better represent real TES systems, this constraint is replaced with the one limiting the charging and discharging power magnitudes of TES at each moment by 20% of the maximum required thermal load as

$$\begin{aligned} P_{HTES}^{\max,ch}, P_{HTES}^{\max,dis} &= 0.2\, L_h \\ P_{CTES}^{\max,ch}, P_{CTES}^{\max,dis} &= 0.2\, L_c \end{aligned} \tag{A2.3}$$

Accordingly, new optimization results will be produced. The results corresponding to the one depicted in Fig. 2.3 are displayed in Fig. A2.4. This figure shows that the new constraint, even though more rational than the one before, does not considerably influence the cost results, as understood by comparing the results between Figs. 2.3 and A2.4

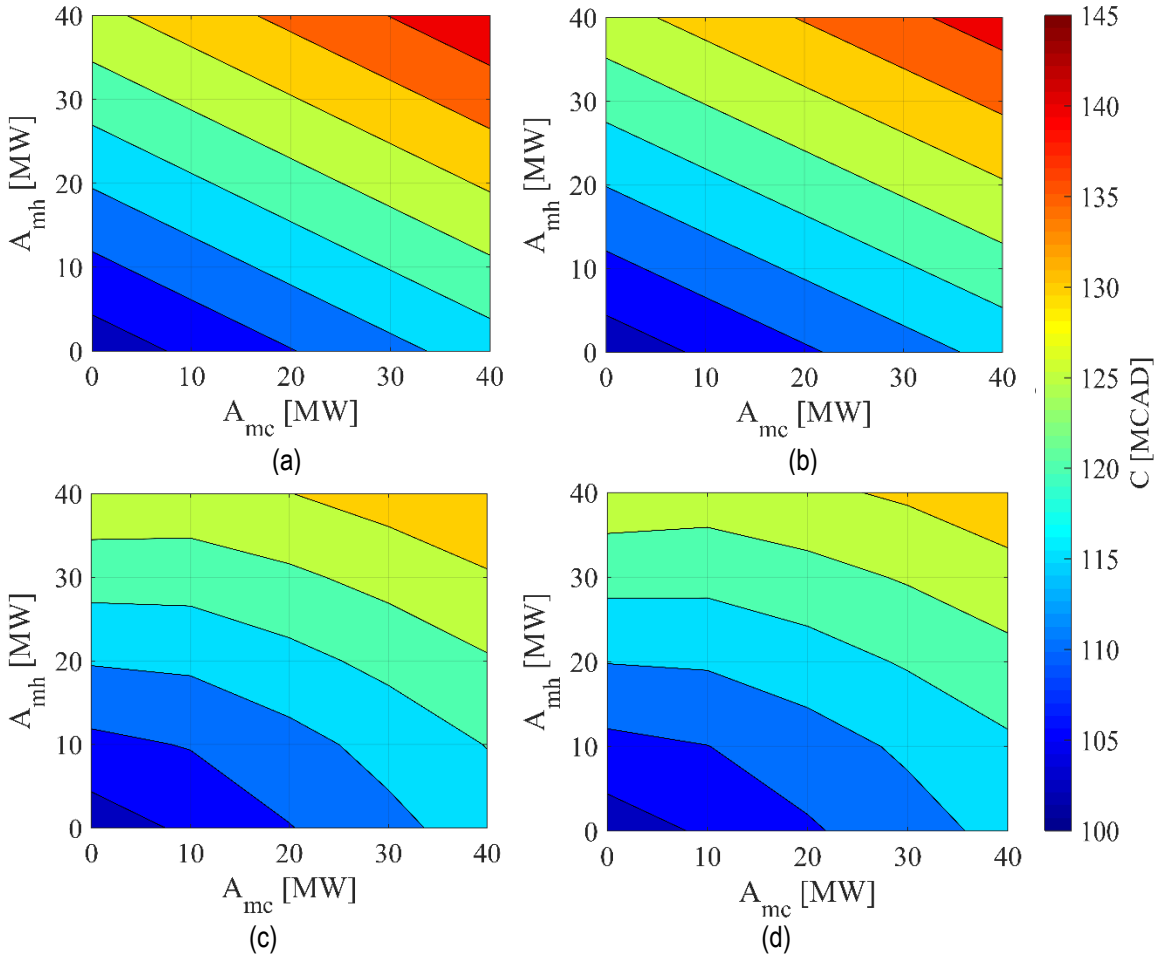

Figure A2.4. Minimized total cost for the energy hubs: (a) Reference (no TES, nor HP); (b) only TES; (c) only HP; (d) both TES and HP.

Bibliographie

[1] N.R.C. Government of Canada, “Energy Use in Canada: Trends Publications,”, https://oee.nrcan.gc.ca/publications/statistics/trends/2017/residential.cfm.

[2] N.R.C. Government of Canada, “Energy Use in Canada: Trends Publications,”, https://oee.nrcan.gc.ca/publications/statistics/trends/2017/commercial.cfm.

[3] “IEA (2021), District Heating, IEA, Paris” https://www.iea.org/reports/district-heating.

[4] H. Ahmadisedigh and L. Gosselin, “Combined heating and cooling networks with waste heat recovery based on energy hub concept,” *Appl. Energy*, vol. 253, p. 113495, Nov. 2019.

[5] P. Favre-Perrod, “A vision of future energy networks,” in *2005 IEEE Power Engineering Society Inaugural Conference and Exposition in Africa*, Jul. 2005, pp. 13–17.

[6] M. Geidl, G. Koeppel, P. Favre-Perrod, B. Klockl, G. Andersson, and K. Frohlich, “Energy hubs for the future,” *IEEE Power Energy Mag.*, vol. 5, no. 1, pp. 24–30, 2007.

[7] M. Geidl, Gaudenz Koeppel, Patrick Favre-Perrod, Bernd Klöckl, Göran Andersson, and Klaus Fröhlich, “The Energy Hub – A Powerful Concept for Future Energy Systems,” presented at the Annual Carnegie Mellon Conference on the Electricity Industry, ETH Zurich, Switzerland, May 2007.

[8] M. Geidl, “Integrated modeling and optimization of multi-carrier energy systems,” 2007. Accessed: Oct. 11, 2017. [Online]. Available: http://e-collection.library.ethz.ch/eserv/eth:29506/eth-29506-02.pdf

[9] M. Geidl and G. Andersson, “A modeling and optimization approach for multiple energy carrier power flow,” in *2005 IEEE Russia Power Tech*, Jun. 2005, pp. 1–7.

[10] M. Geidl and G. Andersson, “Optimal power dispatch and conversion in systems with multiple energy carriers,” 2005, http://www.pscc-central.org/uploads/tx_ethpublications/fp476.pdf

[11] M. Geidl and G. Andersson, “Operational and structural optimization of multi-carrier energy systems,” *Eur. Trans. Electr. Power*, vol. 16, no. 5, pp. 463–477, 2006.

[12] M. Geidl and G. Andersson, “Optimal Power Flow of Multiple Energy Carriers,” *IEEE Trans. Power Syst.*, vol. 22, no. 1, pp. 145–155, Feb. 2007.

[13] M. Schulze, L. Friedrich, and M. Gautschi, “Modeling and optimization of renewables: applying the Energy Hub approach,” in *2008 IEEE International Conference on Sustainable Energy Technologies*, Nov. 2008, pp. 83–88.

[14] A. Maroufmashat, A. Elkamel, M. Fowler, S. Sattari, R. Rochandel, A. Hajimiragha, S. Walker, E. Entchev, “Modeling and optimization of a network of energy hubs to improve economic and emission considerations,” *Energy*, vol. 93, pp. 2546–2558, 2015.

[15] O. Grodzevich and O. Romanko, “Normalization and other topics in multi-objective optimization,” Aug. 2006.

[16] I. G. Moghaddam, M. Saniei, and E. Mashhour, “A comprehensive model for self-scheduling an energy hub to supply cooling, heating and electrical demands of a building,” *Energy*, vol. 94, pp. 157–170, 2016.

[17] Y. Wang, N. Zhang, Z. Zhuo, C. Kang, and D. Kirschen, “Mixed-integer linear programming-based optimal configuration planning for energy hub: Starting from scratch,” *Appl. Energy*, vol. 210, pp. 1141–1150, Jan. 2018.

[18] B. Guler, E. Çelebi, and J. Nathwani, “A ‘Regional Energy Hub’ for achieving a low-carbon energy transition,” *Energy Policy*, vol. 113, pp. 376–385, Feb. 2018.

[19] G. T. Ayele, P. Haurant, B. Laumert, and B. Lacarrière, “An extended energy hub approach for load flow analysis of highly coupled district energy networks: Illustration with electricity and heating,” *Appl. Energy*, vol. 212, pp. 850–867, Feb. 2018.

[20] A. Maroufmashat, M. Fowler, S. Sattari Khavas, A. Elkamel, R. Roshandel, and A. Hajimiragha, “Mixed integer linear programing based approach for optimal planning and operation of a smart urban energy network to support the hydrogen economy,” *Int. J. Hydrog. Energy*, vol. 41, no. 19, pp. 7700–7716, May 2016.

[21] A. Sharif, A. Almansoori, M. Fowler, A. Elkamel, and K. Alrafea, “Design of an energy hub based on natural gas and renewable energy sources,” *Int. J. Energy Res.*, vol. 38, Mar. 2014, doi: 10.1002/er.3050.

[22] K. AlRafea, M. Fowler, A. Elkamel, and A. Hajimiragha, “Integration of renewable energy sources into combined cycle power plants through electrolysis generated hydrogen in a new designed energy hub,” *Int. J. Hydrog. Energy*, vol. 41, no. 38, pp. 16718–16728, Oct. 2016.

[23] T. Togawa, T. Fujita, L. Dong, M. Fujii, and M. Ooba, “Feasibility assessment of the use of power plant-sourced waste heat for plant factory heating considering spatial configuration,” *J. Clean. Prod.*, vol. 81, pp. 60–69, 2014.

[24] A. Shahmohammadi, M. Moradi-Dalvand, H. Ghasemi, and M. S. Ghazizadeh, “Optimal design of multicarrier energy systems considering reliability constraints,” *IEEE Trans. Power Deliv.*, vol. 30, no. 2, pp. 878–886, 2015.

[25] S. Pazouki and M.-R. Haghifam, “Optimal planning and scheduling of energy hub in presence of wind, storage and demand response under uncertainty,” *Int. J. Electr. Power Energy Syst.*, vol. 80, pp. 219–239, 2016.

[26] F. Brahman, M. Honarmand, and S. Jadid, “Optimal electrical and thermal energy management of a residential energy hub, integrating demand response and energy storage system,” *Energy Build.*, vol. 90, no. Supplement C, pp. 65–75, Mar. 2015.

[27] M. Batić, N. Tomašević, G. Beccuti, T. Demiray, and S. Vraneš, “Combined energy hub optimisation and demand side management for buildings,” *Energy Build.*, vol. 127, pp. 229–241, 2016.

[28] F. Kamyab and S. Bahrami, “Efficient operation of energy hubs in time-of-use and dynamic pricing electricity markets,” *Energy*, vol. 106, pp. 343–355, 2016.

[29] M. Mohammadi, Y. Noorollahi, B. Mohammadi-ivatloo, and H. Yousefi, “Energy hub: From a model to a concept – A review,” *Renew. Sustain. Energy Rev.*, vol. 80, pp. 1512–1527, Dec. 2017.

[30] S. Moradi, R. Ghaffarpour, A. M. Ranjbar, and B. Mozaffari, “Optimal integrated sizing and planning of hubs with midsize/large CHP units considering reliability of supply,” *Energy Convers. Manag.*, vol. 148, pp. 974–992, Sep. 2017.

[31] A. Sheikhi, A. M. Ranjbar, H. Oraee, and A. Moshari, “Optimal operation and size for an energy hub with CCHP,” *Energy Power Eng.*, vol. 3, no. 05, p. 641, 2011.

[32] A. Sheikhi, A. M. Ranjbar, and H. Oraee, “Financial analysis and optimal size and operation for a multicarrier energy system,” *Energy Build.*, vol. 48, no. Supplement C, pp. 71–78, May 2012.

[33] R. Croteau and L. Gosselin, “Correlations for cost of ground-source heat pumps and for the effect of temperature on their performance,” *Int. J. Energy Res.*, vol. 39, no. 3, pp. 433–438, Mar. 2015.

[34] D. Setlhaolo, S. Sichilalu, and J. Zhang, “Residential load management in an energy hub with heat pump water heater,” *Appl. Energy*, vol. 208, pp. 551–560, Dec. 2017.

[35] “https://www.energir.com/en/business/price/natural-gas-price/.”

[36] “Rate L - Business” http://www.hydroquebec.com/business/customer-space/rates/rate-l-industrial-rate-large-power-customers.html.

[37] “GHG emissions and electricity | Hydro-Québec.” http://www.hydroquebec.com/developpement-durable/centre-documentation/taux-emission-ges.html.

[38] “Mandatory reporting of certain emissions of contaminants into the atmosphere; draft regulations, Gazette N° 23 du 2010-06-09 Page : 1397.” http://www2.publicationsduquebec.gouv.qc.ca/dynamicSearch/telecharge.php?type=1&file=2010A%2F9832.PDF.

[39] H. P. Williams, *Model Building in Mathematical Programming*. John Wiley & Sons, 2013.

[40] P. Byrne, J. Miriel, and Y. Lenat, “Experimental study of an air-source heat pump for simultaneous heating and cooling–part 1: basic concepts and performance verification,” *Appl. Energy*, vol. 88, no. 5, pp. 1841–1847, 2011.

[41] K. Kontu, S. Rinne, and S. Junnila, “Introducing modern heat pumps to existing district heating systems – Global lessons from viable decarbonizing of district heating in Finland,” *Energy*, vol. 166, pp. 862–870, Jan. 2019.

[42] P. Byrne, J. Miriel, and Y. Lénat, “Modelling and simulation of a heat pump for simultaneous heating and cooling,” in *Building simulation*, 2012, vol. 5, pp. 219–232.

[43] H. Averfalk, P. Ingvarsson, U. Persson, M. Gong, and S. Werner, “Large heat pumps in Swedish district heating systems,” *Renew. Sustain. Energy Rev.*, vol. 79, pp. 1275–1284, Nov. 2017, doi: 10.1016/j.rser.2017.05.135.

[44] A. David, B. V. Mathiesen, H. Averfalk, S. Werner, and H. Lund, “Heat Roadmap Europe: Large-Scale Electric Heat Pumps in District Heating Systems,” *Energies*, vol. 10, no. 4, p. 578, Apr. 2017.

[45] L. Brange, J. Englund, and P. Lauenburg, “Prosumers in district heating networks – A Swedish case study,” *Appl. Energy*, vol. 164, pp. 492–500, Feb. 2016.

[46] H. Ö. Paksoy, *Thermal energy storage for sustainable energy consumption: fundamentals, case studies and design*, vol. 234. Springer Science & Business Media, 2007.

[47] A. Gil, M. Medrano, I. Martorell, A. Lázaro, P. Dolado, B. Zalba et al., “State of the art on high temperature thermal energy storage for power generation. Part 1—Concepts, materials and modellization,” *Renew. Sustain. Energy Rev.*, vol. 14, no. 1, pp. 31–55, 2010.

[48] E. S. Barbieri, F. Melino, and M. Morini, “Influence of the thermal energy storage on the profitability of micro-CHP systems for residential building applications,” *Appl. Energy*, vol. 97, pp. 714–722, 2012.

[49] I. Dincer and M. Rosen, *Thermal energy storage: systems and applications*. John Wiley & Sons, 2002.

[50] D. Haeseldonckx, L. Peeters, L. Helsen, and W. D’haeseleer, “The impact of thermal storage on the operational behaviour of residential CHP facilities and the overall CO 2 emissions,” *Renew. Sustain. Energy Rev.*, vol. 11, no. 6, pp. 1227–1243, 2007.

[51] B. Zalba, J. M. Marín, L. F. Cabeza, and H. Mehling, “Review on thermal energy storage with phase change: materials, heat transfer analysis and applications,” *Appl. Therm. Eng.*, vol. 23, no. 3, pp. 251–283, 2003.

[52] A. Sharma, V. V. Tyagi, C. R. Chen, and D. Buddhi, “Review on thermal energy storage with phase change materials and applications,” *Renew. Sustain. Energy Rev.*, vol. 13, no. 2, pp. 318–345, 2009.

[53] Y. Sun, S. Wang, F. Xiao, and D. Gao, “Peak load shifting control using different cold thermal energy storage facilities in commercial buildings: a review,” *Energy Convers. Manag.*, vol. 71, pp. 101–114, 2013.

[54] P. Palensky and D. Dietrich, “Demand side management: Demand response, intelligent energy systems, and smart loads,” *IEEE Trans. Ind. Inform.*, vol. 7, no. 3, pp. 381–388, 2011.

[55] A. M. Khudhair and M. M. Farid, “A review on energy conservation in building applications with thermal storage by latent heat using phase change materials,” *Energy Convers. Manag.*, vol. 45, no. 2, pp. 263–275, 2004.

[56] F. Dinter and D. M. Gonzalez, “Operability, Reliability and Economic Benefits of CSP with Thermal Energy Storage: First Year of Operation of ANDASOL 3,” *Energy Procedia*, vol. 49, no. Supplement C, pp. 2472–2481, Jan. 2014.

[57] I. V. Postnikov, V. A. Stennikov, E. E. Mednikova, and A. V. Penkovskii, “A Methodology for Optimziation of Component Reliability of Heat Supply Systems,” *Energy Procedia*, vol. 105, no. Supplement C, pp. 3083–3088, May 2017.

[58] *2016 ASHRAE Handbook—HVAC Systems and Equipment (SI),*. 2016. Accessed: Jan. 20, 2020.

[59] R. Ooka and S. Ikeda, “A review on optimization techniques for active thermal energy storage control,” *Energy Build.*, vol. 106, pp. 225–233, Nov. 2015.

[60] X. Lu, Z. Liu, L. Ma, L. Wang, K. Zhou, and N. Feng, “A robust optimization approach for optimal load dispatch of community energy hub,” *Appl. Energy*, vol. 259, p. 114195, Feb. 2020.

[61] C. Chen, H. Sun, X. Shen, Y. Guo, Q. Guo, and T. Xia, “Two-stage robust planning-operation co-optimization of energy hub considering precise energy storage economic model,” *Appl. Energy*, vol. 252, p. 113372, Oct. 2019.

[62] A. Heidari, S. S. Mortazavi, and R. C. Bansal, “Stochastic effects of ice storage on improvement of an energy hub optimal operation including demand response and renewable energies,” *Appl. Energy*, vol. 261, p. 114393, Mar. 2020.

[63] M. Jadidbonab, E. Babaei, and B. Mohammadi-ivatloo, “CVaR-constrained scheduling strategy for smart multi carrier energy hub considering demand response and compressed air energy storage,” *Energy*, vol. 174, pp. 1238–1250, May 2019.

[64] Z. Yuan, S. He, A. Alizadeh, S. Nojavan, and K. Jermsittiparsert, “Probabilistic scheduling of power-to-gas storage system in renewable energy hub integrated with demand response program,” *J. Energy Storage*, vol. 29, p. 101393, Jun. 2020.

[65] H. Ahmadisedigh and L. Gosselin, “How can combined heating and cooling networks benefit from thermal energy storage? Minimizing lifetime cost for different scenarios,” *Energy*, vol. 243, p. 123112, Mar. 2022.

[66] J. Götze, J. Dancker, and M. Wolter, “A general MILP based optimization framework to design Energy Hubs,” - *Autom.*, vol. 67, no. 11, Art. no. 11.

[67] H. Hajabdollahi, “Investigating the effects of load demands on selection of optimum CCHP-ORC plant,” *Appl. Therm. Eng.*, vol. 87, pp. 547–558, 2015.

[68] E. Shahrabi, S. M. Hakimi, A. Hasankhani, G. Derakhshan, and B. Abdi, “Developing optimal energy management of energy hub in the presence of stochastic renewable energy resources,” *Sustain. Energy Grids Netw.*, vol. 26, p. 100428, 2021.

[69] S. Ayyappan, K. Mayilsamy, and V. V. Sreenarayanan, “Performance improvement studies in a solar greenhouse drier using sensible heat storage materials,” *Heat Mass Transf.*, vol. 52, no. 3, pp. 459–467, 2016.

[70] I. Sarbu and C. Sebarchievici, “A comprehensive review of thermal energy storage,” *Sustainability*, vol. 10, no. 1, p. 191, 2018.

[71] Y. Mu, W. Chen, X. Yu, H. Jia, K. Hou, C. Wang et al., “A double-layer planning method for integrated community energy systems with varying energy conversion efficiencies,” *Appl. Energy*, vol. 279, p. 115700, 2020.

[72] H. W. Stanford III, *HVAC water chillers and cooling towers: fundamentals, application, and operation*. CRC Press, 2011.

[73] *Technology Data Catalogue for Electricity and district heating production*. Danish Energy Agency and Energinet, 2020, https://ens.dk/sites/ens.dk/files/Statistik/technology_data_catalogue_for_el_and_dh_-_0009.pdf

[74] “Technology Data for Energy storage”, Dansih Energy Agency, 2018, https://ens.dk/sites/ens.dk/files/Analyser/technology_data_catalogue_for_energy_storage.pdf

[75] M. Ghorab, “Energy hubs optimization for smart energy network system to minimize economic and environmental impact at Canadian community,” *Appl. Therm. Eng.*, vol. 151, pp. 214–230, 2019.

[76] R. Bahmani, H. Karimi, and S. Jadid, “Cooperative energy management of multi-energy hub systems considering demand response programs and ice storage,” *Int. J. Electr. Power Energy Syst.*, vol. 130, p. 106904, Sep. 2021.

[77] M. Capone, E. Guelpa, and V. Verda, “Multi-objective optimization of district energy systems with demand response,” *Energy*, vol. 227, p. 120472, Jul. 2021.

[78] A. Imanloozadeh, M. Nazififard, S. A. Sadat, “A new stochastic optimal smart residential energy hub management system for desert environment”, International Journal of Energy Research - Wiley Online Library.”

[79] G. Pan, W. Gu, Z. Wu, Y. Lu, and S. Lu, “Optimal design and operation of multi-energy system with load aggregator considering nodal energy prices,” *Appl. Energy*, vol. 239, pp. 280–295, Apr. 2019.

[80] S. M. Thiem, “Multi-modal on-site energy systems: development and application of a superstructure-based optimization method for energy system design under consideration of part-load efficiencies,” PhD Thesis, Universitätsbibliothek der TU München, 2017.

[81] E. Fabrizio, M. Filippi, and M. Torbino, “Operational optimization of actual energy systems by means of the energy hub theory,” *Build Simul Syd.*, pp. 2793–2798, 2011.

[82] S. Deng, Q. Wu, Z. Jing, L. Wu, F. Wei, and X. Zhou, “Optimal capacity configuration for energy hubs considering part-load characteristics of generation units,” *Energies*, vol. 10, no. 12, p. 1966, 2017.

[83] J. H. Zheng; J. Huang; S. Deng; Q. H. Wu; M. Li; X. Zhou et al., “Comparison and error analysis of off-design and design models of energy hubs,” *CSEE J. Power Energy Syst.*, vol. 5, no. 4, pp. 454–465, 2019.

[84] L.-L. Li, Z.-F. Liu, M.-L. Tseng, S.-J. Zheng, and M. K. Lim, “Improved tunicate swarm algorithm: Solving the dynamic economic emission dispatch problems,” *Appl. Soft Comput.*, vol. 108, p. 107504, Sep. 2021.

[85] S. Thiem, V. Danov, M. Metzger, J. Schäfer, and T. Hamacher, “Project-level multi-modal energy system design - Novel approach for considering detailed component models and example case study for airports,” *Energy*, vol. 133, pp. 691–709, Aug. 2017.

[86] R. Yokoyama, Y. Hasegawa, and K. Ito, “A MILP decomposition approach to large scale optimization in structural design of energy supply systems,” *Energy Convers. Manag.*, vol. 43, no. 6, pp. 771–790, Apr. 2002.

[87] T. Wakui and R. Yokoyama, “Optimal structural design of residential cogeneration systems with battery based on improved solution method for mixed-integer linear programming,” *Energy*, vol. 84, pp. 106–120, May 2015.

[88] P. Voll, M. Jennings, M. Hennen, N. Shah, and A. Bardow, “The optimum is not enough: A near-optimal solution paradigm for energy systems synthesis,” *Energy*, vol. 82, pp. 446–456, Mar. 2015.

[89] R. Evins, K. Orehounig, V. Dorer, and J. Carmeliet, “New formulations of the ‘energy hub’model to address operational constraints,” *Energy*, vol. 73, pp. 387–398, 2014.

[90] W. Karush, “Minima of functions of several variables with inequalities as side constraints,” *M Sc Diss. Dept Math. Univ Chic.*, 1939.

[91] H. Kuhn and A. Tucker, “Nonlinear programming In Proceedings of 2nd Berkeley symposium (pp. 481–492),” *Berkeley Univ. Calif. Press. Sch.*, 1951.

[92] H. W. Kuhn and A. W. Tucker, *Proceedings of 2nd berkeley symposium*. Berkeley: University of California Press, 1951.

[93] Y. Huang, P. Ding, Y. Wang, S. Li, K. Yang, and Y. Li, “A bilevel optimal operation model of multi energy carriers system considering part load rate and demand response,” *Sustain. Energy Technol. Assess.*, vol. 45, p. 101035, 2021.

[94] W. Huang, N. Zhang, Y. Wang, T. Capuder, I. Kuzle, and C. Kang, “Matrix modeling of energy hub with variable energy efficiencies,” *Int. J. Electr. Power Energy Syst.*, vol. 119, p. 105876, 2020.

[95] H. Hajabdollahi, A. Ganjehkaviri, and M. N. M. Jaafar, “Assessment of new operational strategy in optimization of CCHP plant for different climates using evolutionary algorithms,” *Appl. Therm. Eng.*, vol. 75, pp. 468–480, 2015.

[96] M. Hohmann, R. Evins, and J. Lygeros, “Optimal dispatch of large multi-carrier energy networks considering energy conversion functions,” *Energy Procedia*, vol. 122, pp. 80–85, 2017.

[97] H. Ahmadisedigh and L. Gosselin, “Combined heating and cooling networks with part-load efficiency curves: Optimization based on energy hub concept,” *Appl. Energy*, vol. 307, p. 118245, Feb. 2022.

[98] M.-H. Lin, J. G. Carlsson, D. Ge, J. Shi, and J.-F. Tsai, “A Review of Piecewise Linearization Methods,” 2013. https://www.hindawi.com/journals/mpe/2013/101376.

[99] Y. Yuan, A. A. Bayod-Rújula, H. Chen, A. Martínez-Gracia, J. Wang, and A. Pinnarelli, “An Advanced Multicarrier Residential Energy Hub System Based on Mixed Integer Linear Programming,” *Int. J. Photoenergy*, vol. 2019, 2019.

[100] Z.-F. Liu, L.-L. Li, Y.-W. Liu, J.-Q. Liu, H.-Y. Li, and Q. Shen, “Dynamic economic emission dispatch considering renewable energy generation: A novel multi-objective optimization approach,” *Energy*, vol. 235, p. 121407, Nov. 2021.

[101] K. Orehounig, R. Evins, and V. Dorer, “Integration of decentralized energy systems in neighbourhoods using the energy hub approach,” *Appl. Energy*, vol. 154, pp. 277–289, Sep. 2015.

[102] S. D. Beigvand, H. Abdi, and M. La Scala, “A general model for energy hub economic dispatch,” *Appl. Energy*, vol. 190, pp. 1090–1111, Mar. 2017.

[103] A. Najafi, H. Falaghi, J. Contreras, and M. Ramezani, “Medium-term energy hub management subject to electricity price and wind uncertainty,” *Appl. Energy*, vol. 168, pp. 418–433, Apr. 2016.

[104] “Enersion - Understand the Cost of Current Cooling Technologies,” *Enersion*, Apr. 14, 2017. https://enersion.com/cost-of-current-cooling-technology.

[105] J. Bai, W. Wei, L. Chen, and S. Mei, “Rolling-horizon dispatch of advanced adiabatic compressed air energy storage based energy hub via data-driven stochastic dynamic programming,” *Energy Convers. Manag.*, vol. 243, p. 114322, Sep. 2021, doi: 10.1016/j.enconman.2021.114322.

[106] “L’Énergie au Québec, Ministère de l’Énergie et des Ressources naturelles, Gouvernement du Québec, 2013.” https://mern.gouv.qc.ca/energie/statistiques/index.jsp.

[107] “Waste Heat Recovery: Technology and Opportunities in U.S. Industry,” p. 112.

[108] “https://www.pilotpb.com/uploads/documents/document/fr/46.pdf.”

[109] M. D. Schöpfer, “Absorption chillers: their feasibility in district heating networks and comparison to alternative technologies,” 2015.

[110] G. Kumbaroğlu and R. Madlener, “Evaluation of economically optimal retrofit investment options for energy savings in buildings,” *Energy Build.*, vol. 49, pp. 327–334, 2012.

[111] “Ductwork Installation Cost | Cost to Install Ductwork for Central Air,” *Fixr.com*. https://www.fixr.com/costs/ductwork .

[112] H. Ahmadisedigh, L. Gosselin, and S. Lemelin, “Waste heat assessment of the workshop of a manufacturing plant: Evaluation of the waste heat amount, and waste heat recovery solutions,” https://www.rls-sciences.org/uploads/5/5/4/4/55448469/ahmadisedigh_poster.pdf